Chemistry of Diffuse Molecular Clouds towards Sagittarius B2

Sgr B2 方向にある希薄な分子雲の化学組成

東京大学大学院理学系研究科天文学専攻

白鳥　裕

Chemistry of Diffuse Molecular Clouds towards Sagittarius B2

Sgr B2方向にある希薄な分子雲の化学組成

A Thesis for the Degree of Doctor of Science
Submitted to Department of Astronomy, Faculty of Science,
The University of Tokyo

by Yutaka Shiratori
in December 1993.

List of Contents

Title

Acknowledgments 3

Abstract 4

Chapter 1. Introduction 6

1.1. Interstellar Molecules 6
1.2. Formation Mechanism of Interstellar Molecules 7
1.3. General View of Interstellar Clouds 10
1.4. Problems in the Chemistry of Diffuse Molecular Clouds 13
1.5. Problems in the Chemistry of the SiO Molecule 15
1.6. Outline of This Thesis 16

Chapter 2. Observations and Data Acquisition 18

Chapter 3. Observed Spectra 21

Chapter 4. Physical Properties of the Observed Diffuse Molecular Clouds 27

4.1. Introduction 27
4.2. Determination of Gas Kinetic Temperature of the Observed Diffuse Molecular Clouds 28
4.2.1. Determination of Gas Kinetic Temperature using the NH3 Lines 28
4.2.2. Determination of Gas Kinetic Temperature using the CO Lines 32
4.3. Determination of Molecular Hydrogen Density of Diffuse Molecular Clouds 34
4.3.1. Determination of Molecular Hydrogen Density using the CS Lines 34
4.3.2. Determination of Molecular Hydrogen Density using the SiO Lines 35
4.4. Summary of Chapter 4 36

Chapter 5. Chemical properties of Diffuse Molecular Clouds 37

5.1. Introduction 37
5.2. Determination of Molecular Column Densities 37
5.3. Physical and Chemical Properties of Individual Features 41
5.4. Correlation of Molecular Lines 44
5.4.1. Correlation of Molecular Line Intensities Multiplied by Velocity Widths 45
5.4.2. Correlation of Molecular Column Densities 46
5.5. Summary of Chapter 5. 48

Chapter 6. Discussion 49

6.1. Introduction 49
6.2. Physical Properties of Diffuse Molecular Clouds 49
6.3. Influence of UV Flux and Other Effects on Chemical Properties of Observed Diffuse Molecular Clouds 50
6.3.1. Abundance Correlations in group A 51
6.3.2. Abundance Correlations in group B 58
6.3.3. Influence of Other Effects on Chemical Properties among Observed Diffuse Molecular Clouds 61
6.4. Comparison of Chemical Properties of Diffuse Molecular Clouds with Other Kinds of Clouds 62

Chapter 7. Conclusions 65

References 67

Appendixes 78

A.1. Physical and Chemical Properties of Sagittarius B2 78
A.2. Chopper-Wheel Method 81
A.3. Determination of Rotational Temperature Using NH3 lines 82
A.4. LVG (Large Velocity Gradient) Model Calculation 84
A.5. Determination Method of Molecular Column Densities 87
A.6. Determination Method of Correlation Coefficients 89

Tables 90

Figures 140

Acknowledgments

First of all, the author wishes to express his sincere gratitude to Professor Masaki Morimoto and to Professor Yutaka Uchida, who undertakes an academic adviser for me after the retirement of Professor Masaki Morimoto. Especially, he is grateful to Professor Masaki Morimoto for offering him an opportunity to study diffuse molecular clouds, helpful guidance and valuable suggestions throughout this thesis. The author would like to thank Drs. Kentarou Kawaguchi, and Osamu Kameya for their great deal of valuable advice and suggestions, continuing encouragement and critical reading of this manuscript. He also expresses his profound appreciation to Dr. Masatoshi Ohishi, who allowed him to use unpublished data and gave him valuable comments on this work. He also gives his utmost appreciation to Dr. Satoshi Yamamoto for valuable discussions and suggestions. The radioastronomical observations in this thesis were carried out at Nobeyama Radio Observatory under close collaboration with Professor Masaki Morimoto, Drs. Kentarou Kawaguchi, Osamu Kameya, Masatoshi Ohishi, Naomi Hirano, J. S. Greaves, Glenn J. White, and Mr. Shin-ichi Ishikawa.

Next, he is grateful to Professor Toshihiro Omodaka for giving an opportunity of studying in Kagoshima University, and allowing him to use a work-station for analyzing his data. He also wishes to thank Drs. Katunori M. Shibata, Keiji Ueno, Eiji Nishihara, Messrs. Seiji Katagiri, and Taka'aki Jike for teaching him how to make figures by a Macintosh computer. He also appreciates Messrs. Nobuyuki Yamaguchi, Ryuichi Matsuba, and Yuzuru Shimodaira for helping him to prepare tables in this thesis. He also thanks Dr. Toshihiko Sasaki, Mr. Ley Furuya, Mmes. Miharu Imuta, and Setsuko Koike for sending him research materials during staying in Kagaoshima. The author also thanks Drs. Makoto Miyoshi, Yoshihiro Chikada, Yasuhiro Hirahara, Saeko S. Hayashi, Yutaka Hayano, and Masahiko Hayashi and Messrs. Takeshi Miyaji, Ki'ichi Okita, Tomio Kanzawa, Shinji Toyomasu and many students of the Graduate University for Advanced Studies for their help and warm encouragement throughout this work. The author thanks Professors Minoru Tanaka, Tomoyuki Miyazaki, Drs. Akihiro Nakamura, Yuuji Horie, Messrs. Sigeru Yasuda, Tomonari Suzuyama, and Takahiro Kitagawa and many colleagues for their kind encouragement during his stay of Kagoshima.

Finally, he wishes to thank his family all for their encouragement and being patient helping during studying this thesis. It is his great pleasure to thank all of them.

Abstract

In this thesis, the authors carried out a systematic study on physical and chemical properties of diffuse molecular clouds towards Sgr B2. By using Nobeyama 45-m telescope, we observed 32 transitions belonging to 12 molecular species, and identified nine velocity components at 22, 3, -20, -28, -42, -46, -76, -92 and -105 km/s which are located on the line-of-sight from Sgr B2 to the Sun.

We derived kinetic temperatures of the diffuse molecular clouds by using NH_3 absorption lines to be 24 ~ 30 K. We did not find differences in the kinetic temperature among the observed clouds. The molecular hydrogen density ($n(H_2)$) of each diffuse molecular cloud is determined by large-velocity-gradient (LVG) model calculations of the ^{28}SiO (J = 1-0, J = 2-1), and $C^{32}S$ (J = 1-0, J = 2-1) transitions. The densities lie between 1×10^2 and 4×10^2 cm^{-3}. The differences in the densities are not recognized among clouds. Visual extinctions of the diffuse molecular clouds are determined to be in the range of 1.3 ~ 4.1 mag. The sizes are determined to be 0.05 ~ 0.21 pc by comparing the visual extinctions and the densities. According to these results, the density and the temperature of the diffuse molecular cloud are found to be nearly as same as the higher density regions of the diffuse clouds.

We derived the column densities of the observed molecules, and investigated mutual correlations one another. We found that the correlations of the observed molecules in the diffuse molecular clouds can be divided into two groups. A positive correlation is found among ^{13}CN, $H^{13}CN$, $HN^{13}C$, HC_3N, $H^{13}CO^+$, NH_3, and SiO molecules. These molecules are classified as group A. On the other hand, the $C^{34}S$ and C_3H_2 abundances show a positive correlation, and may be shown among these molecules and SO and CH_3OH. These molecules are classified as group B. The molecules belonging to group A show no apparent correlation with those belonging to group B. A primary reason may be due to difference in photodissociation rates and molecular formation mechanism.

We found that some of the observed molecules correlate with visual extinction. The column densities of ^{13}CN, $H^{13}CN$, HC_3N, NH_3 have peaks at 1.5 ~ 1.8 mag, and decrease as visual extinction further increase. On the other hand, those of the $C^{18}O$, SO, CH_3OH and possibly $C^{34}S$, C_3H_2 molecules (group B) increase with visual extinction. Those of SiO, and $H^{13}CO^+$ show no relation with visual extinction. The reason is conjectured as follows: the ^{13}CN, $H^{13}CN$, HC_3N, NH_3 molecules are relatively difficult to be dissociated by the UV photon compared with the CS, C_3H_2, CH_3OH, and SO molecules. Therefore, increments

in abundances of the group B species with visual extinction is large compared with the case of the group A molecules.

The difference in chemical reaction may partly explain a lack of significant correlation between the groups. The dissociative recombination reaction of $HCNH^+$ with electron is thought to be important to form CN, HCN, and HNC, which are well correlated to one another. The abundance correlation between CN and HC_3N can be well explained if a small part of CN is converted to HC_3N by a neutral-neutral reaction. The CS, c-C_3H_2, and CH_3OH molecules are thought to be formed from the same starting ion (CH_3^+). The molecular abundances of NH_3 and CN are expected to anti-correlate to each other, if C^+ destroys NH_3 to produce the precursor ion H_2NC^+ for CN. However, both molecules are correlated well. The reason is unclear. The HCO^+ molecule is thought to be formed from C^+ and OH, which are abundant in diffuse molecular clouds. Therefore, the molecular abundance of HCO^+ may be increased as in the case of HCN. The SiO molecule has similar behavior as the case of HCO^+, because the Si^+ ion is also increased by UV flux in the diffuse molecular clouds.

Finally, we compared chemical composition of the observed diffuse molecular clouds with those of dense molecular clouds. The relative abundances of ^{13}CN, $H^{13}CN$, $H^{13}CO^+$, and $HN^{13}C$ to CO in the observed diffuse molecular clouds are almost similar to those of TMC-1. On the other hand, the SO and HC_3N abundances are smaller by factor $3 \sim 4$ (± 1.7). These results may be explained by differences in visual extinction and production chemistry of these molecules.

Chapter 1. Introduction

1.1. Interstellar Molecules

Interstellar medium has complex hierarchical structures. The temperature of the interstellar medium ranges from 10 K to 10^6 K, and the density ranges from 10^{-2} to 10^7 cm^{-3}. The studies of the physical and chemical properties of the interstellar medium are conducted in the wide frequency range from ultraviolet (UV) to radio. Especially the density and temperature region from the diffuse cloud (Fig 1; Av ~ 1 mag, $n(H_2) \leqq 100$ cm^{-3}, Tk ~ 25-100 K) to the dense molecular cloud (Fig 1; $n(H_2) \geqq 10^4$ cm^{-3}, Tk ~ 10 K) are well studied by many observers with molecular line observations and theorists with forcible model calculations. Interstellar medium is thought to be evolving from the diffuse clouds to the dense molecular clouds.

The molecular lines first detected in the interstellar space are optical absorption lines of CH, CH^+, and CN in the diffuse clouds in front of the several stars (Swings and Rosenfeld 1937; McKellar 1940; Douglas and Herzberg 1941), where the electronic transitions were used for observations.

After their discoveries, development of radio telescope enabled us to detect many fundamental molecules in interstellar space, which have permanent electronic dipole moments. In 1960's, the spectral lines of OH (Weinreb et al. 1963), NH_3 (Cheung et al. 1968), CO (Wilson, Jefferts, and Penzias 1970), and H_2CO (Palmer et al. 1969) were detected at the region covering centimeter and millimeter wavelength. These molecules have been widely observed and employed as probes of physical conditions of interstellar clouds, such as kinetic temperature, molecular hydrogen density, mass, velocity structure, and so on.

The efforts to assign the spectral lines detected in the interstellar objects have been made through a number of technical developments for spectroscopy of various chemical species. At present, more than 100 interstellar molecules have been identified in various astronomical sources, such as the circumstellar envelope of the late type star IRC+10216, the active star-forming region such as Orion Molecular Cloud-1 (OMC-1), Sagittarius B2 (Sgr B2; neighborhood of the center of our Galaxy), and the dense molecular cloud such as Taurus Molecular Cloud-1 (TMC-1). Most molecular lines are observed in emission. The detected molecules are listed in Table 1.

1.2. Formation Mechanism of Interstellar Molecules

Knowledge of molecules in interstellar space and circumstellar envelopes is important to understand chemistry in extreme physical conditions of density and temperature and in long time scale which cannot be realized in the laboratory. Chemical reactions that produce the interstellar molecules are limited to exothermic two body reactions, as well as the cosmic ray and/or UV ionization processes. Attempts to explain the observed molecular abundances in diffuse clouds were carried out on the basis of non-thermodynamic equilibrium models by Kramers and ter Haar (1946), and Bates and Spitzer (1951). These researchers considered basic formation and destruction processes in some detail through radiative association, photodissociation, photoionization, and dissociative recombination, but were unable to reproduce the observed abundances of the known interstellar molecules CH and CH^+. Because of the difficulties encountered with the early gas-phase reaction schemes, subsequent models focused on grain surface processes for formation of molecules. Plausible models were made for the formation of the H_2 molecule on grains (Hollenbach and Salpeter 1971), but the productions of other molecules were not fully explained due to uncertainties in composition of the grain surface, surface reactions, and desorption processes. Around the same time, Solomon and Klemperer (1972) and Herbst and Klemperer (1973) realized that reactions between ions and neutral species could be very rapid at the low temperatures prevailing in interstellar clouds, and therefore reintroduced the gas-phase reaction schemes. In 1970's, the basic chemical models were constructed with these gas-phase reactions (Solomon and Klemperer 1972; Watson 1973; Watson 1974; Herbst and Klemperer 1973). These models explained well the abundances of observed simple molecules.

However, there are several observational results which cannot be explained only by ion-molecule reactions. Other processes such as grain surface reactions, and high-temperature reactions induced by shock wave, and photodestruction and photoionization processes by stellar radiation have often been suggested for such cases.

There are direct evidences for existence of small solid particles in interstellar medium. Dust grains play certainly an important role in interstellar chemistry through surface reactions such as that forming H_2 molecules and molecular accretion processes on the grain surface, as well as in protecting molecules in interiors of molecular clouds from photodissociating radiation. Many of the current theoretical efforts on grain chemistry, including studies by Hasegawa and

Herbst (1993) and Hasegawa, Herbst, and Leung (1992), have concentrated on studying effects of grain surface chemistry on the chemical evolution of molecular clouds in dense, well shielded regions.

It has been recognized for many years that shocks propagate in the interstellar medium. Supernovae explosion, collisions between interstellar clouds, turbulent motions within clouds, and expansion of compact HII regions can be an origin of supersonic motions which give rise to shocks. Observational support of the shock hypothesis is found in spectroscopic measurements of molecular H_2 (Beckwith et al. 1978; Nadeau and Geballe 1979; Simon et al. 1979; Ogden et al. 1979; Scoville et al. 1982; Davis, Larson, and Smith 1982), highly rotationally excited CO (Watson et al. 1980, Storey, Watson, and Townes 1981; Stacey, Langer, and Genzel 1982; Watson et al. 1985), and vibrationally excited CO (Geballe and Garden 1987) in the Orion molecular cloud. In the shocked gas, endothermic ion-molecule reactions such as

$$C^+ + H_2 = CH^+ + H - 4640\ K$$

may become important. Elitzer and Watson (1978, 1980) have suggested that this reaction is responsible for CH^+ formation in the diffuse clouds. Shock also plays an important role in molecular desorption processes from dust grain. Effects of low-velocity shocks ($V \sim 10$ km/s) on grain mantles consisting of hydrogenated amorphous carbon (HAC) have been investigated by Brown et al. (1989) in diffuse cloud models. These authors proposed that polycyclic aromatic hydrocarbon (PAH) molecules may be released from the mantles into the gas phase.

UV radiation induces the photodissociation and photoionization processes of molecules. Stief et al. (1972) showed that the lifetimes against photodissociation of small interstellar molecules increase dramatically as a function of visual extinction. Black and Dalgarno (1977) showed how strongly stellar UV radiation incident upon a cloud affects the molecular composition of the cloud. The complete neglect of photodissociation and photoionization in dense molecular clouds has always been a contentious subject. The effects by interstellar UV radiation are possibly negligible. However, several authors argue that preferential forward scattering from cosmic ray radiation by the grains could result in more UV radiation inside clouds than customarily assumed. Nevertheless, use of the customary grain parameters (Mathis, Metzger, and Panagia 1983) shows that even at a rather small visual extinction of $Av = 5$, most photodestructive

processes are not rapid compared with competing gas phase processes. This conclusion is based on a compendium of photodissociation and ionization rates compiled by Herbst and Leung (1986), who utilized the available literature regarding cross sections and branching ratios for photodestructive processes involving neutral polyatomic species. However, Prasad and Tarafdar (1983) studied the effects of internal UV fields in molecular clouds generated by cosmic ray excitation of molecular hydrogen. These authors concluded that phtodestruction rates of up ~ 10^{-14} s^{-1} of the CO molecule could be expected.

The laboratory measurements of the rate coefficients were made by various techniques and the results were summarized, for example, by Huntress (1977) and Prasad and Huntress (1980). These chemical networks have been enlarged to explain the production of more complex molecules, including the polyatomic molecules found in the dense molecular dark clouds. Suzuki (1979) constructed a chemical network including over 2800 gas-phase reactions, and calculated the time dependent abundances of 234 molecular species. They showed that the time scale for the calculated abundance to attain steady state is at t ~ 2×10^{16} sec (~ 10^9 years), which is longer than the evolutionary time scale of dense clouds. Graedel, Langer, and Frerking (1982) developed a time-dependent model of dense molecular clouds to study the dominant chemical processes in carbon and oxygen isotope fractionation, formation of nitrogen-containing molecules, and evolution of product molecules as a function of cloud density and temperature. They treated 1067 individual reactions of 63 species in their calculations. Several of the observed molecules (e.g., CO, H_2CO, OH) have abundances which agree with their calculation and seem to be well explained by the basic aspects of the ion-molecule chemistry. However, abundances of some species such as NH_3 do not agree with those predicted by the calculations. Herbst and Leung (1989) made a time-dependent calculation of the gas-phase model including the carbon-chain molecules with 9 carbon atoms. They showed that the gas-phase reactions in the dense molecular clouds can produce large abundance of very complex molecules such as carbon-chain molecules, which have peak abundances only at periods before a steady state. Herbst and Leung (1990) have extended the one-phase, pseudo-time-dependent approach to include 2577 gas phase chemical reactions involving 276 species up to nine carbon atoms (HC_9N) in size. Their results show that the abundances of both small and large molecules in the well-studied source TMC-1 are well accounted for at early time, although there are several important exceptions.

Suzuki et al. (1992) carried out survey observations of CCS, HC_3N, HC_5N

and NH_3 toward 49 dense molecular clouds to examine an existence of systematic correlation between the chemical evolution and the physical evolution of dense molecular clouds. They found the column density of CCS shows a good positive correlation with those of HC_3N and HC_5N, whereas it shows no correlation or probably an anti-correlation with that of NH_3 (Fig. 2a, 2b). Suzuki et al. (1992) also performed a numerical calculations consisting of 99 chemical species including H, C, O, N, S, He, and Mg, and involving 431 chemical reactions, which cover most of the standard reaction pathways for production and destruction of small carbon-chain and hydrocarbon molecules whose numbers of carbon atoms are less than 3 (Suzuki 1983; Herbst 1983). The correlation and anti-correlation in the column densities observed by Suzuki et al. (1992) are qualitatively interpreted as an effect of chemical evolution of dense molecular clouds. The carbon-chain molecules are theoretically inferred to be formed effectively in the earlier stages of the chemical evolution, while the other molecules, such as NH_3, HN_2^+, HCO^+, SO, and SO_2 are responded to be slowly formed at late stages in the clouds. Such gas-phase reaction schemes are suitable for reproducing the chemical compositions of the relatively placid region such as the dense molecular clouds. However, in active star-forming regions, other processes such as grain-surface reactions, endothermic reactions via interstellar shock waves, and radiation processes are to be included.

On the other hand, in diffuse clouds, all observed molecules are correlated well with visual extinctions of the clouds (e.g., Dickman et al. 1983). The chemical composition of the diffuse clouds are thought to be similar in most observed clouds. Since the early work of Bates and Spitzer (1951) and Solomon and Klemperer (1972), many steady-state models have been developed to describe the chemistry in diffuse clouds.

1.3. General View of Interstellar Clouds

We give a short summary about characteristics of diffuse clouds. Next, we describe the characteristics of translucent clouds and high-latitude clouds which have slightly higher density than diffuse clouds. Finally, characteristics of dense molecular clouds are described.

A study of the diffuse clouds is conformed by observing absorption lines in the optical and the UV region, because their visual extinction is less than 1 mag. Therefore, many studies are made by observing the objects lying near the solar system which have low extinction (e.g., ζ Oph, χ Per, α Cam). ζ Oph cloud is the

most studied of all diffuse clouds (e.g., Herbig 1968; Morton 1975). ζ Oph is the excitation source for the surrounding diffuse HII region S27 (Sharpless 1959), and CO, CN, and CH are detected in a foreground cloud at mean velocity ~ 0.2 km/s. There is marginal evidence for a difference in the CH and CH^+ velocities by ~ 1-2 km/s (Wilson 1981). Reasonable agreement is found in the column densities derived from optical (UV) absorption and radio emission line studies for both CO (Dickman et al. 1983) and CH (Lang and Wilson 1978), indicating that there is very little molecular material behind the star. The results of ζ Oph clouds which are made by the UV absorption studies show that physical properties of the diffuse clouds are as follows: $N(CO) \leqq 10^{15}$ cm^{-2}, Av ~ 1 mag, size ~ 1-3 pc (the size is much higher than that of dense core in molecular clouds ~ 0.1 pc), and Tk ~ 20-100 K (Snow 1980). However these studies are made by low velocity resolution (e.g., Jenkins, Savage, and Spitzer 1986; 2.4 km/s). On the other hand, the cloud is observed by the CO molecular line with high velocity resolution, and found to be Tk ~ 20-30 K, $n(H_2)$ ~ 200-500 cm^{-3} (van Dishoeck and Black 1986). Chemical characteristic of the diffuse clouds is as follows: most elements in gas phase have atomic or ionic form depending their ionization potential, and molecular abundance are very low. Moreover, only simple diatomic molecules such as CH, CH^+, OH, CO, C_2, and CN are detected (van Dishoeck and Black 1986). On the other hand, CS is not detected, since this molecule is expected to be less abundant than CH etc. Another characteristic of the diffuse cloud is almost no difference in the chemical composition among the clouds. This is shown by the fact that the column density of the H_2 molecule always correlates with those of other molecules (CO, Federman et al. 1980; CH, CH^+; Federman 1982; CN; Federman, Danks, and Lambert 1984).

In recent years, a growing body of data has become available for more reddened lines-of-sight with Av = 2 ~ 5 mag ($N(H_2) \geqq 10^{21}$ cm^{-2}). These clouds are of interest because they provide the bridge between diffuse and dense molecular clouds, and may give insight into the chemical processes occurring in both regions. They are denoted as "translucent" clouds, to indicate that photochemical processes play an important role in the chemistry throughout the cloud, even though the photodissociation rates diminish rapidly toward the center. Although the translucent clouds are usually taken to refer to isolated small clouds, they may also represent the outer edges of dense molecular clouds. Translucent clouds have the virtue that they can be studied observationally not only by millimeter emission lines, but also by absorption line techniques (e.g., van Dishoeck and Black 1988), provided that a suitable background star is available

(CO; e.g., Knapp and Bowers 1988). Compared with the diffuse clouds, the column densities of CH, C_2 and CN are larger by up to an order of magnitude, whereas the CO column density is larger by several orders of magnitude (van Dishoeck and Black 1989). A good example of a translucent cloud is provided by the small cloud in front of the B1 supergiant HD 169454 investigated by Jannuzi et al. (1988), who obtained Tk = 15 K, $n(H_2) \sim 300$ cm^{-3} by observations of C_2. The CO column density in this cloud lies implies that translucent clouds are in the critical physical condition where a large fraction of the available carbon is converted into the CO molecules. Another interesting example of a translucent cloud is that toward HD 29647. This cloud has been studied by Crutcher (1985) and was found to have $n(H_2) \sim 800$ cm^{-3}, Tk = 10 K by observation of CO. van Dishoeck and Black (1989) reported absorption-line observations of CH, C_2 and CN in a number of translucent molecular clouds towards reddened stars. The column densities of C_2 and CH are found to be strongly correlated with each other, and probably with the column density of H_2. Large variations between the C_2, CH and CN abundances, pose a major problem for understanding of the chemistry. Following ideas have been reported for this problem: (1) variable element depletion, (2) variations in the UV radiation field and extinction curve, and (3) uncertain rates for reactions that are essential for the nitrogen chemistry.

Another class of diffuse or translucent clouds are the high-latitude molecular clouds detected by Magnani, Blitz, and Mundy (1985) through millimeter observations of CO. Visual extinctions of these clouds are similar to those (Av ~ 1 mag) of the diffuse clouds such as the ζ Oph and χ Per clouds, but their CO column densities and CO/H_2 ratios are at least an order of magnitude higher than those of diffuse clouds (Lada and Blitz 1988). As discussed by van Dishoeck and Black (1988), such high CO column densities for small Av can be produced within the steady-state framework only if the clouds are exposed to a UV radiation field that is weaker than the average background radiation field by a factor of 2 ~ 4. These clouds are observed by CO emission lines, and do not always lie in front of bright OB stars. The observations are mainly performed by Gredel et al. (1992) for the cloud toward HD210121. This cloud is discovered by de Vries and van Dishoeck (1988) on the basis of the IRAS 100 μm data. This cloud has located at suitable position that it is not the outer extension of a giant molecular cloud or a dark cloud located close to the galactic plane. Therefore, it is much suited for an investigation than many other clouds as the sample. There is a lot of CO molecule, but it does not yet become the dominant carbon-bearing species in this cloud. The CO millimeter lines are therefore weak. The C_2 excitation suggests that

temperature is less than 20 K, although the molecular hydrogen density is somehow uncertain, Tk $\lesssim$ 20K, and a rather low, but uncertain density is in the range of 500-1000 cm^{-3}. The CN excitation derived from the absorption lines, combined with sensitive searches for the CN millimeter emission line, indicates molecular hydrogen densities are in the range of 1500-2500 cm^{-3}.

Magnani, Blitz, and Wouterloot (1988) have derived the abundances of OH and H_2CO in a number of high-latitude clouds through observations at centimeter wavelengths. Within the large observational uncertainties, the OH column densities are in the range of $10^{14} \sim 10^{15}$ cm^{-2}, an order of magnitude larger than those found the diffuse clouds, while the H_2CO column densities are in the range of $10^{12} \sim 10^{13}$ cm^{-2}. H_2CO has not yet been detected in any diffuse clouds. de Vries and van Dishoeck (1988) have detected absorption lines of interstellar CH and CH^+ for clouds with strong interstellar Na features. The observed CH column densities are of the order of 10^{13} cm^{-2}, and are not significantly larger than those found in the diffuse clouds. CH^+ has been detected in one high-latitude cloud, and its column density of 6×10^{12} cm^{-2} is lower than that found in the ζ Oph cloud.

Finally, physical and chemical properties of the dense molecular clouds are described. The dense molecular clouds have a more complex structure than diffuse clouds, the translucent clouds, and high-latitude clouds. The existence of the dense molecular clouds was known by observing the weakened background star light in optical observations. The dense molecular clouds are studied by many observers from optical to radio wavelength. Many observations are conformed to TMC-1 in the Taurus complex as a representative object. The physical property of this cloud is obtained by observations with various molecular emission lines, and it is found that $n(H_2) \sim 10^4$-10^5 cm^{-3} in the center region and $10 \sim 100$ cm^{-3} in the edge of the cloud, and $Tk \sim 10$-20 K. The chemical compositions of the dense molecular clouds are studied by observing rotational spectral in the millimeter and centimeter-wave region. Chemical composition of the dense molecular clouds are different from source to source whether star formation is taking place or not (e.g., Suzuki et al. 1992, Hirahara et al. 1992).

1.4. Problems in the Chemistry of Diffuse Molecular Clouds

We define the region which is mainly observed by absorption lines (e.g., HCN, HCO^+; Nyman 1983, CS, C_2H; Nyman 1984, HCO^+, HCN; Linke, Stark, and Frerking 1981, C_3H_2; Matthews and Irvine 1985) in millimeter-wave except for the CO lines as 'Diffuse Molecular Clouds'. Absorption line features belonging

to the diffuse molecular clouds are observed toward many astronomical objects (e.g., Cas A; Bartla, Walmsley, and Wilson 1984; W49, W51, DR21; Nyman 1983; Sgr A, Sgr B2; Linke et al. 1981). However, it is difficult to find these clouds, because they are only observed toward the strong continuum point (mostly one points), so that their wide space distribution is not known in general.

The CO (J = 1-0) line was observed as emission in these diffuse molecular clouds, while other lines were observed as absorption of the continuum source. From two level excitation analysis for a 20 K cloud, the critical density is 200 cm^{-3} for CO. On the other hand, those are 1000 and 5000 cm^{-3} for HCO^+ and HCN, respectively. This means that the molecular hydrogen density is in the range of 200-1000 cm^{-3}.

Up to now, chemical composition of the diffuse molecular clouds has been thought to be similar (e.g., Nyman 1983, Linke et al. 1981). However, this thought is based on a few observations with low S/N ratios.

Since absorption lines are in general very weak, long integration times and low-noise receivers are necessary. If a continuum source is a point source, a use of large telescope is essential to obtain the higher continuum brightness temperature and the many molecular absorption lines.

One exception is the observation of the diffuse molecular clouds in front of W49A (Miyawaki, Haseagawa, and Hayashi 1988). Two absorption features of CS (J = 1-0) have been detected at V_{lsr} = 39 and 60 km/s. The column density of CS for the 60 km/s absorbing feature is about half of that for the 39 km/s gas, while the column densities of other molecular species such as H_2CO, HCO^+, C_2H, and OH in the 60 km/s gas are 2-6 times higher than those in the 39 km/s gas. However, the data is not enough to study in detail whether characteristic features of diffuse molecular clouds in front of W49A, and general tendency of chemical differences among diffuse molecular clouds.

Recently, many absorption lines were observed with good S/N ratios towards the Sgr B2 using the Nobeyama 45-m telescope (Greaves et al. 1992). However, they analyzed the spectrum of main isotopic species except for CS. Therefore, the optical depths were not estimated accurately. Shiratori et al. (1995) used data of rare isotope species as well as those of the main isotope species for each molecule with good S/N ratio in order to estimate optical depth. Shiratori et al. (1995) studied mutual correlation in the brightness temperature of molecular absorption lines (^{28}SiO, $H^{13}CO^+$, $C^{34}S$, $H^{13}CN$, C_3H_2), and found the molecular abundance in the diffuse molecular clouds are different from source to source. Unfortunately the relation of the correlation with physical properties (for example,

molecular hydrogen density, and kinetic temperature) of the diffuse molecular clouds is not known because of the large error of the physical properties. Also a possible pathway of the molecular formation has not been establishment yet because of poor observational information on molecular abundances.

1.5. Problems in the Chemistry of the SiO Molecule

Interstellar SiO was detected at millimeter wavelengths (Wilson et al. 1971) shortly after the discovery of CO (Wilson et al. 1970). Since then, CO has been known to be the most widely distributed molecule other than H_2 in the interstellar medium. In contrast, SiO has been detected mainly in regions with high density and high temperature associated with outflows from young stellar objects. Although silicon is likely to be strongly depleted on dust grains in dense clouds, and the SiO lines have a higher critical density for rotational excitation to excite than CO, the almost complete lack of detection in quiescent regions cannot be understood solely in these reasons. Interstellar silicon chemistry was first discussed in detail by Turner and Dalgarno (1977); other early work was carried out by Solomon and Klemperer (1972), Prasad and Huntress (1980), and Millar (1980). Silicon chemistry in shocks has been studied by Hartquist, Oppenheimer, and Dalgarno (1980) and more recently Neufeld and Dalgarno (1989). Circumstellar silicon chemistry has been investigated by Scalo and Slavsky(1980) and Clegg, Ijzendoorn, and Allamandola (1983). The gas phase chemistry of silicon in dense molecular clouds has been investigated using a pseudo-time dependent model by Herbst et al. (1989). Recent theoretical and experimental studies of silicon reactions and new astronomical observations now provide stimulation to develop further studies of the interstellar silicon chemistry.

From radio observations, it is apparent that the interstellar chemistry of silicon differs from those of carbon, oxygen, nitrogen, and sulfur. The elemental abundance of Si is twice those of S and only one order of magnitude less than that of C, N, or O. A number of molecules containing C, N, O, and S are known as interstellar molecules, whereas gas phase silicon is detected only as SiO, SiS and SiC_2 (Morris et al. 1975; Irvine et al. 1985). Furthermore these Si bearing molecules are detected and only in hot dense regions perturbed by star formation, and circumstellar envelopes of highly evolved red giants. The SiO emission lines are detected toward massive-star forming regions, such as W49 and W51 (Downes et al. 1982, Wright et al. 1983, Ziurys and Friberg 1987, Ziurys 1988). Recently, Bachillar, Menten, and del Rio-Alverez (1990) detected the J = 3-2 line

of SiO toward Barnard 1 (B1). This source is one of dense molecular cloud cores in the Perseus OB2 association, and is known to be a formation site of a low mass star. This is the first report on the detection of SiO toward a low-mass star forming region in a dense molecular cloud. More recently, the SiO lines are detected in other low-mass star forming regions, L1448 (Bachiller, Martin-Pintado, and Fuente 1991) and L1157 (Mikami et al. 1992, Umemoto et al. 1992). The SiO line (J = 2-1) in L1157 is as strong as 3.2 K in brightness temperature, and it arises from an interaction region between the outflow and dense gas. In L1448 the SiO line is detected in "molecular bullets" in the high velocity outflow.

On the other hand, the lines of SiO are not detected in the dense molecular cloud (Tk $\leqq$ 20K) like TMC-1 and L134N (Ziurys, Friberg and Irvine 1989; relative abundance in TMC-1 estimated by Ziurys et al. (1989) is $X(SiO) = N(SiO)/N(H_2) < 2.4 \times 10^{-12}$). A possible interpretation for these observational results is that the Si containing molecules are heavily depleted into dust grains, and hence, observable amount of SiO no longer remains in the gas phase of cold dense molecular clouds. Energetic phenomena associated with massive star-formation or supernova explosion may release Si or SiO from dust grains into the gas phase. However, the absorption lines of SiO was observed toward a strong continuum source of Sgr B2, suggesting that SiO exists in diffuse molecular clouds in front of Sgr B2 (Ohishi 1991). In order to understand the SiO production, the correlation of SiO with other molecules would essentially be important.

1.6. Outline of This Thesis

In this thesis, we observed many molecular lines toward Sgr B2 and analyzed them in order to clarify molecular distribution in diffuse molecular clouds. The diffuse molecular clouds towards Sagittarius B2 (Sgr B2) are the most suitable sources for studying the chemical composition, because of the following reasons:

(1) Sgr B2 is one of the strongest continuum sources in our Galaxy, and many absorption lines can be detected with good S/N ratios.

(2) There are many diffuse molecular clouds in front of Sgr B2, and we can study chemical abundance variation among these clouds at the same time.

(3) Sgr B2 is located at 100 pc from the center of our Galaxy (Fig. 3). Therefore, we can study not only our neighboring diffuse molecular clouds, but also other clouds which lie near the Galactic center.

Physical and chemical properties of Sgr B2 itself will be described in Appendix A.1.

In Chapter 2, the observations of the diffuse molecular clouds and the data acquisitions are described. In Chapter 3, the qualitative description about the results of the observations is given. In Chapter 4, the physical properties such as kinetic temperature and molecular hydrogen of the diffuse molecular clouds are determined. In Chapter 5, the quantitative analysis of chemical composition of the diffuse molecular clouds are carried out. In Chapter 6, discussions of the results obtained in Chapter 5 are described. Finally, conclusion of this thesis is given in Chapter 7.

Chapter 2. Observations and Data Acquisition

Our spectroscopic observations of Sgr B2 were made with 45-m telescope at the Nobeyama Radio Observatory (NRO) April and May 1989. The reference point used was (MD5) R.A. (1950) = $17^h44^m10.6^s$, Dec(1950) = -28° 22'05"; Fig. 4. Observed molecular lines were ^{28}SiO (J = 1-0) and ^{29}SiO (J = 1-0) at 43 GHz region, ^{28}SiO (J = 2-1) and $H^{13}CO^+$ (J = 1-0) at 86 GHz. We used two frontends for the 43 GHz and the 86 GHz bands. The frontend for 43 GHz was an SIS (Superconductor-Insulator-Superconductor) mixer receiver and was operated in double-sideband mode. The aperture efficiency and the beam efficiency of the telescope were 0.48 and 0.67, respectively. System noise temperature (SSB; Single-sideband mode) on the sky was 600-900K at elevation of 20° including contribution from atmosphere. This receiver did not install SSB filter. So the line intensities were corrected to the value at the center of the line by the H53α recombination line which observed at February, 1985 by using cooled Schottky Barrier diode mixer receiver with SSB filter. Imaging rejection ratio was about 6 dB at SiO line frequency. The other frontend for 86 GHz was a cooled Schottky Barrier diode mixer receiver. System noise temperature (referred to above the Earth's atmosphere) was 900 ~ 1600 K at elevation of 20° in single-sideband mode. The aperture efficiency and the beam efficiency of the telescope were 0.31 and 0.48, respectively. The half-power beam widths (HPBW) were 39" at 43 GHz and 20" at 86 GHz. The values correspond to 2.0 pc at 43 GHz and 1.0 pc at 86 GHz assuming the distance of 8.5 kpc to the Sgr B2.

Eight arrays of the 2048 channel acoustic-optical spectrometer (AOS-W) were used for the backends. Each array had a channel interval of 125 kHz and an effective frequency resolution of 250 kHz, which correspond to 1.7 km/s at 43 GHz and 0.85 km/s at 86 GHz, respectively. Baselines were determined by position switching, with an off position at ΔR.A. = -30'. The raw data for the 'on' and 'off' positions were inspected in regions of the spectra which were free of lines, in order to obtain a first order estimate of the continuum level. The pointing accuracy was checked every 2 or 3 hour using the SiO (J = 1-0 v = 1) maser emission from VX-Sgr at 43 GHz, and was estimated to be less than 10". Intensity scale was calibrated against a blackbody at the ambient temperature (295 K) using the Chopper-Wheel method (Ulich and Haas 1976; Appendix A.2). The intensity scale using this method was the antenna temperature (T_A^*), which was corrected for the atmospheric and ohmic losses. R.m.s. noise temperatures obtained were 0.05K at 43 GHz and 0.10 K at 86 GHz.

In addition to the presently observed data, we analyzed those of Greaves et al. (1992), Ohishi et al. (1995), Morimoto et al. (1983), and Lis (1989) simultaneously. The molecular lines used in this thesis are summarized in Table 2 with their frequencies, and the observed r.m.s. noise temperatures.

Greaves et al. (1992) observed the CS (J = 1-0), $C^{34}S$ (J = 1-0), $H^{13}CN$ (J = 1-0), and C_3H_2 J(Ka,Kc) = [2(1,2)-1(0,1)] line with the NRO 45-m telescope. The receivers and the spectrometer which they used were the same as we used. Observed r.m.s. noise levels range from 0.03 to 0.5 K.

The data of the line survey were obtained in wide frequency range from 8 to 113 GHz except 50 ~ 70 GHz. Those were observed by Ohishi et al. (1995) with the NRO 45-m telescope from 1986 to 1993. The r.m.s. noise values of the line survey were between 0.01 K and 0.24 K, and the average r.m.s. noise value was 0.03 K. There were frequency gaps of 25 % in the 8 ~ 50, 75 ~ 115 GHz frequency range, as shown in Fig. 5. According to the observations by Turner (1991) and Cummins, Link and Thaddeus (1986), no strong absorption lines are reported in these frequency gap. However, it should be noted that the beam sizes of these observations are much different from that the data by Ohishi et al. (1995).

Morimoto et al. (1983) observed the $H^{12}CO^+$ (J = 1-0) line with the Nobeyama 45-m telescope, November 1982. The frontend for their observation was the same as we used. The system noise temperature was 1000 K at elevation of 20° in single-sideband mode. The values of the aperture efficiency and the beam efficiency of the telescope were 0.35 and 0.48, respectively. Observed r.m.s. noise level was 0.3 K.

Lis (1989) observed the ^{12}CO (J = 1-0) and ^{13}CO (J = 1-0) lines using the 14 m telescope at Five College Radio Astronomical Observatory (FCRAO), October and December 1986 and June 1988 at the same reference point as we used. The frontend for their observation was a cooled Schottky Barrier diode mixer receiver. The value of the beam efficiency was 0.45. The system noise temperature was 800 K (SSB) in the observations of Sgr B2. The half-power beam width (HPBW) was 42", which corresponds to 1.8 pc assuming the same distance as we used. A quasi-optical single sideband filter was used for image rejection. Pointing and temperature calibration were carried out by observing Saturn. Integration times were 90 seconds. The r.m.s. noise levels were 0.1 K at the ^{12}CO frequency and 0.04 K at the ^{13}CO frequency.

We identified absorption lines as follows: the rest frequencies of some of used molecular lines are not known. All molecular lines belonging to the Sgr B2 itself except for H_2CO line are observed with emission profiles or mixture of

emission and absorption profiles (Fig. 6). If an emission line of Sgr B2 is observed, it is used to derive the rest frequency by using the reference velocity. If the mixture line is observed, two methods are used. When the recombination line was observed in the same spectrometer in which the absorption line was observed, the rest frequency of the absorption line is derived by assuming the rest frequency of the recombination line as a reference. When the recombination line was not observed in the same spectrometer as the absorption line, the mixture line radiated from Sgr B2 itself is used. However, the mixture line is not known where the location of peak is by influence of the absorption line, we considered only molecular candidate which is known in the range of 50 MHz. Finally, the energy level of the transition of each molecule is calculated to confirm that the transition could be obtained as an absorption. If the energy level is not so high as those of other molecules, we recognize it as an absorption line. Thus, totally 32 transitions due to 12 molecules are identified as absorption lines.

We corrected velocity shift using the three strong absorption or emission of the $C^{32}S$ (J = 1-0) lines as reference velocities, which correspond to V_{lsr} = 62km/s of $C^{32}S$ (J = 1-0) belongs to Sgr B2 itself and V_{lsr} = 3, -105 km/s belong to the diffuse molecular clouds towards Sgr B2. Examples are shown in Fig. 7. The error of the velocity measurement was estimated to be less than 5 km/s by considering line width of three velocity components as shown in Fig. 6.

Baselines of our data and a part of other data are corrected by linear fitting. The baselines of other data of Greaves et al. (1992), Lis (1989), Morimoto et al. (1982), and Ohishi et al. (1995) have already been corrected. We used these data without further correction. The results are shown in Fig. 8a ~ 8d. Since continuum level was removed by linear fitting, the baseline in Fig. 6 corresponds to the continuum level. The inaccuracies caused by removing the baselines produced by these baseline correction were less than r.m.s. noise temperature.

Figure 6 shows the CS (J = 1-0) spectra. Absorption lines were observed with many velocity components between the V_{LSR} = -120km/s and 120 km/s, and we identified 10 components at 62, 22, 3, -20, -28, -42, -46, -76, -92 and -105 km/s, as shown in Fig. 7. These features, except for the 62 km/s component belonging to Sgr B2 itself, were explained by molecules in the foreground clouds toward Sgr B2. Figure 8a ~ 8d show all absorption line features used in this thesis. The identification of the velocity components is slightly different from those of Greaves et al. (1992). We found the 22 km/s velocity component in $H^{13}CO^+$ was the same as the 30 km/s velocity component by Greaves et al. (1992). Also they found a component at -25 km/s, but it was nominated to be due to two components, -20 km/s and -28 km/s by the CS (J = 1-0) observation. The -92 km/s component was not found by Greaves et al (1992), but it was recognized clearly as strong absorption in the SiO (J = 1-0 and J = 2-1) lines. So the number of clouds is nine in this thesis while that of Greaves et al. (1992) is seven. Some of these absorption features are also seen in other atomic and molecular line mapping observations; HI; Burton and Liszt 1980, H_2CO; Whiteoak and Gardner 1979, Bieging et al. 1980, OH; Cohen and Few 1976, CO; Bania 1977, Bally et al. 1987. By using these data, the observed velocity components are thought to belong to the following diffuse molecular clouds.

(l) 22 km/s feature:

The positions of this cloud is unknown. The absorption lines of the SO(J_N = 3_2-2_1), SiO (J = 1-0 and J = 2-1), NH_3, and HC_3N are not detected, because of disturbance due to strong and broad emission lines belonging to Sgr B2 itself. On the other hand, the $H^{13}CO^+$ and ^{13}CN lines show strong absorption features, and other lines such as CS, HCN, HNC, NH_3, and CH_3OH show weak absorption features. The HNC line is weakly observed with narrow line width. The $C^{32}S$ (J = 1-0) line is also weakly detected with broad velocity width. On the other hand, the $C^{32}S$ (J = 2-1) line has strong absorption with narrow width. Therefore, this velocity component has high density region with small velocity range and the low density outer region. Similar result is found in the $C^{34}S$ (J = 2-1 and J = 1-0) lines. The ^{13}CO (J = 1-0) emission maps by Bally et al. (1988) show a ring structure at this velocity around the Sgr B2 directions where only weak emission is seen. They concluded that it was unlikely that ^{13}CO emission was absorbed by cold gas, and hence that there was a genuine absence of material. However, according to Fig.

8d, ^{12}CO line is seen in absorption at this velocity. On the other hand, the ^{12}CO line is seen in emission at other velocities. According to this, the +22 km/s cloud is thought to be slightly lower than the average density of other clouds. Furthermore, this line has broad velocity width, presumably due to a mixture of two velocity components as mentioned before.

(2) 3 km/s feature:

This absorbing cloud spreads widely according to the H_2CO survey observation by Whiteoak and Gardner (1979). It is also recognized by other molecular mapping observations (e.g., HI; Rouger and Oort 1960, Burton and Liszt 1978, Liszt and Burton 1980, OH; Cohen and Few 1976, CO; Scoville, Solomon, and Penzias 1975, Liszt et al. 1977, Bania 1977, Bally et al. 1987, NH_3; Kaifu et al. 1973). These observations indicate that this cloud is lying at a distance of a few hundred pc from the sun, and may have several velocity components. However, we assume that this cloud has one component in this thesis, since it is difficult to resolve individual components.

This component corresponds to one of the most strongest absorption feature of the observed lines, and is observed for the most molecular species up to HC_5N. The CO line at this velocity shows the mixed line profile with the +3 km/s velocity component and the Sgr B2 itself. The $H^{12}CN$ and $H^{13}CN$ lines have strong absorption. The +3 km/s velocity component of the $H^{13}CN$ line can be distinguished from other velocity components, however, the $H^{12}CN$ line can not. The $H^{12}CN$ molecule may be much abundant but become optically thick, since the $H^{13}CN$ line is shown strong absorption. Similarly, the $HN^{13}C$, $C^{32}S$ (J = 2-1, J = 1-0), HC_3N (J = 4-3, J = 5-4), C_3H_2, and CH_3OH lines are observed strongly with wide velocity width. The C_3H_2 and CH_3OH lines may be a mixture of two velocity components. On the other hand, the $H^{12}CN$, SiO (J = 1-0 and J = 2-1) lines show strong and flat bottomed line profile. Thus, these lines may become optically thick. In contrast, the $H^{13}CO^+$ line shows narrow width, although it is fairly strong. Therefore, this molecule is confined within a narrow velocity region.

The NH_3 lines are detected in absorption up to J,K = 7,7-7,7, and the HC_3N lines are up to J = 5-4. Such high excitation transitions are not observed at other velocity components. Thus, the gas kinetic temperature of this velocity component may be higher than the other velocity components. It will be determined qualitatively in section 4.2.

(3) -20 and -28 km/s features:

These two components are identified by other molecular mapping observations as in t e case of the +3 km/s velocity components (e.g., HI; Menon and Ciotti 1970, Burton and Liszt 1978, Liszt and Burton 1980, CO; Liszt, Sanders, and Burton 1975, Liszt et al. 1977). Especially, the HCO^+ line shows absorption line profile at these two velocity towards Sgr A (Linke et al. 1981). It is thought that these two features may be due to the 4.5 kpc arm from the Galactic center according to these observations. Since the molecules at the central part of the arm are more highly excited than those of the near and far sides of the arm, absorption lines at the central part are weaker than those of the side of the arm. Consequently, two absorption corresponding to the side of the arm are seen.

The ^{12}CO and ^{13}CO lines may have complex line profiles, as shown Fig. 8d. On the other hand, the $C^{32}S$ (J = 1-0, J = 2-1), and C_3H_2 ($2_{1,2}$-$1_{0,1}$) lines show in strong absorption line profiles. The $C^{18}O$ (J = 1-0), $C^{34}S$ (J = 1-0), ^{28}SiO (J = 1-0), $H^{13}CN$ (J = 1-0), NH_3 (J,K = 1,1-1,1, 2,2-2,2), and HC_3N (J = 4-3) lines have weak absorption. The $C^{32}S$ (J = 2-1) line has different intensities between these two velocity components. Similar tendencies are seen for the $C^{34}S$ (J = 1-0) line. On the other hand, the line intensities of $C^{32}S$ (J = 1-0), $H^{13}CN$, C_3H_2 are seen in similar intensities. This reason may result from these clouds are located before and behind the shock, since the expanding arm moves with supersonic velocity. The detailed discussion will be described in chapter 6. Other lines which are not given above were not observed at these two velocities.

(4) -42 and -46 km/s features:

These two components are reported in other molecular mapping observations as in the case of the +3 km/s feature (e.g., HI; Rouger and Oort 1960, Burton and Liszt 1978, Liszt and Burton 1980, OH; Cohen and Few 1976, CO; Scoville, Solomon, and Jefferts 1974, Liszt et al. 1977, Bania 1977, Bally et al. 1987, NH_3; Kaifu et al. 1973). It is thought that these clouds are lying in the expanding arm with about 3 kpc distance from the Galactic center according to these observations.

The ^{13}CO line may have self-absorption belonging to the -42 km/s velocity component, as shown in Fig. 8d. However, since the ^{12}CO line does not have self-absorption, the dump of the ^{13}CO line may not be self-absorption. On the other hand, the $H^{12}CN$ (J = 1-0) and ^{12}CN (N = 1-0) lines show strong absorption with flat-bottomed line profiles. The SO ($J_N = 3_2$-2_1), $C^{32}S$ (J = 1-0 and J = 2-1), $C^{34}S$ (J = 1-0), C_3H_2 ($2_{1,2}$-$1_{0,1}$), and $H^{13}CO^+$ (J = 1-0) lines are observed with strong

and clearly discrete two absorption line profiles. The $H^{13}CN$ (J = 1-0), and NH_3 (J,K = 1,1-1,1) lines are impossible to be resolved into two velocity components. And ^{13}CN (N = 1-0), CH_3OH, and ^{28}SiO (J = 1-0) lines are weakly detected. As similar with the -20 and -28 km/s features, the $C^{32}S$ (J = 1-0 and J = 2-1), $C^{34}S$ (J = 1-0), C_3H_2 ($2_{1,2}$-$1_{0,1}$), $H^{13}CO^+$ (J = 1-0) lines at -42 km/s velocity component have strong absorption with narrow width. However, those at -46 km/s have slightly weak absorption with wide line widths. On the other hand, the characteristic of the SO line is that the internal velocity widths at these velocity components are narrow (5 ~ 8 km/s), but similar intensities. Other molecules are not detected.

(5) -76, -92, and -105 km/s features:

It is thought that these three components may be lie in the nuclear disk within about 1 kpc radius nearby the Galactic center. Therefore, we consider these velocity components as diffuse molecular clouds near the center of our Galaxy. On the other hand, the observed features except for -76, -92, and -105 km/s features are thought to correspond to diffuse molecular clouds outside the Galactic center. This nuclear disk consists of a large amount of gas and dust, which has non-circular motion (Bania 1977, Liszt and Burton 1978, Bally et al. 1988). The physical conditions of the gas in the galactic center clouds are very different from those in the disk at a few kpc from the center, which has higher density (> 10^4 cm^{-3}) observed by CS rotational lines (Bally et al. 1987) and higher gas kinetic temperature (> 60 K) according to the results derived using NH_3 and CH_3CN observations (Güsten et al. 1985). And the galactic center clouds are located in an environment where cosmic ray, magnetic field, and UV flux are high.

The -105 km/s feature shows the strongest absorption next to the +3 km/s feature for the most of the observed absorption lines. The ^{13}CN line is weakly detected, but other lines have been observed with strong absorption features. Especially, the ^{28}SiO (J = 1-0), $C^{32}S$ (J = 1-0 and J = 2-1), $H^{13}CO^+$, NH_3 lines were observed intensely. The $C^{32}S$ (J = 1-0 and J = 2-1), $H^{13}CO^+$ lines are observed with wide velocity width. The $H^{13}CO^+$ line may be a mixture of two velocity components. The peaks of NH_3 (J,K = 1,1-1,1, 2,2-2,2) are located between -105 and -92 km/s. These lines have non-Gaussian and asymmetric line profiles. The $HN^{13}C$, and HC_3N J = 4-3 lines are weakly detected.

The -92 km/s feature has slightly weaker absorption than the -105 km/s feature, and some of molecules are difficult to distinguish it from the -105 km/s feature. This tendency is seen for the SiO (J = 1-0 and J = 2-1), CS (J = 1-0 and J

= 2-1), $H^{13}CN$, C_3H_2 ($2_{1,2}$-$1_{0,1}$), NH_3 (J,K = 1,1-1,1, 2,2-2,2, and 3,3-3,3) and ^{13}CN. Only the ^{28}SiO (J = 1-0) line shows stronger line profile than the -105 km/s.

For the -76 km/s velocity component, all molecular absorption lines are weak and narrow except the $C^{32}S$ (J = 1-0 and J = 2-1), C_3H_2 ($2_{1,2}$-$1_{0,1}$) lines that gives fairly strong features. The ^{13}CN and NH_3 (J,K = 1,1-1,1, 2,2-2,2, and 3,3-3,3) lines at this velocity component are weakly detected, and other lines are not observed.

The $C^{34}S$ lines at these velocity components are not detected. However, other velocity components are seen in strong absorption, and the $C^{32}S$ (J = 1-0 and J = 2-1) lines at -76, -92, and -105 km/s have strong absorption features. The discussion on this will be given in section 6.3.2.

The most prominent features are that the ^{12}CN, $H^{12}CN$, $H^{12}CO^+$ lines show flat bottomed profiles with very wide line width in Figure 8c, indicating that these molecular lines are optically thick ($\tau \sim 1$-2) in the wide velocity range of the diffuse molecular clouds. The optical depth for each velocity component is the same. This means that the excitation temperature (Tex) of each cloud is almost same. On the other hand, other molecular absorption lines have narrow line width. This indicates these molecules are confined in narrow velocity range. Moreover, the line profiles in one velocity component are different from one species to another. Especially, the CS (J = 2-1), $H^{13}CN$ (J = 1-0), and $H^{13}CO^+$ (J = 1-0) lines show different line profiles, although they have nearly the same upper-state energy levels. Therefore, an origin of the differences in the line profiles may be due to the different abundance rather than due to the different excitation condition.

The intensities of the ^{13}CN and $H^{13}CO^+$ lines at +22 km/s are stronger than those of the ^{12}CN and $H^{12}CO^+$ lines. The reason may be the influence of the emission line belonging to the Sgr B2 itself. On the other hand, the intensities of the $H^{13}CN$ line at +3 km/s and the $H^{13}CO^+$ line at +3 and -42 km/s are also stronger than those of the $H^{12}CN$ and $H^{12}CO^+$ lines. The reason may be result from the error of the removing baselines. This will be discussed in detail in section 5.2.

The observed brightness temperatures and the velocity widths are listed in Table 3 and Table 4, respectively. The error of brightness temperatures were estimated from the r.m.s. noise temperatures in both side of the lines. The velocity widths were determined by assuming Gaussian line profiles (half-power line width). Since some of lines are not expressed by a Gaussian profile because of overlapping of several velocity components, those line widths may have larger

error. Determination of molecular column densities will be discussed in Chapter 5.

Chapter 4. Physical Properties of the Observed Diffuse Molecular Clouds

4.1. Introduction

In this chapter, we argue some physical properties of the diffuse molecular clouds.

Generally, line intensities of various molecules are used to derive their physical conditions such as kinetic temperatures, molecular hydrogen densities, and other properties of the clouds. Inversion transitions of ammonia and the ^{12}CO (J = 1-0) and ^{13}CO (J = 1-0) transitions are used for determinations of gas kinetic temperature. Numerical calculations based on the large-velocity-gradient (LVG) approximation are used for determination of molecular hydrogen density and fractional abundance of molecules per unit velocity gradient from the observed SiO, CS transitions.

Physical properties determined in this chapter are average value of the line-of-sight. In the diffuse molecular clouds, there may also be contamination of higher density or lower density regions. However, the density variation in diffuse molecular clouds is smaller than that in dense molecular cloud, that is, it is spread by one-to-two order magnitude in the region from a few pc to a few tens pc. On the other hand, that of the dense molecular clouds is spread by three order of magnitude in the region from 0.1 pc to 0.01 pc.

If the observed line is optically thin, the line intensity is proportional to ($T_{bg}+T_C-T_{ex}$), where T_{bg} is the brightness temperature of the cosmic background radiation, T_C is the brightness temperature of the background continuum source Sgr B2, and T_{ex} is the excitation temperature of the molecular line. If a cloud has relatively higher density, T_{ex} becomes larger and approach to ($T_{bg}+T_C$), and the absorption line intensity becomes weaker. Therefore, the excitation temperature of higher density region in the diffuse molecular clouds is closer continuum level. Thus, the contamination from the higher density region is small. Furthermore, since only diatomic molecular lines are detected in optical, polyatomic molecules, may not be produced in lower density region. The effect of the contamination from higher or lower density region seems to be small. The determination of the gas kinetic temperatures of diffuse molecular clouds will be described in section 4.2. Section 4.3 will describe determination of molecular hydrogen densities of diffuse molecular clouds. Finally, section 4.4 will describe summary of this chapter.

4.2. Determination of Gas Kinetic Temperature of the Observed Diffuse Molecular Clouds

4.2.1. Determination of Gas Kinetic Temperature using the NH_3 Lines

Firstly, we determined the gas kinetic temperatures by using the NH_3 lines, assuming that an uniform NH_3 gas is lying in front of continuum source Sgr B2. Since the NH_3 lines are observed in absorption, we used T_{mb} (brightness temperature of molecular absorption line), which corresponds to the bottom brightness temperature of absorption lines, instead of the brightness temperature of emission line T_B. The absorption lines may arise at several velocity components along the line-of-sight. According to the wide survey observation such as Whiteoak and Gardner (1979), each velocity component become strong at one region except for the +3 km/s velocity component, which may arise at several velocity components. Therefore, we treat each absorption line as one diffuse molecular cloud, so the derived physical parameters are the mean values over the substructures within the line-of-sight.

Because transitions between the metastable inversion doublets are usually much faster than those to other rotational states with different K-values, they can be approximated as a two-level system. Then, if the brightness temperatures T_{mb} of $NH_3(1,1)$ and $NH_3(2,2)$ are known, the rotational temperature $T_R(2,2;1,1)$ is given by

$$T_R(2,2;1,1) = \frac{-41.5}{\ln\left(\frac{-0.282}{\tau_m(1,1)}\ln\left[1-\frac{T_{mb}(1,1)}{T_{mb}(2,2)}\{1-\exp(-\tau_m(1,1))\}\right]\right)}, \quad (1)$$

where T_{mb} is the brightness temperature of the NH_3 absorption lines and $\tau_m(1,1)$ is the optical depth of $NH_3(1,1)$ (see Appendix A.3).

The brightness temperature T_{mb} is given by,

$$T_{mb} = T_A^*/\eta, \quad (2)$$

where T_A^* is the antenna temperature of the NH_3 absorption lines and η is the beam efficiency (0.45).

If $T_{mb}(1,1)$, $T_{mb}(2,2)$ and $\tau_m(1,1)$ are given, $T_R(2,2;1,1)$ is determined from eq. (1). Because of large transition probabilities of the downward relaxation in the nonmetastable states and the small collisional coupling between K-ladders, the metastable populations may resemble a Boltzman distribution. Thus, as shown by Ho and Townes (1983), T_R is a good indicator of the gas kinetic temperature Tk. Martin et al. (1982) show that the rotational temperature T_R derived from NH_3 is a well correlate with the kinetic temperature Tk derived from CO with similar angular resolutions toward a variety of regions. Walmsley and Ungerechts (1983) have performed statistical equilibrium calculations demonstrating that, after corrections for the depopulation effects, the NH_3 and CO temperatures are in good agreement.

The radiative transfer equation is given by

$$T_{mb}(1,1) = \{J(Tex)-T_C^{BG}-J(Tbg)\}\{1-\exp(-\tau_m(1,1))\}, \quad (3)$$

where Tex is the excitation temperature of NH_3, Tbg is the brightness temperature of the cosmic background radiation, and T_C^{BG} ($=T_{cont}/\eta$) is the observed specific intensity of the background continuum source Sgr B2. J(T) is the Planck function ($J(T) = (h\nu/k)\{\exp(h\nu/kT)-1\}^{-1}$), h is the Planck constant, k is the Boltzmann constant, and ν is the molecular transition frequency.

If the excitation temperature Tex of diffuse molecular clouds is equal to Tbg, the brightness temperature is transformed to

$$T_{mb}(1,1) = -T_C^{BG}\{1-\exp(-\tau_m(1,1))\},$$

$$= -T_C^{BG}\tau_m(1,1). \quad (4)$$

If the NH_3 line is optically thin, the optical depth $\tau_m(1,1)$ is given by

$$\tau_m(1,1) = -(1-\frac{T_{mb}(1,1)}{T_C^{BG}}),$$

$$= -\frac{T_{mb}(1,1)}{T_C^{BG}}. \quad (5)$$

We used the data of $T_{mb}(1,1)$ and $T_{mb}(2,2)$ of the NH_3 lines obtained by

Ohishi et al. (1995) in this thesis. The continuum brightness temperature T_c^{BG} is referred to Akabane et al. (1988), who used Bonn 100-m telescope. However, the beam size of the continuum observation is 42" (Bonn 100-m telescope), that is different from that of the NH_3 line observation, 80" (NRO 45-m telescope). Therefore, we corrected the continuum brightness temperature to the same beam size of the line data as follows: We assume the continuum source is a point source judging from the VLA observation, which shows this continuum brightness temperature is radiated from the very small source (2"×2" at 22 GHz; Vögel, Genzel, and Palmer 1987).

If the continuum source is a point source, the antenna temperature is given by

$$T_A^* = \frac{1}{2k} P_n A e S_\nu. \tag{6}$$

where S_ν is the flux density received by the antenna and Ae is the effective area of the antenna. P_n is the weight considering the Gaussian beam. Thus, the antenna temperatures of the telescope with the different beam size (40", 80") are given by

$$T_A^*(40") = \frac{1}{2k} P_n A e S_\nu, \tag{7}$$

and

$$T_A^*(80") = \frac{1}{2k} P_n' \ Ae' \ S_\nu'. \tag{8}$$

Even if the beam size is different, the flux density in each beam size, S_ν and S_ν', have the same value. If the continuum brightness temperature at 40" is given, then the equation (7) and (8) yield,

$$T_A^*(80") = \frac{P_n' \ Ae'}{P_n \ Ae} T_A^*(40"). \tag{9}$$

Assuming that the aperture efficiencies η and η' are constant, the equation (9) is transformed to

$$T_B(80") = \frac{P_n' \ Ae'}{P_n \ Ae} T_B(40"). \tag{10}$$

According to Akabane et al. (1988), the continuum brightness temperature at 22 GHz (40") was 14.52 K. However, the temperature corrected by this method was 11.0 K (Table 5). The error (0.3 K) mainly originates from the error of the observed continuum brightness temperature. Although the real continuum size is 2"×2", we assumed the continuum source is a point source. The error due to this assumption is 3/100 of the continuum brightness temperatures. This value is comparable to the original error of the observed brightness temperature.

The rotational temperatures $T_R(2,2;1,1)$ derived using the NH_3 absorption lines range from 26K to 30 K, as listed in Table 6. When the continuum brightness temperature Tc changes 1 K, the optical depth τ_m of the absorption lines changes only 0.01. As shown in Table 5, the r.m.s. noise of the continuum brightness temperature is 0.3 K. Therefore, the error of the rotational temperature due to the error of the continuum brightness temperature is less than 0.01 K. The absorption lines used in this thesis were observed with good S/N ratio (r.m.s. noise temperature is 0.4 K). Therefore, the error contributed by the inspection of the baseline and the reading error of the bottom of the absorption lines are small. Thus, the total error of the rotational temperature is estimated to be 3 K, originating from $T_{mb}(1,1)/T_{mb}(2,2)$ calculation. When we consider total errors synthetically, it is concluded that the rotational temperature of each diffuse molecular cloud is presumably not different very much.

Bartla et al. (1984) derived the rotational temperature of $T_R(2,2;1,1) = 20 \sim 30$ K using the $NH_3(1,1)$ (2,2) absorption lines towards the Cas A (The absorption lines seem to be due to the Orion arm and the Perseus arm). The values are similar to the present results (24 ~ 30 K), although absorbing regions are different from those in the present observation.

Tieftrunk et al. (1994) derived the (1,1), (2,2) rotational temperature from the $NH_3(1,1)$ (2,2) absorption lines towards the Sgr B2 using the Effelsberg 100-m telescope. They derived $T_R(2,2;1,1) = 35 \pm 2$ K for the -10 to 20 km/s velocity component, and $T_R(2,2;1,1) = 26 \pm 3$ K for the -95 to -105 km/s velocity component. These values are not contradict with our results. However, they estimated the kinetic temperatures $T_K = 60 \pm 10$ K for the -10 to 20 km/s velocity component and 35 ± 5 K for the -95 to -105 km/s velocity component, respectively, on the base of the results given in Fig. 1 of Danby et al. (1988), who derived the relationship between the rotational temperature and the kinetic temperature, assuming the molecular hydrogen density of $n(H_2) = 10^5$ cm^{-3}. Such high molecular density is not plausible in the diffuse molecular clouds, although

Danby et al. (1988) insist that the results are not very sensitive to the cloud density. However, in a low density region such a diffuse molecular cloud, since the high energy levels of ammonia are not populated, the kinetic temperature becomes nearly close to the rotational temperature between J,K = 1,1 and 2,2.

The difference between the rotational temperature and the kinetic temperature is smaller than the total error of the rotational temperature. Therefore, we used the rotational temperatures derived in this section as a kinetic temperature.

4.2.2. Determination of Gas Kinetic Temperature using the CO Lines

The kinetic temperatures Tk of the observed diffuse molecular clouds are also derived using the ^{12}CO emission lines, whose brightness temperatures are listed in Table 7. Assuming that the emission of CO is radiated from a uniform cloud in front of the Sgr B2, the observed brightness temperature T_B is given as follows (A.3.1),

$$T_B(CO) = \{J(Tex)-T_C^{BG}-J(Tbg)\}\{1-\exp(-\tau_m(1,1))\}. \quad (11)$$

Assuming that the line is optically thick and completely thermalized by frequent collision with H_2, the kinetic temperature (Tk) of diffuse molecular clouds is thought to be equal to the excitation temperature (Tk = Tex).

The data of Lis (1989) are used for the brightness temperatures of the CO lines. The background continuum temperature is assumed to be 2.7 K. The continuum brightness temperature at the beam size 30" is used in this thesis, since there are no data of the continuum brightness temperature over the 115 GHz at the beam size 42", which is the same beam size as the CO observations of FCRAO 14 m telescope. We used the continuum brightness temperatures of Lis (1989) at 231 GHz and that of Salter et al. (1989) at 90 GHz. By the same method as in the case of the NH_3 absorption lines, the continuum brightness temperature obtained at beam size 30" was 13.2 K. The temperature corrected to 40" beam size was 12.1 K, as listed in Table 5. The error of this value comes mainly from the data of Lis (1989), who reported 105 ± 26 Jy.

We considered whether the assumption that the ^{12}CO J = 1-0 line is optically thick is correct. The optical depth of ^{12}CO was determined from the ^{12}CO J = 1-0 and ^{13}CO J = 1-0 observations of Lis (1989) assuming the same excitation temperature for both isotopic species and the terrestrial abundance ratio of

$[^{12}C]/[^{13}C] = 90$. The determined optical depth of each cloud is listed in Table 7, and it is apparent that the ^{12}CO molecules in all clouds are optically thick. Real $^{12}C/^{13}C$ ratio may be smaller than the value which is used in this thesis (for example, $^{12}C/^{13}C$ at Sgr B2 is 28; Gomez-Gonzalez et al. 1986). Therefore, real optical depths may be slightly smaller by a factor 1-2 than the present results. We will discuss whether the ^{12}CO lines are thermalized or not in section 4.3 after the molecular hydrogen densities are derived.

By using eq. (11), the kinetic temperatures of the observed diffuse molecular clouds are derived to be 12.7 ~ 13.7 K, as listed in Table 7. The errors in these kinetic temperatures originate from the errors in the brightness temperature of the background continuum and the brightness temperature of the CO emission lines. The error (1σ r.m.s.) due to the brightness temperature of the CO line is about 0.1 K. However, the continuum brightness temperature accompany a large error, as described before. In the case of the NH_3 lines, the contribution of the continuum brightness temperature is small, since the NH_3 lines are optically thin. Therefore, the error of the continuum brightness temperature is multiplied by the optical depth (τ_m). Since the CO lines are optically thick, the error of the continuum brightness temperature directly affects the gas kinetic temperature. The error of the continuum brightness temperature at 115 GHz is 2.3 K. Therefore, the total error of that is about 2.4 K. When considering this total error, the gas kinetic temperature of each diffuse molecular cloud is presumably not different.

We compare the kinetic temperatures derived using CO with the rotational temperatures derived using NH_3. The result is shown in Fig. 9. No apparent positive correlation is shown, and the kinetic temperature derived from ^{12}CO lines are lower than the rotational temperature from NH_3 lines by about 10 K. One reason is, in the present analysis, we assume the CO has no self-absorption. However, the ^{12}CO line is presumably self-absorbed, since it already becomes optically thick. Indeed, the +22 km/s velocity component shows a strong absorption by ^{12}CO itself. Since ^{12}CO is observed as an emission line, the higher density region than the diffuse molecular clouds influences the determination of kinetic temperature. However, such region is not spread widely and beam filling factor of the telescope may be smaller than 1. The influence of the beam filling factor on this results will be discussed in section 6.2.

As a result, we will use the rotational temperature derived from the NH_3 lines as a gas kinetic temperature of the observed diffuse molecular clouds.

4.3. Determination of Molecular Hydrogen Density of Diffuse Molecular Clouds

The molecular hydrogen density ($n(H_2)$) of the diffuse molecular clouds are determined from the $C^{32}S$ (J = 1-0, J = 2-1) and ^{28}SiO (J = 1-0, J = 2-1) absorption lines using the large velocity gradient (LVG) model approximation (Goldreich and Kwan 1974; Scoville and Solomon 1974; see Appendix A.4).

4.3.1. Determination of Molecular Hydrogen Density using the CS Lines

Firstly, we used the CS lines in order to determine the molecular hydrogen densities. Observed parameters of these molecular absorption lines are listed in Table 3 and Table 4. We used the continuum brightness temperature at 49 GHz determined from the Nobeyama 45-m telescope observation of Akabane et al. (1988) (Table 5; 4.5K at beam size 43") and that at 98 GHz determined from the observation at 90 GHz of Salter et al. (1989) (Table 5; 5.8K at beam size 30"). It is noted that the beam size at 98 GHz is different from that at 49 GHz. However, the absorption profile is naturally weighted according to the spatial distribution of the background continuum, which may be similar at 49 GHz and 98 GHz. Therefore, the difference in beam sizes presumably do not influence the determination of excitation temperature and optical depth.

If we assume a simple case of a uniform molecular cloud (CS) lying in front of a continuum source, the brightness temperature is given as followed by the eq. (3).

Here we assume as follows:

(1) Absorbing cloud lies wholly in front of the continuum source.

(2) No emitting cloud lies in the line-of-sight.

(3) Since a source coupling factor is not known, we assume it as unity.

Large velocity gradient (LVG) model calculations are performed using the CS J = 1-0 and J = 2-1 lines. We used the value of Green and Chapman (1978) for the collisional cross sections with the hydrogen molecule. The gas kinetic temperature was assumed to be 28 K, which is the average rotational temperature derived using the NH_3 (1,1) and (2,2) lines, as described in section 4.2.1. The velocity widths ΔV used in this calculation are listed in Table 4. The optical depth and the excitation temperature for the CS J = 1-0 line are calculated against molecular hydrogen density and column density of CS per velocity width. The

results are shown in Fig. 10a. The solid lines indicate the optical depths of the CS molecules. On the other hand, the dashed lines are the excitation temperatures. The possible solutions for each velocity component are shown in Fig. 10b. Similar results for the CS J = 2-1 lines are shown in Fig. 10c and Fig. 10d. Table 8 lists the determined molecular hydrogen densities and the column densities of CS in the observed diffuse molecular clouds .

As a result, the molecular hydrogen densities ($n(H_2)$) of the diffuse molecular clouds are found between 10^2 and 10^3 cm^{-3}. The value of the +22 km/s velocity component is not derived, since the emission line belonging to the Sgr B2 itself is strong. Errors of these results are estimated by changing the brightness temperatures and the velocity widths of the CS lines. The average of molecular hydrogen density is 1.6×10^2 cm^{-3}; those of the +3 km/s and -105 km/s velocity components may be slightly higher, and those of -20 and -28 km/s velocity components may be slightly lower. However, when considering possible errors in the brightness temperature and velocity width, the difference in the molecular hydrogen densities of diffuse molecular clouds are presumably not large. The molecular hydrogen densities obtained in this thesis are consistent with those ($n(H_2) \leqq 2\times10^2$ cm^{-3} assuming Tk = 10 K) reported by Miyawaki et al. (1989) within a factor of 2 for most of the source, although absorbing gas is in different region from our observation. The present values $(1 \sim 3)\times10^2$ cm^{-3} are slightly smaller than that of Greaves et al. (1992) who reported $n(H_2) = 1\times10^3 cm^{-3}$ from the CS observations. However, when considering the error of our data and Greaves et al. (1992), our data do not contradict of the results of Greaves et al. (1992). The kinetic temperature derived from the ^{12}CO lines is lower than that determined by NH_3 by 10 K. It is important to estimate the influence of kinetic temperature on the large-velocity gradient model calculation. When the same model calculation is carried out by assuming Tk = 13 K, it is found that the molecular hydrogen density becomes higher by 1.5 ~ 2 factor, and the abundance of CS becomes lower by 1.5 ~ 2, compared with the case of Tk = 28 K.

4.3.2. Determination of Molecular Hydrogen Density using the SiO Lines

The SiO lines are also used to calculate the molecular hydrogen densities and column densities of SiO molecules using the LVG method in order to compare the result with the molecular hydrogen densities derived using the CS lines. Observed parameters of these molecular absorption lines are listed in Table 3 and Table 4.

Since the SiO J = 1-0 lines of the +22 and -76 km/s and the J = 2-1 lines of the +22, -20, -28, -42, -46, and -76 km/s velocity components are not detected, LVG calculations are carried out only for the +3, -92, and -105 km/s velocity components. The collisional cross sections with the hydrogen molecule are not known for SiO. Therefore, we used the value of CS molecule instead of SiO (Green and Chapman 1978), because it has a nearly similar dipole moment (3.1 for SiO and 2.0 for CS) and similar molecular weights (both 44 for $^{28}Si^{16}O$ and $^{12}C^{32}S$). The results are shown in Fig. 11a ~ 11d with the similar presentation as the CS lines (Fig. 10a ~ 10d), and the derived parameters are listed in Table 9. We estimated the error of this results by changing the brightness temperature and velocity widths of the SiO lines, and found the nearly similar results with CS. The average molecular hydrogen density is $10^{2.3}$ cm^{-3}. We did not find a large density variation in the observed diffuse molecular clouds.

Then, we correlated the molecular hydrogen densities derived from the SiO lines with those from CS. The result is shown in Fig. 12. This is likely well correlated. This suggests that which the molecular lines used do not affect the results.

4.4. Summary of Chapter 4.

(1) The gas kinetic temperatures of the diffuse molecular clouds were derived using ^{12}CO emission lines and NH_3 absorption lines. The kinetic temperatures determined by ^{12}CO are 12.7 ~ 13.7 K, and the rotational temperatures determined by NH_3 are 24 ~ 30 K. The difference may be caused by self-absorption of the CO molecule and/or the fact that in the case of the ^{12}CO emission line, the higher density region in the diffuse molecular clouds influences the determination of the kinetic temperature of CO. Therefore, we used the data derived from the NH_3 lines.

(2) The molecular hydrogen density ($n(H_2)$) of each diffuse molecular cloud is determined from ^{28}SiO J = 1-0, J = 2-1 and $C^{32}S$ J = 1-0, J = 2-1 data using the large velocity gradient (LVG) model approximation. The densities lie between 1×10^2 and 4×10^2 cm^{-3}.

(3) The differences in the gas kinetic temperature and in the hydrogen density among clouds are not recognized within the error limit.

Chapter 5. Chemical properties of Diffuse Molecular Clouds

5.1. Introduction

In this chapter, we will derive chemical abundances of observed molecules in the diffuse molecular clouds, and compare those one another and consider possible relationship between the physical and chemical properties of individual clouds.

Since in the calculations of column densities, there are errors arising from excitation temperatures, velocity widths, the line intensities, and continuum brightness temperatures, we first consider correlation in the molecular line intensities multiplied by line widths ($T_{mb}(X)\Delta V$) instead of the column densities. This method uses the relation that the column density of the molecule N(X) is proportional to $T_{mb}(X)\Delta V$ if molecular lines are optically thin. The error of this method may be smaller than that using molecular column densities, because the errors in the brightness temperature and the velocity widths contribute mainly to the result of correlation. Before using this method, we derived the optical depths to judge whether the molecular lines are optically thin. After we studied correlation of $T_{mb}(X)\Delta V$ among various molecules, we inspected the correlation in the column density for further confirmation.

Determinations of molecular column densities are described in section 5.2, where the optical depths and visual extinction will be also derived. The chemical characteristics of individual clouds is summarized in section 5.3. We will also compare the results with physical properties such as visual extinction, gas kinetic temperature, and molecular hydrogen density of individual clouds. The correlation of molecular abundances is presented in section 5.4. We will describe the results derived using $T_{mb}(X)\Delta V$ in section 5.4.1. The results of correlation between molecular column densities will be stated in section 5.4.2. Finally, section 5.5 will state the summary of Chapter 5.

5.2. Determination of Molecular Column Densities

First of all, we derived the optical depths of observed molecular lines.

Firstly, the estimation method as NH_3 lines in the chapter 4.2 is employed for each molecular line by assuming $T_{ex} = T_{bg}$. The optical depths derived using this method are in the range from 0.009 to 0.549, as listed in Table 10a. The uncertainties of these results come from the reading error of the brightness

temperature of lines and continuum brightness temperature, and are estimated in the range from 0.002 to 0.027.

Secondly, for molecules in which both main and isotopic species are observed, we derived the optical depth as follows: the radiative transfer equation for the main molecule and isotopic species are given by analogy with eq. (3) as,

$$T_{mb} = \{J(T_{ex})-T_c^{BG}-J(T_{bg})\}\{1-\exp(-\tau_m)\} \quad \text{for main species,} \qquad (12a)$$

and

$$T_{mb} = \{J(T_{ex})-T_c^{BG}-J(T_{bg})\}\{1-\exp(-d\tau_m)\} \quad \text{for isotope species,} \qquad (12b)$$

where d is an isotopic abundance ratio, which is assumed to be the same as the terrestrial value. We assume the same values for the observed specific intensities of the background continuum source Sgr B2, the brightness temperatures of the cosmic background radiation, and the excitation temperatures of molecular absorption lines of main and isotopic species ($T_c^{BG} = T'^{BG}_c$, $T_{bg} = T'_{bg}$ and $T_{ex} = T'_{ex}$), because observed frequencies of both species are close to each other. The results are listed in Table 10b. Changing T_{mb} of main and isotopic species by r.m.s. noise temperatures, the error of this method is estimated to be in the range from 0.1 to 2.0.

Thirdly, for CS and SiO molecules, the results from the large velocity gradient model calculation are also compared with the results derived in the former LTE calculation and isotopic method. These results and errors derived in section 4.3 are listed in Table 10c.

The optical depths derived from the LTE calculations are in good agreement with those from the LVG model calculations. This suggests that the simplifications and assumptions in the LVG model do not greatly affect the results. However, the results derived using main and isotopic species are not in agreement with those of LTE and LVG calculations. The disagreement comes presumably from the assumed isotope ratio and a procedure baselines of ^{13}CO, ^{12}CN, $H^{12}CN$, $HN^{12}C$, $H^{12}CO^+$. Indeed, judging from the line profiles of ^{12}CN, $H^{12}CN$, these lines possibly become optically thick. If the excitation temperature derived from the LVG calculation in Chapter 4 are used, in the case of optically thick, the brightness temperature of these lines become about 5 and 11.3 K of $H^{12}CN$ and ^{12}CN, respectively. However, the brightness temperatures in this thesis are 0.3 ~ 1.5 K. These values are lower than expected. If we assume T_{mb} of 5 K for $H^{12}CN$

and use $^{12}C/^{13}C = 28$ at the Sgr B2 from the data of Gomez-Gonzalez et al. (1986), the optical depths of $H^{12}CN$ and $H^{13}CN$ become 0.5 ~ 3.7 and 0.018 ~ 0.132. The optical depths of $H^{13}CN$ become consistent with the results derived from LTE calculation. Similarly, the removing of the baselines of the ^{13}CO, ^{12}CN, $HN^{12}C$, and $H^{12}CO^+$ lines may have large error. For $C^{32}S$ and $C^{34}S$, the optical depths derived using main and isotope are not consistent with those from other methods. The reason may be the isotope ratio used in this thesis are presumably different from real values. We used terrestrial abundance ratio as isotope ratio. However, Greaves et al. (1989) derived $^{32}S/^{34}S$ of these diffuse molecular clouds are 7 ~ 16. If these $^{32}S/^{34}S$ ratios are used, the optical depths of $C^{34}S$ become 0.02 ~ 0.08 and these results are in good agreement with those derived from the LTE and LVG calculations. In the case of SiO, the difference in isotope ratio may also be contributed. However, the $^{28}Si/^{29}Si$ ratio of diffuse molecular clouds are not known yet. Therefore, we used $^{28}Si/^{29}Si = 3.31395$ of main/isotope ratio derived from LTE calculation. As a result, the optical depths of ^{28}SiO and ^{29}SiO become 0.20 and 0.06, respectively. These values are consistent with those derived from other methods.

As a result, the optical depths derived from LTE method are consistent with those from LVG calculation and using main and isotope. After that, we will use the results derived from LTE calculations. The optical depths of $C^{18}O$, ^{13}CN, $C^{34}S$, SO, ^{28}SiO, $HN^{13}C$, $H^{13}CO^+$, NH_3, HC_3N, C_3H_2, and CH_3OH are in the range of 0.01 ~ 0.197, and found to be optically thin. On the other hand, that of the $H^{13}CN$ molecule is from 0.039 ~ 0.127 except for +3 km/s velocity component, which has a higher optical depth of 0.318, and this value is a little higher than other velocity components. On the other hand, those of $C^{32}S$ are in the range between 0.098 ~ 0.441. Therefore, these lines are found to be optically thick. Others, those of the ^{13}CO, ^{12}CN, $H^{12}CN$, $HN^{12}C$, and $H^{12}CO^+$ molecules are not determined accurately as mentioned before. From these results, the ^{12}CN, $H^{12}CN$, $C^{32}S$ lines are found to be optically thick.

We derive the column density (N) of observed molecule by using the following formula (see Appendix A.5),

$$N = \frac{\tau}{A} \exp(-Eu/Tex)\, Tex\, \frac{8\pi k\nu^2}{hc^2 g_J}\, Q_{rot}\Delta V, \qquad (13)$$

where A is the Einsein A coefficient, Eu is the energy of upper level, Tex is the excitation temperature, k is the Boltzmann constant, v is the transition frequency,

c is the light velocity, g_J is the rotational degeneracy ($g_J = 2J+1$), and Q_{rot} is the rotational partition function. Molecular constants of the observed molecules are listed in Table 11. The rotational partition function (Q_{rot}) is given by

$$Q_{rot} = \sum_J g_J \exp\left(-\frac{E_J}{kT_{ex}}\right). \qquad (14)$$

Since T_{ex} is low and approximate expression is not valid, each levels are summed up numerically with the contribution of a level becomes less than 0.1 % of the partition function. The rotational partition function of the CH_3OH molecule is estimated only for E-state, which is observed in this thesis, and when determining the column density, that of A-state is determined by multiplying with $\exp(-4.833/T_R)$. The column densities of NH_3 molecules are determined by the following equation proposed by Ungerechts, Walmsley, and Winnewisser (1986),

$$N_{JK}(NH_3) = \frac{3k\,J(J+1)\,\sqrt{\pi}}{8\pi^3\,\sqrt{\ln 2}\;|\,\mu\,|\,K^2\,\nu_{JK}}\,\Delta v \tau_{JK}^{tot}. \qquad (15)$$

The determined column densities are listed in Table 12. The errors come from the assumption of excitation temperatures and continuum temperatures, and factors due to velocity widths and line intensities. We used the average excitation temperature (3.9 K) derived from the LVG analysis of the CS lines. According to Table 8, the differences in excitation temperatures among the observed clouds are small except for +3 km/s (4.8 K). A change in the excitation temperature by 1 K causes a change in the column density of about 30 %. The errors of continuum temperatures and line intensities reflect to the errors of optical depths. The error of the optical depth in this thesis are less than 10 %. Large ambiguity in the determination of the column density comes from the line width, because some observed lines are overlapped each other. The total error in column density is thought to be with a factor 1.5 ~ 2.0.

When molecular lines are not detected, we used the r.m.s. noise temperatures as lower limit of the brightness temperatures of the observed molecules and average velocity widths of the other molecules as line velocity widths. The results are also included in Table 12. The discussion about its abundance of individual cloud will be described in section 5.3. And the results of correlation of molecular column densities will be presented in section 5.4.2.

According to Greaves et al. (1992), the column densities of CS, $C^{34}S$, ^{28}SiO,

$H^{13}CN$, $H^{13}CO^+$, and C_3H_2 are determined to be $0.1 \sim 4.4 \times 10^{13}$ cm^{-2}, $1.0 \sim 6.0 \times 10^{12}$ cm^{-2}, $0.5 \sim 1.3 \times 10^{13}$ cm^{-2}, $1.0 \sim 2.0 \times 10^{12}$ cm^{-2}, $0.1 \sim 0.5 \times 10^{13}$ cm^{-2}, and $0.1 \sim 1.0 \times 10^{13}$ cm^{-2}, respectively. Bartla et al. (1984) obtained the NH_3 column densities of the diffuse molecular clouds towards the Cas A. to be $N(NH_3) = 2.3 \sim 37.6 \times 10^{12}$ cm^{-2}. These values are consistent with our results, although the diffuse molecular clouds observed by Bartla et al. (1984) are different from ours.

We derived the ortho-to-para ratios of the C_3H_2 and NH_3 molecules to be 3:1 and 1:1, respectively. The error are less than 10 %. These ratios are the same as that in high temperature limit. We found the formation temperatures of these molecules do not contradict with the kinetic temperatures derived in section 4.2.

Finally, since the column densities of the $C^{18}O$ lines are obtained, the visual extinctions are also determined using the following formula,

$$Av = \frac{N(C^{18}O)}{(2.5 \pm 0.8) \times 10^{14}} + (1.1 \pm 0.5), \qquad (16)$$

which is the experience formula proposed by Duvert, Cernicharo, and Baundy (1986) for the 0 to $4 \sim 5$ mag range of visual extinction. The column densities of $C^{18}O$ are used from the data of Table 12. The $C^{18}O$ line is observed only at -20, -28, -42, -46 km/s velocity components. The determined visual extinction is in the range of $1.3 \sim 4.1$ mag, as listed in Table 14. The errors are mainly originated from the determination of column densities of $C^{18}O$, and are estimated to be in the range of $0.8 \sim 1.5$. Moreover, the visual extinctions of -76, -92, -105 km/s velocity components are determined using the ^{13}CO lines. The terrestrial abundance ratio of $[^{13}CO]/[C^{18}O]$ was used as a conversion factor.

5.3. Physical and Chemical Properties of Individual Features

The column densities of each velocity components are shown in Fig. 13a ~ 13c. The characteristic of each velocity component is as follows.

(1) +22 km/s feature

The molecular hydrogen density and temperature are not determined from the CS and SiO lines because these lines are disturbed by strong emission from the +62 km/s cloud belonging to the Sgr B2 itself. However, since the ^{12}CO line is observed as absorption, this velocity component may have lower density than other velocity components. Since all transitions of the $C^{32}S$, SO, ^{28}SiO, NH_3, and

HC_3N lines are also affected by the Sgr B2 itself, the upper limit of the column densities are estimated. Similarly, the upper limit of the column densities of the $C^{18}O$ and CH_3OH molecules are estimated, since these lines are not detected. On the other hand, column densities of the $C^{34}S$, $H^{13}CN$, $HN^{13}C$, and C_3H_2 molecules are found to be nearly similar with those at other clouds (9.3×10^{11} cm^{-2}, 8.5×10^{11} cm^{-2}, 7.5×10^{11} cm^{-2}, and 2.7×10^{11} cm^{-2}). $H^{13}CO^+$, and ^{13}CN abundances are an order of magnitude higher than those of other clouds (1.5×10^{13} cm^{-2}, 4.6×10^{13} cm^{-2}).

(2) +3 km/s feature

The $C^{18}O$ line is not detected. The column densities of other molecules at this velocity are 2 ~ 5 times higher than those of other clouds. Especially, those of the $H^{13}CN$, C_3H_2 are an order of magnitude higher than those of other clouds (3.5×10^{13} cm^{-2}, 4.6×10^{13} cm^{-2}). However, this velocity components may be the mixture of several clouds as described in chapter 3.

(3) -20 and -28 km/s features

The column densities of the SO, $HN^{13}C$, and CH_3OH molecules and the -28 km/s velocity component of $H^{13}CO^+$ are not determined, since these lines are not detected. However, the $C^{18}O$ lines is detected to give column density of 1.8×10^{14} cm^{-2} at -20 km/s velocity component and 9.5×10^{13} cm^{-2} at -20 km/s velocity component, respectively. The visual extinctions of -20, -28 km/s components may be slightly higher than those of +22 and +3 km/s features (1.8 mag at -20 km/s velocity component and 1.5 mag at -20 km/s velocity component). The molecular hydrogen densities at these velocity components are not different from those at other velocity components within the error. The column densities of the HC_3N molecules are determined from the data of J = 4-3 (9.3×10^{11} cm^{-2} at both velocity components), since this transition is only observed. The column density of the SiO molecules is also derived from the data of J = 1-0 transition (4.5×10^{12} cm^{-2} at both velocity components). Some of other molecules are correlated well with the column densities of the $C^{18}O$ molecules and visual extinction. The detailed discussion will be described later.

(4) -42 and -46 km/s features

The $C^{18}O$ lines at these velocity components are observed as strong absorption, and the column density of $C^{18}O$ is higher than those of other velocity components (7.6×10^{14} cm^{-2} at -42 km/s velocity component and 9.5×10^{13} cm^{-2} at

-46 km/s velocity component). Therefore, the visual extinction of these components are higher than other velocity components (4.1 mag at -42 km/s velocity component, and 2.4 mag at -46 km/s). The column densities of the SO, $C^{34}S$ and C_3H_2 molecules at -42, -46 km/s velocity component are higher than those of other clouds (10^{12} cm^{-2} and 5.0×10^{11} cm^{-2}, 1.7×10^{12} cm^{-2} and 1.3×10^{12} cm^{-2}, and 5.3×10^{12} cm^{-2} and 4.3×10^{12} cm^{-2}). On the other hand, the column densities of the ^{13}CN, ^{28}SiO, $H^{13}CN$, $H^{13}CO^+$ molecules are lower than those of other velocity components. The column density of the $HN^{13}C$ molecules are not determined, since these lines are not detected. The column densities of the $C^{34}S$ molecules are determined from the data of J = 1-0, since the $C^{34}S$ J = 2-1 lines are not observed. Similarly, the HC_3N molecular abundance at -46 km/s is determined from the data of J = 5-4. The lower limit of the HC_3N molecule at -42 km/s is nearly the same as that at -46 km/s (5.2×10^{12} cm^{-2} at -42 km/s velocity component and 4.3×10^{12} cm^{-2} at -46 km/s velocity component). Cox, Güsten and Henkel (1988) obtained the C_3H_2 column density of the diffuse molecular cloud (the 3 ~ 4 kpc expanding arm) toward the Sgr A, to be $N(C_3H_2) = 5\times10^{12}$ cm^{-2}. On the other hand, Link et al. (1981) derived $N(HCO^+) = 1.3\times10^{13}$ cm^{-2} towards the Sagittarius A. If we use the $^{12}C/^{13}C = 28$ at the Sgr B2 from the data of Gomez-Gonzalez et al. (1986), we obtain $N(H^{13}CO^+) = 6.5\times10^{11}$ cm^{-2}. This is consistent with our results.

(5) -76, -92, and -105 km/s features

The column densities of all observed molecules at -105 km/s velocity are higher than other clouds except for the +3 km/s velocity component. The reason will be discussed in sections 6.3. However, the column densities of the $C^{18}O$, $C^{34}S$, SO, and CH_3OH molecules are not determined, since these lines are not detected. Similarly, these lines are not observed at -76 and -92 km/s. Therefore, the visual extinctions are determined using the ^{13}CO lines, as stated before. The visual extinction of these velocity components are in the range of 1.3 ~ 1.4 mag. The column densities of observed molecules at the -76 and -92 km/s features are nearly similar with those at -20 ~ -46 km/s. Moreover, the molecular lines at -76 km/s are slightly weaker than those at -92 and -105 km/s. The column densities of the ^{28}SiO, $H^{13}CN$, and HC_3N molecules are not determined. Linke et al. (1981) derived the HCO^+ column density of the lines which are absorbing cloud towards the Sagittarius A. Using the galactic center value as the abundance ratio $^{12}CO/^{13}CO = 28$ as employed before, the $H^{13}CO^+$ column densities near the Galactic center (-76, -92, and -105 km/s) are $N(H^{13}CO^+) < 1.6\times10^{13}$ cm^{-2}. These

results are consistent with the present results.

We will consider the correlation of the column densities with the visual extinction. The results are shown in Fig. 14a ~ 14c. Here, those at +3, +22 km/s velocity components are not included, since the visual extinction at these velocity components are not determined. The column densities at -105 km/s velocity components are higher than other velocity components, the reason will be discussed in chapter 6.

The column densities of ^{13}CN, $H^{13}CN$, HC_3N, and NH_3 are small below 1.5 mag. However, these molecules reach the peak at 1.5 ~ 1.8 mag, and then decreased. On the other hand, those of SO, CH_3OH reach the peak at 2.5 ~ 4.5 mag. This tendency between column densities and visual extinction is shown in $C^{34}S$, and C_3H_2, although these molecules may be different from the SO, CH_3OH molecules. The visual extinction derived using the data of $C^{18}O$ in the range of 1.5 ~ 4.1 mag and from the data of ^{13}CO in the range of the below 1.5 mag. Therefore, there is a discontinuity between 1.5 ~ 4.1 mag and below 1.5 mag. The column densities of the $HN^{13}C$ molecule are determined only at +3, +22, and -105 km/s velocity components. The column densities of SiO are higher at clouds with extinction below 1.2 mag, although this molecule is not detected at -76 km/s velocity component (1.4 mag). Those of $H^{13}CO^+$ are determined only in the clouds with visual extinction mag. Only at 4 mag the $H^{13}CO^+$ column density is slightly higher than other velocity components.

From these results, observed species are classified into; (1) the column densities of ^{13}CN, $H^{13}CN$, HC_3N, and NH_3 are peak at 1.5 ~ 1.8 mag, and decreased with the increase of visual extinction. (2) those of the $C^{18}O$, SO, CH_3OH and possibly $C^{34}S$, and C_3H_2 molecules increase with visual extinction, and reach the peak at 2.5 ~ 4.5 mag. (3) those of the SiO, and $H^{13}CO^+$ molecules may have no relation with visual extinction. These results will be discussed in section 6.3.

5.4. Correlation of Molecular Lines

In order to clarify the chemical relation among molecules in the observed diffuse molecular clouds, we focus on the correlation of their column densities. However, in the case of the column density, the error of the excitation temperature, partition function, brightness temperature of molecular line, continuum brightness temperature, and the line widths influence the total error.

Therefore, the comparison of the column density or relative abundance ratio accompanies larger error, and these errors may hide correlation of molecular lines. Then, firstly we correlate molecular lines intensities multiplied by line widths. Secondly, we inspected correlation among molecular column densities in order to confirm these results.

5.4.1. Correlation of Molecular Line Intensities Multiplied by Velocity Widths

The molecular line intensities and velocity widths are listed in Table 3 and Table 4, respectively. Since this method is applicable if molecular lines are optically thin. Therefore, only optically thin molecular lines are used. When many transitions of one molecule are observed, the transition with the best S/N ratio is used. The values of $T_{mb}(X)\Delta V$ are listed in Table 13. The errors come from the reading errors of the brightness temperature and velocity width of each molecular line, and are in the range of 0.06 ~ 1.54 Kkm/s. These $T_{mb}(X)\Delta V$ are plotted each other, as shown in Fig. 15a ~ 15c. The values of ^{13}CN are correlated well with those of $H^{13}CN$ (Fig. 15a). The overall $[H^{13}CN]/[^{13}CN]$ ratio is ~ 4.65. Here, as mentioned in section 5.3, the column densities of $H^{13}CN$ and ^{13}CN at the +3 km/s velocity components and that of ^{13}CN at the +22 km/s velocity component have extraordinary larger than other velocity components. Therefore, these velocity components are not included. The abundance ratio of the ^{13}CN molecule and the $H^{13}CN$ molecule is similar among all observed clouds. Considering the excitation condition of the ^{13}CN and that of the $H^{13}CN$ are similar, this result is possibly not due to excitation but to the difference in chemical composition. It is possibly because the $T_{mb}\Delta V(H^{13}CN)/T_{mb}\Delta V(^{13}CN)$ abundance ratio is diluted by the bottom of the ^{13}CN line at the +3 km/s velocity component, and so the real abundance ratio seem to be larger. A similar positive correlation is found in the brightness temperatures of $C^{34}S$ and those of C_3H_2 (Fig. 15b). The +3 km/s velocity component is removed as in the case of Fig 15a. The overall $[C_3H_2]/[C^{34}S]$ ratio is ~ 3.39. However, the $C^{34}S$ lines near the center of our Galaxy (-76, -92, and -105 km/s) are not detected. On the other hand, those of outside the center of our Galaxy (+22, +3 -20, -28, -40, and -46 km/s) are observed. This suggests that the chemistry near the center of our Galaxy may be different from that of outside region. Such a tendency is firstly found in the present study. It will be discussed in section 6.3 again. On the other hand, the brightness temperatures multiplied by velocity widths of C_3H_2 shows no apparent

positive correlation with that of $H^{13}CN$ (Fig. 15c).

The correlation coefficients are calculated by the method described in Appendix A.6. In calculating these correlation coefficients, the +3 km/s velocity components and +22 km/s velocity components are not included. The reason is as follows: the $T_{mb}(X)\Delta V$ values of all molecules at the +3 km/s velocity components are much larger than those of other velocity components. Also, the value of +22 km/s velocity components of $H^{13}CN$ and ^{13}CN are large. We estimated the errors of these correlation coefficients by changing r.m.s. noise of the brightness temperatures and velocity widths within r.m.s. noise. We found that the errors of coefficients are in the range of 0.01 ~ 0.03. The calculated correlation coefficients are listed in Table 15, and shown in Fig. 16. According to these, correlation coefficients between ^{13}CN and $H^{13}CN$ is 0.93 and that of $C^{34}S$ and C_3H_2 is 0.83. These are shown in Fig. 15a and 15b. Similar tendencies are shown among the ^{28}SiO, $H^{13}CN$, ^{13}CN, $H^{13}CO^+$, $HN^{13}C$, and NH_3 molecules, and the correlation coefficients among these molecules are in the range of 0.7 ~ 0.9. Similar tendencies are shown among $C^{18}O$ $C^{34}S$, and C_3H_2, and the correlation coefficients are in the range of 0.80 ~ 0.91. On the other hand, that of $H^{13}CN$ and C_3H_2 is 0.37, and show no apparent correlation as shown in Fig 15c. Similar tendencies are shown between C_3H_2 and ^{13}CN, $C^{34}S$ and $H^{13}CN$, which values are 0.34, and 0.35, respectively.

5.4.2. Correlation of Molecular Column Densities

In the section 5.4.1, we had correlations among observed species by using the values of the brightness temperatures multiplied by velocity widths, and found some molecules showed good correlation to one another. However, this method has an ambiguous factor in the case of optically thin. For example, since the column density is estimated from only one transition, the excitation temperature may be different.

Therefore, there is a possibility that the correlations found in section 5.4.1 are artificial. We studied correlation relation among the column densities in this section for confirmation. Examples, which are plotted as the same molecules as used in Fig. 15a ~ 15c, are presented in Fig. 17a ~ 17c.

The obtained column densities of $H^{13}CN$ are plotted against those of ^{13}CN (Fig. 17a). The column densities of $H^{13}CN$ are found to be positively correlated with those of ^{13}CN. The correlation becomes worse compared with the case of the previous section, but the tendency of the correlation can be recognized. The

uncertainties of these column densities are larger than the results in the previous section. However, since the errors of continuum brightness temperature, those of brightness temperatures of molecular lines, and excitation temperatures are changed systematically, the error of the results becomes smaller, and the influence of these errors on the results are small. We investigate the influence of the velocity width and the excitation temperature to the correlation coefficients, and found this influences on the results are not systematically, but works relatively small. As a result, the correlation derived in this section is not hidden by the errors of 0.01 ~ 0.02. A similar positive correlation is seen between the column densities of $C^{34}S$ and C_3H_2 (Fig. 15b). The overall abundance ratio, $N[H^{13}CN]/N[^{13}CN]$ is ~ 1.00, and that $N[C^{34}S]/N[C_3H_2]$ is ~ 0.79. The positive correlation of the $H^{13}CN$ column density with the ^{13}CN column densities may indicate that the production chemistry of $H^{13}CN$ is closely related to those of ^{13}CN. And the positive correlation of those of $C^{34}S$ and C_3H_2 indicate that the production chemistry of $C^{34}S$ is closely related to those of C_3H_2.

The correlation coefficients among the other molecules by this method are listed in Table 16, and are shown in Fig. 18. According to these, a correlation coefficient between ^{13}CN and $H^{13}CN$ is 0.80, and has positive correlation, as shown in Fig. 17a. Similar results are shown among the ^{13}CN, $H^{13}CN$, NH_3, $H^{13}CO^+$ molecules. The correlation coefficients among these molecules are in the range of 0.7 ~ 0.9, except between the NH_3 and $H^{13}CO^+$ molecules (0.64). A possible correlation between these molecules and the SiO molecule is seen, and the correlation coefficients are range from 0.5 to 0.78. Of these molecules, whose correlation coefficients can not be calculated the correlation coefficients since the numbers of the data are small, the line profiles of the HC_3N and $HN^{13}C$ lines are similar with that of the $H^{13}CN$ lines. Therefore, the column densities of these molecules may be correlated well with that of the $H^{13}CN$ molecule. A correlation coefficient between $C^{34}S$ and C_3H_2 is 0.81, and has good correlation as shown in Fig. 17b. The line profiles of the SO and CH_3OH lines are similar with that of the C_3H_2 lines. Therefore, the column densities of these molecules may be correlated well to that of the C_3H_2 molecule.

On the other hand, the column density of $H^{13}CN$ shows no correlation or probably an anti-correlation with that of C_3H_2 (Fig. 17c). And the correlation coefficient of $H^{13}CN$ and C_3H_2 is 0.40, and show no apparent correlation as shown in Fig 17c.

As a result, we found that the correlations of the observed molecules in the diffuse molecular cloud can be divided into two groups. The positive correlation

are seen among ^{13}CN, $H^{13}CN$, NH_3, $H^{13}CO^+$, $HN^{13}C$, and HC_3N molecules, and may be between these molecules and the SiO molecule. These molecules are treated as group A. On the other hand, $C^{34}S$ and C_3H_2 are seen in positive correlation, and may also be seen among these molecules and possibly SO and CH_3OH. These molecules are treated as group B. The molecules belonging to group A and those belonging to group B do not show no apparent correlation.

A similar tendency is reported by Miyawaki et al. (1988). The column density of CS of the 60 km/s absorbing feature is about half of that of the 39 km/s gas, while the column densities of other molecular species in the 60 km/s gas are 2 ~ 6 times higher than those in the 39 km/s gas.

5.5. Summary of Chapter 5.

(1) We had the correlation between molecular lines intensities multiplied by line widths and between molecular column densities. Thus, chemical differences of the diffuse molecular clouds are reconfirmed.
(2) We found that the observed molecules in the diffuse molecular clouds can be divided into two groups from both methods. The positive correlation are seen among ^{13}CN and $H^{13}CN$, NH_3, $H^{13}CO^+$, and possibly $HN^{13}C$, and HC_3N molecules These molecules correlate with the SiO molecule. These molecules are classified as group A. On the other hand, $C^{34}S$ and C_3H_2 are seen in positive correlation, and may also correlate with SO and CH_3OH. These molecules are classified as group B. The molecules belonging to group A and those belonging to group B do not show no apparent correlation.
(3) We also found column densities of some of the observed molecules may depend on visual extinction. The column densities of the ^{13}CN, $H^{13}CN$, HC_3N, NH_3 reach at the peak at 1.5 ~ 1.8 mag, and decreased with the increase of visual extinction. On the other hand, those of the $C^{18}O$, SO, CH_3OH and possibly $C^{34}S$, C_3H_2 molecules increase with visual extinction. Others, those of the SiO, and $H^{13}CO^+$ molecules show no relation with visual extinction.

Chapter 6. Discussion

6.1. Introduction

In the former chapter, we derived the column densities of observed molecules, and studied their mutual correlation to consider relationship with physical properties of observed diffuse clouds. We found the differences in the chemical constituent of the diffuse molecular cloud and apparent correlation between the molecular abundances and visual extinction. The origin of these results will be considered on the basis of molecular formation mechanism in this chapter.

Firstly, we summarize the gas kinetic temperatures and molecular hydrogen densities of observed diffuse molecular clouds, and compare with those of the dense molecular clouds, diffuse clouds, translucent clouds, and high-latitude clouds in section 6.2. The origin of chemical differences among diffuse molecular clouds and correlation between visual extinction and molecular column densities will be discussed by considering the results of model simulation and other observational results. We will discuss about the influence of UV radiation and differences in evolutionary stage among the diffuse molecular clouds in section 6.3. Finally, section 6.4 will describe the comparison of chemical properties of diffuse molecular clouds with other kinds of clouds such as diffuse clouds, translucent clouds, high-latitude clouds, and dense molecular clouds.

6.2. Physical Properties of Diffuse Molecular Clouds

In Chapter 4, we derived the gas kinetic temperatures and molecular hydrogen densities as plotted in Fig. 19. The representative values of the temperature and density of HI gas region, diffuse clouds, translucent clouds, high-latitude clouds, and dense molecular clouds are also shown in Fig. 19. The molecular hydrogen densities and the gas kinetic temperatures of the diffuse molecular clouds are nearly the same as those of the higher density region of the diffuse clouds. On the other hand, according to Magnani et al. (1988), the CS, HCN, and HCO^+ lines towards translucent clouds are observed as emission. Therefore, the molecular hydrogen densities of the translucent clouds may be higher than those of observed diffuse molecular clouds. The densities and temperatures of high-latitude clouds are nearly similar to those of the diffuse clouds. However, the CO/H_2 ratio is higher by factor 2 ~ 4 than that of diffuse

cloud.

The sizes of the diffuse molecular clouds are approximately derived by the ratio of the H_2 column densities and the molecular hydrogen densities, where the H_2 column densities ($N(H_2)$) are obtained by multiplying the column densities of ^{12}CO by 10^4 ($H_2/^{12}CO$ ratio in TMC-1). The sizes determined by this method are in the range of 0.05 ~ 0.21 pc, as listed in Table 14. Although the error of this method may be an order of magnitude, the derived sizes are the same order of magnitude as those of dense molecular clouds.

In the section 4.2, we assumed that the beam filling factor is unity in order to derive the gas kinetic temperatures. However, when we consider that the telescope beam size is 42" at 40 GHz, the beam filling factor may be less than unity (0.05 ~ 0.21) for most molecules. In the case of NH_3, if the NH_3 (1,1) absorbing region is equal to the NH_3 (2,2) absorbing region, T_R (2,1) does not change from the present result even if the beam filling factor is not unity. On the other hand, if the beam filling factor is not unity, the kinetic temperature derived from the CO emission line become higher. This may be one of the reasons to explain that the kinetic temperature derived from the ^{12}CO lines are not in agreement with that derived using the NH_3 absorption lines.

6.3. Influence of UV Flux and Other Effects on Chemical Properties of Observed Diffuse Molecular Clouds

In section 5.4, we found that the observed molecules in the diffuse molecular cloud can be classified into two groups (A group; ^{13}CN, $H^{13}CN$, NH_3, $HN^{13}C$, HC_3N, $H^{13}CO^+$, and SiO; B group; $C^{34}S$, C_3H_2, SO, and CH_3OH). No apparent positive correlation is found, for example, between $H^{13}CN$ and C_3H_2, and the difference in abundances is found between the center of the Galaxy and the outside of the Galaxy. The possible reasons for this anti-correlation are due to the difference in physical condition (density, temperature, UV flux etc.), or that in evolutionary stage of each diffuse molecular cloud. The following factors may cause the anti-correlation in column densities.

(1) Difference in molecular hydrogen density
(2) Difference in kinetic temperature
(3) Difference in UV flux
(4) Difference in cloud evolution

We derived the kinetic temperatures and molecular hydrogen densities in chapter 4. According to these, no apparent differences in these physical properties

among the observed diffuse molecular clouds are recognized. This means the chemical composition of the observed diffuse molecular clouds may not be much dependent on molecular hydrogen densities and kinetic temperature.

It is thought that the diffuse cloud is in chemically and physically equilibrium stage. On the other hand, dense molecular cloud is not in chemically equilibrium stage, and the molecular abundances are subjected to the time-evolved calculation. The presently observed diffuse molecular clouds have similar physical conditions as diffuse clouds. Therefore, the chemical composition may be close to equilibrium condition, but may also be effected by non-equilibrium condition in some degree. Therefore, we must consider both situation of diffuse cloud and dense molecular cloud. Unfortunately, only a few theoretical calculations treating the intermediate stage have been reported so far, such as Graedel et al. (1982).

First of all, we will discuss a possibility of the influence of UV flux on chemical differences in observed diffuse molecular clouds. In diffuse cloud, photodissociation plays an important role for destruction of molecular species, because the visual extinction of the diffuse molecular cloud in the range of 1.3 ~ 4.1 mag, as shown in Table 14. In Chapter 5, we found some of the observed molecules may have some relation to visual extinction. For these consideration, Table 17 lists photodissociation energies and rates of the observed molecules.

We will discuss about production mechanisms for the molecules belonging to the group A in section 6.3.1. The formation pathways of the molecules which are belonging to the group B will be discussed in section 6.3.2. Next, section 6.3.3 will discuss about other effects on the chemical compositions of the diffuse molecular clouds.

6.3.1. Abundance Correlations in group A

In Chapter 5, we found that (1) the molecular abundances of ^{13}CN, $H^{13}CN$, $HN^{13}C$, HC_3N, NH_3, and $H^{13}CO^+$, and possibly SiO correlates well with one another, and (2) the column densities of ^{13}CN, $H^{13}CN$, HC_3N, NH_3 have peaks at 1.5 ~ 1.8 mag as shown in Fig. 14a except for the +22 km/s velocity component. There is discontinuity in the column density between the region with larger magnitude than 1.5 and smaller magnitude than 1.5, because the visual extinctions of the former are determined from ^{13}CO lines and those of the latter are from $C^{18}O$ lines.

Figure 20 shows the schematic illustration of the proposed model for the production mechanisms of these molecules, which are considered in this thesis.

Firstly, we will discuss the possible production mechanism of the CN, HCN, and HNC molecules. Gas phase channels for CN production in diffuse clouds have been described in many literature (cf. Prasad and Huntress 1980; Federman et al. 1994). The following ion-molecule reactions are proposed for the CN production,

$$C^+ + NH \rightarrow CN^+ + H, \quad (17a)$$
$$CN^+ + H_2 \rightarrow HCN^+ + H, \quad (17b)$$
$$HCN^+ + e^- \rightarrow CN + H, \quad (17c)$$
$$HCN^+ + H_2 \rightarrow HCNH^+ + H, \quad (17d)$$
$$HCNH^+ + e^- \rightarrow CN + H_2, \quad (17e)$$
$$\rightarrow HCN + H, \quad (17f)$$
$$\rightarrow HNC + H. \quad (17g)$$

These reactions are thought to be effective in the lower density region such as diffuse molecular clouds (Federman et al. 1994). According to Federman et al. (1994), the observed steep dependence of CN on H_2 in the diffuse clouds suggests that the following neutral-neutral reactions are also important for the CN production,

$$CH + N \rightarrow CN + H, \quad (18a)$$
$$C_2 + N \rightarrow CN + C. \quad (18b)$$

These neutral-neutral reactions contribute to CN production in the higher density region than Av = 3 mag. The rate coefficients of these reactions (18a, b) are reported to be $2.0\times10^{-11}(T/300)^{0.5}$ cm^3s^{-1} by Messing et al. (1981), and $1.7\times10^{-11}(T/300)^{0.5}$ cm^3s^{-1} by Federman et al. (1994), respectively.

The HNC molecule is a metastable isomer of HCN and the production seems to be mainly due to ion-molecule reactions. If HNC is produced by a chemical equilibrium reaction scheme, the abundance of HNC would be smaller than that of HCN by more than a factor of 6000, due to the energy difference of 0.65 eV between HNC and HCN. On the other hand, the well known recombination reaction (17f, g) would produce HCN and HNC with about 1:1 abundance ratio (Herbst 1978), as in observations towards dense molecular clouds (Irvine and Schloeb 1984). However, the branching ratios for reactions (17e ~ 17g) are not measured in laboratory.

We derived the $N[H^{13}CN]/N[HN^{13}C]$ abundance ratios. Since the fractional reaction of ^{12}C and ^{13}C is unknown, we assumed $N[H^{13}CN]/N[HN^{13}C]$ =

$N[H^{12}CN]/N[HN^{12}C]$. Both the $H^{13}CN$ and $HN^{13}C$ lines are observed at +22 km, +3 km/s, and -105 km/s velocity components, and in other clouds the $HN^{13}C$ line is not observed because of weak absorption intensity. The $N[H^{13}CN]/N[HN^{13}C]$ abundance ratios derived towards diffuse molecular clouds are 1.07, 10.47, and 3.02, at +22 km, +3 km/s, and -105 km/s velocity components respectively. These relatively small values indicate that the HCN and HNC molecules are formed by ion-molecule reaction scheme (17 f, g). It is noted that Nyman and Millar (1989) derived N[HCN]/N[HNC] = 0.56 in the diffuse molecular cloud towards Cas A. In the observed clouds with Av = 1 ~ 4 mag, if CN, HCN, and HNC are produced mainly by recombination reaction (17e ~ 17g), their abundances correlate one another.

The precursor ion $HCNH^+$ for these molecules is also thought to be produced by the following reactions;

$$C^+ + H_2 \rightarrow CH_2^+, \quad (19a)$$
$$CH^+ + H_2 \rightarrow CH_2^+ + H, \quad (19b)$$
$$CH_2^+ + N \rightarrow HCN^+ + H, \quad (19c)$$
$$NH_2 + C^+ \rightarrow HCN^+ + H, \quad (19d)$$
$$HCN^+ + H_2 \rightarrow HCNH^+ + H. \quad (19e)$$

Reaction (19a) has small rate constant, owing to the radiative association mechanism. On the other hand, CH^+ is known to be abundant, although the production mechanisms is still under discussion. Since NH_2 is mainly destroyed through photodissociation in the average interstellar radiation field at Av ~ 1 mag, contribution of (19d) may be small.

In the high UV radiation field, both the HCN and HNC molecules are easily photodissociated and the CN molecule is produced by the following reactions,

$$HCN + h\nu \rightarrow H + CN, \quad (20a)$$
$$HNC + h\nu \rightarrow H + CN. \quad (20b)$$

The photodissociation rate of reaction (20a) is reported to be $1.1\times10^{-9}\exp(-2.08Av)\ s^{-1}$ by Lee (1984).

Photodissociation by UV photons is thought to be a major destruction process for the CN molecules in diffuse clouds (Federman et al. 1994).

$$CN + h\nu \rightarrow C + N, \quad (21)$$

where the rate is $5.8\times10^{-10}\exp(-7.04Av)s^{-1}$ from Table 17 (Roberge et al. (1991)). In the case of Av = 1.3, photodissociation rate of CN is three orders of magnitude smaller than that of HCN. We derived an order of larger CN molecular abundance than HCN in two observed diffuse molecular clouds with Av = 1.3. However, a large photodissociation rate 7×10^{-10} s^{-1} had been suggested for the CN molecule by Lavendy, Gandara, and Robbe (1984) using SCF and CI methods. As pointed out by van Dishoeck and Black (1986), the limited size of base set in the calculation of Lavendy et al. (1984) may have led to an overestimate of the rate. The observed abundance ratio $N[^{13}CN]/N[H^{13}CN]$ implies that the photodissociation rate may be between that of Roberge et al. (1991) and that of Lavendy et al. (1984). The CN photodissociation occurs primarily at short-wavelengths, $\lambda < 1050$ Å, in harmony with the fact that no CN photodissociation is observed experimentally for $\lambda > 1060$ Å (Nee and Lee 1985). In the strong UV region, the HCN and HNC molecules are easily dissociated to produce the CN molecule. Indeed, the CN molecule is detected in the outer envelopes of the carbon star such as IRC+10216 with a shell-structure (Keady and Ridgway 1993), and is thought to be produced by photodissociation of the HCN molecule by the external UV radiation. Therefore, the HCN and HNC molecules are thought to be destroyed by the reaction (20a, b) in the strong UV flux region. When the UV flux is weaken, the HCN and more complex molecular abundances may be increased.

The $N[^{13}CN]/N[H^{13}CN]$ ratio in +22 km/s velocity component is determined to be 53.7. On the other hand, that in -42 km/s velocity component it is 2.88. In the +22 km/s cloud, the ^{12}CO line is observed as absorption. On the other hand, the line is observed as emission towards other velocity components. Therefore, this +22km/s cloud is relatively low density region ($n(H_2) \lesssim 10^2$ cm^{-3}), and the UV flux in this cloud is strongest among observed diffuse molecular clouds. The large relative abundance of the CN molecule at this velocity component may be mainly explained by this strong UV field. The -42 km/s cloud has Av = 4.1, and the relative abundance of HCN is increased due to less photodissociation of HCN.

Secondly, we will discuss the production scheme of the HC_3N molecule. Several reaction schemes have been proposed for the interstellar HC_3N (cyanoacetylene) production, as summarized by Knight et al. (1986). One mechanism for HC_3N production is the dissociative recombination reaction of $H_2C_3N^+$ with electron. This ion is thought to be produced in the following

reaction mainly,

$$C_3H_3^+ + N \rightarrow H_2C_3N^+ + H. \quad (22)$$

This $H_2C_3N^+$ ion will produce the HC_3N and HNCCC by recombination reaction. However, the HNC_3 abundance was found to be much smaller than that of HC_3N (Kawaguchi et al. 1992a, b) in TMC-1.

Recently, Herbst and Leung (1990) proposed neutral-neutral reactions for HC_3N production in addition to the ion-molecule reactions,

$$C_2H_2 + CN \rightarrow HC_3N + H. \quad (23)$$

The rate coefficient of reaction (23) is 2.2×10^{-10} cm^3s^{-1}, and is found to be very rapid in the laboratory experiments by Lichtin and Lin (1986). According to Takano et al. (1991), among the J = 5-4 rotational transitions of the three ^{13}C isotopic species of HC_3N, the $HCC^{13}CN$ line intensity is stronger than those of $H^{13}CCCN$ and $HC^{13}CCN$ lines by factor 2. This result is not contradicted with the neutral-neutral reactions of Herbst and Leung (1990), because in reaction (23), the unpaired electron on the C atom of CN attacks acetylene to produce HC_3N. If reaction (23) is a main route for production of HC_3N, and only small part of CN abundance is converted to HC_3N , the abundance correlation between CN and HC_3N can be well explained.

Thirdly, the formation and destruction mechanism of the NH_3 molecule will be discussed. The NH_3 molecular abundance is correlated with that of CN. The gas-phase production of NH_3 has been discussed in detail by Herbst, DeFrees, and McLean (1987), and Galloway and Herbst (1989). According to these, the production starts from the N^+ formation by the following reaction:

$$N_2 + He^+ \rightarrow N^+ + He + N. \quad (24)$$

The N^+ ion has surplus translation energy to overcome the small endothermicity (18.54 meV) of the following hydrogenation reaction (Martquette et al. 1985):

$$N^+ + H_2 \rightarrow NH^+ + H. \quad (25)$$

The rate coefficient of reaction (25) is assumed to be 1.1×10^{-14} cm^3s^{-1} by Herbst

and Leung (1989). Further hydrogenation of NH^+ leads to NH_4^+ to produce NH_3 by recombination reaction.

The formed NH_3 is destroyed by photodissociation and/or by reaction primarily with C^+.

$$NH_3 + h\nu \rightarrow NH_2 + H, \quad (26a)$$
$$NH_3 + C^+ \rightarrow H_2NC^+ + H. \quad (26b)$$

The molecular abundances of NH_3 and CN are expected to be anti-correlation, because C^+ destroys NH_3 to produce the precursor ion H_2NC^+ for CN. However, both molecules are correlated well. Therefore, the reason why the NH_3 and CN molecules correlated well is unknown.

Finally, we will consider the possible production scheme of the $H^{13}CO^+$ and SiO molecules. These molecular abundances are correlated with that of the CN molecule, but found to have no apparent correlation with visual extinction.

The HCO^+ molecule is thought to be produced and destroyed by the following reactions,

$$C^+ + OH \rightarrow CO^+ + H, \quad (27a)$$
$$CH^+ + O \rightarrow CO^+ + H, \quad (27b)$$
$$CO^+ + H_2 \rightarrow HCO^+ + H, \quad (27c)$$
$$HCO^+ + e^- \rightarrow CO + H, \quad (27d)$$
$$CO + H_3^+ \rightarrow HCO^+ + H_2. \quad (27e)$$

In diffuse clouds, the principal source of CO^+ is the reaction of C^+ with OH (27a) (van Dishoeck and Black 1986, 1988). Contributions of the other reactions, for example reaction (27b), are small. Because of similarity in physical properties between diffuse clouds and the observed diffuse molecular clouds, we think the reaction (27a) is also effective in the diffuse molecular clouds. Since the abundance of the H_3^+ ion is proportional to that of H_2, the reaction (27e) is less effective for HCO^+ production in the diffuse molecular clouds than in the dense molecular clouds. In the diffuse molecular clouds, the C^+ abundance is increased by UV flux. The molecular abundance of OH is also higher than that in a diffuse cloud. Therefore, the HCO^+ molecular abundance is increased compared with that in diffuse cloud. Groβmann et al. (1990) reported the radio observations of ^{12}CO, ^{13}CO, OH, and H_2CO towards the high-latitude clouds, and found that the OH

abundance is higher than that in dense molecular cloud and even somewhat higher than that in diffuse cloud.

One pathway for SiO production is due to the destruction of grain by the shock wave in interstellar clouds. Another pathway is due to ion-molecule reactions.

The former is largely accepted for the SiO production in the star-forming regions with outflow. Indeed, a large amount of the SiO molecule are observed in sources such as OMC-1 and B1. However, more than 40 km/s velocity shock wave is necessary to destroy the silicate-type grain (Seab and Shull 1983). Such high velocity is not discovered toward the diffuse molecular clouds. Therefore, the former mechanism may not be effective for the SiO production in the observed diffuse molecular clouds.

On the other hand, another pathway by ion-molecule reaction may be important for the lower density and lower temperature region such as the diffuse molecular clouds. The SiO molecule is thought to be produced via following ion-molecule reactions

$$Si^+ + OH \rightarrow SiO^+ + H, \quad (28a)$$

$$SiO^+ + H_2 \rightarrow SiOH^+ + H, \quad (28b)$$

$$SiOH^+ + e^- \rightarrow SiO + H. \quad (28c)$$

where Si^+ and OH reaction (28a) has no activation energy and is fast to produce SiO^+ with Langevin rate. Also, SiH + O → SiO + H is thought to be another process. However, this reaction is slow because of neutral-neutral reaction. In the diffuse cloud, the Si^+ ion is detected (Pwa and Pottasch 1986), and a large amount of OH is observed (cf. Bieging 1976). According to these, a detectable amount of SiO is thought to be produced by eqs. (28a ~ 28c).

Recent experimental data accompanying the Si^+, Si (Wlodek, Fox, and Bohme 1987; Bohme, Wlodek, and Fox 1988; Wlodek and Bohme 1988, 1989) and the theoretical thermodynamical data accompanying the Si atoms (Qi, Panzat, and Berthier 1984; Flores and Largo-Cabrerizo 1987; Wong et al. 1988) are used for the many theoretical reaction calculations. Herbst et al. (1989) carried out chemical network calculations including about 300 reactions and obtained the SiO abundance relative to the H_2 molecule to be 4×10^{-8}. However, the result is not consistent with the observational results by Ziurys et al. (1989), who assumed a temperature dependent reaction which contains an activation energy term ([SiO] exp(-Eact/Tgas)), because the SiO molecule is not detected in the low kinetic

temperature (~ 10 K) region such as TMC-1. The kinetic temperatures of the observed diffuse molecular clouds are higher than those of the dense molecular clouds. Therefore, some amount of SiO may be produced in the region.

6.3.2. Abundance Correlations in group B

We found (1) the column densities of CS, C_3H_2, CH_3OH, and SO are correlated well one another, and (2) those of the $C^{18}O$, SO, CH_3OH and possibly $C^{34}S$, C_3H_2 molecules increase with visual extinction.

Firstly, we will consider the reason why these molecules are increased with visual extinction.

The CS molecule once formed can be destroyed by photodissociation, photoionization, charge-transfer reactions, and reactions with H_3^+. However, the latter three processes are not important as destruction mechanisms, since they form either CS^+ or HCS^+,which for the most part lead back to CS. Thus, the dominant destruction route of CS in diffuse molecular clouds is photodissociation. Although the dissociation energy of CS (7.36 eV) is not largely different from that of CN (7.48 eV), and the photodissociation rate may be different. Unfortunately, the photodissociation rate of CS is highly uncertain. The photodissociation process of CS is probably similar to that for CO, with the difference that the dissociation energies and ionization thresholds are smaller by 3 ~ 4 eV in CS. Recent laboratory studies of the vacuum UV absorption spectrum of the isovalent CO molecule (Letzelter et al. 1987; Yoshino et al. 1995), have demonstrated that the photodissociation of the CO molecule proceeds through a series of discrete absorption into predissociating states. The photodissociation of CO is discussed in detail by van Dishoeck and Black (1988) and Viala, Roueff and Abgrall (1988). The corresponding spectrum for CS is only partly known. High resolution spectra of CS at VUV wavelengths (Stark, Yoshino, and Smith 1987) show many diffuse bands. In particular, the strong B-X (0,0) and C-X(0,0) bands of CS are rapidly predissociated, in contrast to CO. If the oscillator strengths for these bands in CS are similar to those of CO, the photodissociation rate of interstellar CS must be significantly larger than that of CO. The photodissociation rate of CO is 1.8×10^{-10} s^{-1} and the value is not different from that of CN, which is estimated to be $k = 5.8 \times10^{-10}\exp(-7.04Av)$ (Roberge et al. 1991). According to Drdla, Knapp and van Dishoeck (1989), the CS photodissociation rate is estimated to be about 2×10^{-10} $s^{-1} \sim 1\times10^{-9}$ s^{-1}. The molecular abundances of CS is increased with visual

extinction as shown in Fig. 14b, although there is discontinuity between 1.3 ~ 1.5 mag and below 1.5 mag. CN is also increased with visual extinction. However, the increase of the CS molecule is larger than that of the CN molecule. The CS molecules are observed with weak profiles in optical spectrum in diffuse clouds. On the other hand, the CN lines are strongly observed (CS; Drdla et al. 1989; CN; Federman et al. 1984).

Miyawaki et al. (1988) reported that the CS column densities in the observed two diffuse molecular clouds towards W49A are different from those of other molecules (H_2CO, HCO^+, C_2H, and OH). They insist the reason is due to the difference in UV flux among the two clouds as follows: The ionization energy of sulfur is less than that of carbon, and the diffuse S^+ region in molecular clouds could penetrate deeper than C^+ regions. Therefore, they speculate that sulfur is mostly ionized there, and sulfur-bearing molecules such as CS become less abundant, while hydrogen and carbon remain neutral, and hydrocarbons such as H_2CO, HCO^+, C_2H, and OH are in normal abundances.

The $C^{34}S$ lines were not detected near the central region of our Galaxy, where we consider the region within the radius of 500 pc from the galactic center as the central region of our Galaxy. On the other hand, the $C^{34}S$ line was strongly observed in other clouds. The $C^{32}S$ lines were strongly observed toward all the observed diffuse molecular clouds. The reason is under discussion.

The main destruction reactions of SO, CH_3OH, and c-C_3H_2 are also thought to be photodissociation process in diffuse molecular clouds,

$$SO + h\nu \rightarrow S + O, \quad (29)$$

$$CH_3OH + h\nu \rightarrow H_2CO + H_2, \quad (30)$$

$$c\text{-}C_3H_2 + h\nu \rightarrow C_3H + H. \quad (31)$$

The dissociation energies of CH_3OH and SO are 5.36 eV and 4.07 eV, respectively. Therefore, these molecules are easily dissociated. On the other hand, the dissociation energy of c-C_3H_2 is unknown. However, this molecule is not detected in diffuse clouds, and the electronic transitions which seem to be in the UV wavelength region, are not measured in the laboratory. This means that c-C_3H_2 seems to be easily dissociated by the UV radiation. Indeed, the molecular abundances of CH_3OH, SO, and possibly c-C_3H_2 are increased with visual extinction like as CS, as shown in Fig. 14b.

The proposed synthesis model of these molecules are shown in Fig. 21. A significant amount of CS is thought to be formed in diffuse molecular clouds

through the series of gas-phase reactions.

$$C^+ + H_2 \rightarrow CH_2^+, \quad (32a)$$
$$CH_2^+ + H_2 \rightarrow CH_3^+, \quad (32b)$$
$$CH_3^+ + e^- \rightarrow CH + H_2, \quad (32c)$$
$$S^+ + CH \rightarrow CS^+ + H, \quad (32d)$$
$$S^+ + C_2 \rightarrow CS^+ + C, \quad (32e)$$
$$CS^+ + H_2 \rightarrow HCS^+ + H, \quad (32f)$$
$$HCS^+ + e^- \rightarrow CS + H. \quad (32g)$$

The rate coefficients of reactions (32d) ~ (32g) are 6.2×10^{-10} cm^3s^{-1}, 8.1×10^{-10} cm^3s^{-1}, 1.5×19^{-9} cm^3s^{-1}, and $3.0\times10^{-7}(T/300)^{0.5}$ cm^3s^{-1}, respectively, which are taken from Prasad and Huntress (1980). An additional formation route is through the neutral-neutral reactions of S with CH and C_2 to form CS directly. It is important to note that CS^+ is able to react with H_2, which allows the chemistry to proceed, although there is some competition with the dissociative recombination of CS^+. The dissociative recombination of HCS^+ with electrons, reaction (32g), is unusually slow (Millar et al. 1986), but HCS^+ is also unreactive with H_2 and other abundant interstellar species. Thus essentially most of HCS^+ still leads to CS.

Both in the laboratory and in space, c-C_3H_2 can be formed by electron recombination with the $C_3H_3^+$, as follows (Virtilek, Gotlieb, and Thaddeus 1987):

$$CH + C^+ \rightarrow C_2^+ + H, \quad (33a)$$
$$C_2^+ + H_2 \rightarrow C_2H^+ + H, \quad (33b)$$
$$C_2H^+ + H_2 \rightarrow C_2H_2^+ + H, \quad (33c)$$
$$C_2H_2 + C^+ \rightarrow C_3H^+ + H, \quad (33d)$$
$$C_3H^+ + H_2 \rightarrow C_3H_3^+ + hv, \quad (33e)$$
$$C_3H_3^+ + e^- \rightarrow c\text{-}C_3H_2 + H, \quad (33f)$$
$$\rightarrow C_3H + H_2, \quad (33g)$$
$$\rightarrow HCCC + H_2, \quad (33h)$$
$$\rightarrow c\text{-}C_3H + H_2, \quad (33i)$$

where CH is produced by (32c).

Although the isometric form is not specified, Herbst, Adams, and Smith (1984) and Millar and Nejad (1985) calculated fractional abundances for the C_3H_2 with respect to H_2 in a TMC-1 type cloud to be the range $10^{-8} \sim 10^{-7}$.

On the other hand, the CH_3OH molecule is thought to be formed as follows:

$$CH_3^+ + H_2O \rightarrow CH_3OH_2^+, \quad (34a)$$
$$CH_3OH_2^+ + e^- \rightarrow CH_3OH + H. \quad (34b)$$

According to these reactions, the CS, c-C_3H_2 and CH_3OH molecules are formed from the same ion CH_3^+ which is decreased in the density region where C^+ is transformed from C^+ to CO.

On the other hand, the reactions for SO production are considered as follows (Swade 1989),

$$S + OH \rightarrow SO + H, \quad (35a)$$
$$SH + O \rightarrow SO + H. \quad (35b)$$

According to these reactions, the SO molecule is not thought to be connected with the CS, c-C_3H_2, and CH_3OH molecules. However, the molecular abundance of OH is high in the diffuse molecular clouds as stated before. The SH molecular abundance is unknown, since the observable frequencies of this molecule are in submillimeter wavelength region which is not easy for observation from ground based telescope. However, the H_2S and SO molecules are observed in absorption and found to be high abundance in the diffuse molecular clouds towards W49 and Sgr B2 (Tieftrunk et al. 1994).

6.3.3. Influence of Other Effects on Chemical Properties among Observed Diffuse Molecular Clouds

Thirdly, we discuss an influence of the difference in the evolutionary stage on the chemical properties of the observed diffuse molecular clouds. Chemical equilibrium in the interstellar medium is determined by the time that productions and destructions of the molecules reach equilibrium. The molecular compositions are thought to be already in equilibrium in the diffuse clouds. On the other hand, those are not in equilibrium in the dense molecular clouds. The diffuse molecular clouds may be in chemically equilibrium, because the physical properties of the observed diffuse molecular clouds are similar with those of the diffuse clouds. The chemical equilibrium is attained in the case of the ion-molecular reactions. However, if the slow reactions such as some neutral-neutral reactions play important roles in molecular synthesis, chemical compositions in the diffuse

molecular clouds may show time variation.

The column densities of the c-C_3H_2, $C^{34}S$, and SO molecules at -42, -46 km/s velocity components are higher by an order of magnitude than those of other clouds. These velocity components, which are corresponding to the 3 kpc arm, are thought to be produced by the explosion near the Galactic center at ~ 10^7 yrs before. On the other hand, it is likely to be that the -20, -28 km/s features also correspond to the 4.5 kpc arm which is produced by the explosion near the Galactic center. However, these features are thought to be older than the -42, -46 km/s features. The -76, -92, and -105 km/s features are thought to belong to the youngest velocity components. The reason may be as follows: the SO molecule has neutral-neutral reactions in the production routine, and the c-C_3H_2 molecule has many reactions. The reason why $C^{34}S$ molecule is higher than the other velocity components is unclear. However, the -42, -46 km/s velocity components have higher visual extinction than other velocity components as stated in chapter 5.3. It may be influenced by the difference in visual extinction rather than by the difference in the evolutionary stage. It will be discussed in the next section again.

The column densities of the $C^{32}S$, $C^{34}S$ molecules are different between -20 km/s and -28 km/s velocity components. On the other hand, those of $H^{13}CN$ and C_3H_2 are similar. These clouds are located at the both sides of the 4.5 kpc arm, as stated in chapter 3. This arm moves with supersonic velocity in the direction to the outer Galaxy. The -20 km/s velocity component is located in front of the shock. On the other hand, the -28 km/s velocity component is located in the rear of the shock. Therefore, the $C^{32}S$, $C^{34}S$ molecules may be changed among two velocity components by this shock.

6.4. Comparison of Chemical Properties of Diffuse Molecular Clouds with Other Kinds of Clouds

Table 18 lists the column densities of the observed molecules in the diffuse cloud (ζ Oph), the translucent cloud (HD169454), the high-latitude cloud (HD21021), and the dense molecular cloud (TMC-1). In TMC-1, there are two strongest positions in molecular line intensities. One is " the Cyanopolyyne peak", which is the richest source of carbon-chain molecules. Another one is " the Ammonia peak", which has the NH_3, N_2H^+, and SO molecules more abundant than the cyanopolyyne peak (Hirahara et al. 1992, 1995). These difference in chemical composition can be explained by the difference in chemical evolutionary

stage (Hirahara et al. 1992, 1995).

We derived the $N[^{12}CN]/N[C^{16}O]$ abundance ratio from the observed ^{13}CN and $C^{18}O$ lines, by assuming the terrestrial ratios of $^{13}C/^{12}C \sim 1.1\times10^{-2}$ and $^{18}O/^{16}O \sim 2.0\times10^{-3}$. The $N[^{12}CN]/N[C^{16}O]$ abundance ratio is derived to be 4.0×10^{-3}, $2.0 \sim 4.5\times10^{-3}$, and 3.8×10^{-4} for diffuse clouds, diffuse molecular clouds, dense molecular clouds, respectively. The ratios for the -42, -46 km/s velocity components are 1.5×10^{-4} and 2.5×10^{-4}, respectively, which are closer to those of the dense molecular clouds. The visual extinctions of the -42, -46 velocity components are higher than those of other velocity components. Since the real isotope ratio may be different from the assumed one, the errors are expected to be factor 2 in the ratio. Except for the -42, and -46 km/s velocity components, $N[^{12}CN]/N[C^{16}O]$ abundance ratio of the observed diffuse molecular cloud is similar with those of the diffuse cloud.

We compared relative abundances ($N[X]/N[C^{16}O]$) of the observed diffuse molecular clouds with those of the dense molecular clouds. The observed molecular abunadances are listed in Table 19 and plotted in Fig. 22a ~ 22i.

In the +22 km/s velocity component, the relative abundances of HCN, HNC, CH_3OH, and CS to CO are almost similar with those in TMC-1. However, those of CN and HCO^+ are larger than those in TMC-1. The reason is thought to be due to the effect of UV flux as stated in section 6.3. In the +3 km/s velocity component, the relative abundances of all observed molecules are higher than those in TMC-1 systematically. This is due to that the upper limit of the CO molecule is used. Nevertheless, the HCN abundance is larger than that in TMC-1.

We found that the relative abundances of SO, HC_3N with respect to CO in the observed diffuse molecular clouds are smaller by factor 3 ~ 4 than those in TMC-1 with the errors of factor 1.5 ~ 2.0. The HCO^+ abundance is slightly small , but the value at the -28 km/s velocity component is the upper limit. HCN in the diffuse molecular clouds is more abundant than in TMC-1. These results may be explained by differences in visual extinction and production chemistry of these molecules.

Recently, Tieftrunk et al. (1994) observed the H_2S, SO, and NH_3 (1,1), (2,2) lines toward the Sgr B2 using the Effelsberg 100-m and the IRAM 30-m telescopes, and found the abundances of SO and NH_3 are less by an order of magnitude than those in TMC-1 and L183. Tieftrunk et al. (1994) also insisted that the small abundance of SO is due to the influence of UV flux. However, these results may partly be explained by production chemistry of each molecule. Since the production reaction of the SO molecule includes the neutral-neutral reactions

(35a, b) and that of the NH_3 molecule includes the slightly endothermic reaction (24), both molecules are expected to be less abundant in the observed diffuse molecular clouds.

Chapter 7. Conclusions

We analyzed many molecular absorption lines towards Sgr B2 in order to make clear the variety of molecular abundance in diffuse molecular clouds.

(1) The gas kinetic temperatures of the diffuse molecular clouds were derived using ^{12}CO emission lines and NH_3 absorption lines. The kinetic temperatures determined by ^{12}CO are 12.7 ~ 13.7 K, and the rotational temperatures determined by NH_3 are 24 ~ 30 K. The difference may be caused by self-absorption of the CO molecule and/or the fact that in the case of the ^{12}CO emission line, the higher density region in the diffuse molecular clouds influences the determination of the kinetic temperature of CO.

(2) The molecular hydrogen density ($n(H_2)$) of each diffuse molecular cloud is determined from ^{28}SiO (J = 1-0, J = 2-1) and $C^{32}S$ (J = 1-0, J = 2-1) data using the large velocity gradient (LVG) model approximation. The densities lie between 1×10^2 and 4×10^2 cm^{-3}.

(3) The differences in the gas kinetic temperature and in the hydrogen density among clouds are not recognized within the error limit. We found that physical conditions of the observed diffuse molecular clouds are located between those of diffuse cloud and those of dense molecular cloud, and are nearly close to those of diffuse cloud. The sizes of the diffuse molecular clouds are estimated in the range of 0.05 ~ 0.21 pc with error of an order of magnitude.

(4) A positive correlation is found among ^{13}CN and $H^{13}CN$, NH_3, $H^{13}CO^+$, and possibly $HN^{13}C$, HC_3N, and SiO molecules. These molecules are classified as group A. On the other hand, $C^{34}S$ abundance shows positive correlation with that of C_3H_2, and these molecular abundances may be correlated with those of SO and CH_3OH. These molecules are classified as group B. The molecules belonging to group A do not show apparent correlation with those belonging to group B.

(5) Some of the observed molecules are found to be correlated with visual extinction. The column densities of the ^{13}CN, $H^{13}CN$, HC_3N, NH_3 have peaks at 1.5 ~ 1.8 mag, and decreased with the increase of visual extinction. On the other hand, those of the $C^{18}O$, SO, CH_3OH and possibly $C^{34}S$, C_3H_2 molecules increase with visual extinction. Others, those of the SiO, and $H^{13}CO^+$ molecules show no significant dependence on visual extinction. The reason is conjectured as follows: the ^{13}CN, $H^{13}CN$, HC_3N, NH_3 molecules are relatively strong against UV photodissociation compared with the CS, C_3H_2, CH_3OH, and SO molecules. Therefore, latter molecules may show large increment with visual extinction.

(6) The electron dissociative recombination reaction of $HCNH^+$ with electron is

thought to be important to form the neutral products (CN, HCN, HNC). This explains the observed correlation in molecular abundances of ^{13}CN, $H^{13}CN$, and $HN^{13}C$. The abundance correlation between CN and HC_3N can be well explained, if the HC_3N molecule is produced from a part of CN by a neutral-neutral reaction. On the other hand, the CS, C_3H_2, and CH_3OH molecules are formed partly by a fact that those molecules are formed from the common ion CH_3^+.

(7) The molecular abundances of NH_3 and CN are expected to be anti-correlation, if C^+ destroys NH_3 to produce the precursor ion H_2NC^+ for CN. However, both molecules are correlated well. The reason is unclear in the present state. The HCO^+ molecules is thought to be formed from C^+ and OH. In the diffuse molecular clouds, the C^+ and OH molecules are thought to be abundant, and the molecular abundance of HCO^+ may be increased as that of HCN. The Si^+ ion is also increased by UV flux in the observed diffuse molecular clouds. Therefore, the SiO molecule may be increased by the same reason as the case of HCO^+.

(8) The relative abundances of the ^{13}CN, $H^{13}CN$, $H^{13}CO^+$, and $HN^{13}C$ molecules to CO in the observed diffuse molecular clouds are almost similar with those of TMC-1. On the other hand, the SO and HC_3N abundances are smaller by factor 3 ~ 4 (±1.7). These results may be explained by the differences in visual extinction and the production chemistry of these molecules, since the SO and HC_3N molecules have the neutral-neutral reactions in production mechanism.

References

Akabane, K., Sofue, Y., Hirabayashi, H., Morimoto, M., Inoue, M., and Downes, D., 1988, Publ. Astron. Soc. Japan, 40, 459.

Anicich, V. G., and Huntress, W. T. Jr., 1986, Astrophys. J. Suppl., 62, 553.

Bachiller, R., Martin-Pintado, and J., Fuente, A., 1991, Astron. Astrophys., 243, L21.

Bachiller, R., Menten, K. M., and del Rio-Alvarez, S., 1990, Astron. Astrophys., 236, 461.

Bally, J., Stark, A. A., Wilson, R. W., and Henkel, C., 1987, Astrophys. J. Suppl., 65, 13.

Bally, J., Stark, A. A., Wilson, R. W., and Henkel, C., 1988, Astrophys. J., 324, 223.

Bania, T. M., 1977, Astrophys. J., 216, 381.

Bania, T. M., 1980, Astrophys. J., 242, 95.

Barlow, M. J., 1978, Mon. Not. R. astr. Soc, 183, 367.

Barsuhn, J. and Walmsley, C. M., 1977, Astron. Astrophys., 54, 345.

Bartla, W., Walmsley, C. M., and Wilson, T. L., 1984, Astron. Astrophys., 136, 127.

Bates, D. R., and Spitzer, L. Jr., 1951, Astrophys. J., 113, 441.

Baulch, D. L., Cox, R. A., Crutzen, P. J., Hapson, Jr. R. F., Kerr, J. A., Troe, J., and Watson, R. T., 1982, J. Chem. Ref. Data, 11, 327.

Beckwith, S., Persson, S. E., Neugebauer, G., and Becklin, E. E., 1978, Astrophys. J., 223, 464.

Benson, J. M., and Johnston, K. J., 1984, Astrophys. J., 277, 181.

Bieging, J. H., 1976, Astron. Astrophys., 51, 289.

Bieging, J. H., Downes, D., Wilson, T. L., Martin, A. H. M., and Güsten, R., 1980, Astron. Astrophys. Suppl., 42, 163.

Black, J. H., and Dalgarno, A., 1977, Astrophys. J. Suppl., 34, 405.

Black, J. H., Hartquist, T. W., and Dalgarno, A., 1978, Astrophys. J., 224, 448.

Blake, G. A., Sutton, E. C., Masson, C. R., and Phillips, T. G., 1987, Astrophys. J., 315, 621.

Blitz, L., Magnani, L. and Mundy, L., 1984, Astrophys. J., 282, L9.

Bohme, D. K., Wlodek, S., and Fox, A., 1988, in "Rate Coefficients in Astrochemistry", ed. by Millar, T. J., and Williams, D. A., (Dordrecht: Kluwer), p. 193.

Brown, P. D., Duley, W. W., Jones, A. P., and Williams, D. A., 1989, Mon. Not. R. astr. Soc, 241, 753.
Burton, W. B., and Liszt, H. S., 1978, Astrophys. J., 225, 815.
Burton, W. D., and Liszt, H. S., 1980, Astron. Astrophys. Suppl. Ser., 52, 63.
Carlstrom, J. E., and Vögel, S. N., 1989, Astrophys. J., 337, 408.
Castets, A., Duvert, G., Dutrey, A., Bally, J., Langer, W. D., and Wilson, R. W., 1990, Astron. Astrophys., 234, 469.
Castor, J. I., 1970, Mon. Not. R. astr. Soc., 149, 111.
Cheung, A. C., Rank, D. M., Townes, C. H., Thornton, D. D., and Welch, W. J., 1968, Phys. Rev. Lett., 21, 1701.
Clavel, J., Viala, Y. P., and Bel, N., 1978, Astron. Astrophys., 65, 435.
Clegg, R. E. S., van Ijzendoorn, L. J., and Allamandola, L. J., 1983, Mon. Not. R. astr. Soc, 203, 125.
Cohen, R. J., and Few, R. W., 1976, Mon. Not. R. astr. Soc., 176, 495.
Condors, R. E., Roebbel, J. L., and Weiss, K., 1974, J. Chem. Phys, 60, 5011.
Cox, P., Güsten, R., and Henkel, C., 1988, Astron. Astrophys., 206, 108.
Crutcher, R. M, 1985, Astrophys. J., 288, 604.
Cummins, S. E., Linke, R. A., and Thaddeus, P., 1986, Astrophys. J. Suppl., 60, 819.
Danby, G., Flower, D. R., Valiron, P., Schilke, P., and Walmsley, C. M., 1988, Mon. Not. R. astr. Soc, 235, 229.
Davis, D. S., Larson, H. P., and Smith, H. A., 1982, Astrophys. J., 259, 166.
de Vries, C. P., and van Dishoeck, E. F., 1988, Astron. Astrophys., 203, L23.
Dickman, R. L., 1975, Astrophys. J., 202, 50.
Dickman, R. L., and Clements, D. P., 1983, Astrophys. J., 271, 143.
Dickman, R. L., Somerville, W. B., Whittet, D. C. B., McNally, D., and Blades, J. C., 1983, Astrophys. J. Suppl, 53, 55.
Douglas, A. E., and Herzberg, G., 1941, Astrophys. J., 94, 341.
Downes, D., Genzel, R., Hjalmarson, Å, Nyman, L. Å., and Rönnäng, B. 1982, Astrophys. J., 252, L29.
Draine, B. T., 1978, Astrophys. J. Suppl., 36, 595.
Drdla, K., Knapp, G. R., and van Dishoeck, E. F., 1989, Astrophys. J., 345, 815.
Duley, W. W., and Williams, D. A., 1984, in "Interstellar Chemistry", ed. by Duley, W. W., and Williams, D. A., (London: Academic Press) , p.213.
Duvert, G., Cernicharo, J., and Baundy, A., 1986, Astron. Astrophys., 164, 349.
Elitzer, M., and Watson, W. D., 1978, Astrophys. J., 222, L141.
Elitzer, M., and Watson, W. D., 1980, Astrophys. J., 236, 172.

Federman, S. R., 1982, Astrophys. J., 257, 125.
Federman, S. R., Danks, A. C., and Lambert, D. L., 1984, Astrophys. J., 287, 219.
Federman, S. R., and Glassgold, A. E., 1980, Astron. Astrophys., 89, 113.
Federman, S. R., Glassgold, A. E., Jenkins, E. B., and Shaya, E. J., 1980, Astrophys. J., 242, 545.
Federman, S. R., Strom, C. J., Lambert, D. L., Cardelli, J. A., Smith, V. V., and Joseph, C. L., 1994, Astrophys. J., 424, 772.
Flores, J. R., and Largo-Cabrerizo, J., 1987, Chem. Phys. Let., 142, 159.
Galloway, E. T., and Herbst, E., 1989, Astron. Astrophys., 211, 413.
Garay, G., Reid, M. J., and Moran, J. M., 1985, Astrophys. J., 289, 681.
Gardner, E. F., and Whiteoak, J. B., 1970, Astrophys. Lett., 5, 161.
Gardner, E. F., Whiteoak, J. B., Forster, J. R., and Pankonin, V., 1986, Mon. Not. R. astr. Soc., 218, 385.
Gaustad, J. E., 1963, Astrophys. J., 138, 1050.
Geballe, T. R., and Garden, R., 1987, Astrophys. J., 317, L107.
Genzel, R., Downes, D., and Bieging, J., 1976, Mon. Not. R. astr. Soc., 177, 101p.
Genzel, R., Downes, D., Pauls, T., Wilson, T. L., and Bieging, J., 1979, Astron. Astrophys., 73, 253.
Glassgold, A. E., and Langer, W. D., 1974, Astrophys. J., 193, 73.
Glassgold, A. E., and Langer, W. D., 1976, Astrophys. J., 206, 85.
Glassgold, A. E., Mamon, G. A., and Huggins, P. J., 1991, Astrophys. J., 373, 254.
Goldreich, P. and Kwan, J., 1974, Astrophys. J. 189, 441.
Goldsmith, P. F., Lis, D. C., Hills, R., and Lasenby, J., 1990, Astrophys. J., 350, 186.
Goldsmith, P. F., Snell, R. L., and Lis, D. C. 1987, Astrophys. J., 313, L5.
Gomez-Gonzalez, J., Güelin, M., Cernicharo, J., Kahame, C., and Bogey, M., 1986, Astron. Astrophys., 168, L11.
Gordy, W., and Cook, R. L., 1970, in "Microwave Molecular Spectra", (New York; Wiley-Interscience)
Graedel, T. E., Langer, W. D., and Frerking, M. A., 1982, Astrophys. J. Suppl, 48, 321.
Greaves, J. S., White, G. J., Ohishi, M., Hasegawa, T., Hayashi, M., and Sunada, K., 1992, Astron. Astrophys., 260, 381.
Gredel, R., van Dishoeck, E. F., de Vries, C. P., and Black, J. H., 1992, Astron. Astrophys., 257, 245.

Green, S., and Chapman, S., 1978, Astrophys. J. Suppl., 37, 169.
Groβmann, V., Heithausen, A., Meyerdierks, H., and Mebold, U., 1990, Astron. Astrophys., 240, 400.
Güsten, R., and Downes, D., 1980, Astron. Astrophys., 87, 6.
Güsten, R., and Fiebig, D., 1988, Astron. Astrophys., 204, 253.
Güsten, R., Walmsley, C. M., and Pauls, T., 1981, Astron. Astrophys., 103, 197.
Güsten, R., Walmsley, C. M., Ungerechts, H., and Churchwell, E., 1985, Astron. Astrophys., 142, 381.
Habing, H. J., 1968, Bull. Astr. Inst. Netherlands, 19, 421.
Handa, T., Sofue, Y., Nakai, N., Hirabayashi, H., and Inoue, M., 1987, Publ. Astron. Soc. Japan, 39, 709.
Hartquist, T. W., Oppenheimer, M., and Dalgarno, A., 1980, Astrophys. J., 310, 182.
Harvey, P. M., Camphell, M. F., and Hoffmann, W. F., 1977, Astrophys. J., 211, 786.
Haschick, A. D., and Ho, P. T. P., 1990, Astrophys. J., 352, 630.
Hasegawa, T. I., and Herbst, E., 1993, Mon. Not. R. astr. Soc, 261, 83.
Hasegawa, T. I., Herbst, E., and Leung, C. M., 1992, Astrophys. J. Suppl., 82, 167.
Hasegawa T., Morita, K-I., Okumura, S., Kaifu, N., Suzuki, H., Ohishi, M., Hayashi, M., Ukita, N., 1985, Proc. of a meeting on "Masers, Molecules, and Mass Outflows in Star Forming Regions", p.275.
Herbig, G. H., 1968, Zs. Ap., 68, 243.
Herbst, E., 1978, Astrophys. J., 222, 508.
Herbst, E., 1983, Astrophys. J. Suppl., 53, 41.
Herbst, E., Adams, N. G., and Smith, D., 1984, Astrophys. J., 285, 618.
Herbst, E., Bohme, D. K., Payzant, J. D., and Schiff, H. I., 1975, Astrophys. J., 201, 603.
Herbst, E., DeFrees, D. J., and McLean, A. D., 1987, Astrophys. J., 321, 898.
Herbst, E., and Klemperer, W., 1973, Astrophys. J., 185, 505.
Herbst, E., and Leung, C. M., 1986, Astrophys. J., 310, 378.
Herbst, E., and Leung, C. M., 1989, Astrophys. J. Suppl., 69, 271.
Herbst, E., and Leung, C. M., 1990, Astron. Astrophys., 233, 177.
Herbst, E., Millar, T. J., Wlodek, S., and Bohme, D. K., 1989, Astron. Astrophys., 222, 205.
Herzberg, A., 1961, Proc. Roy. Soc., A., 262, 291.
Hirahara, Y., Masuda, A., Yamamoto, S., Takano, S., Ohishi, M., Suzuki, H.,

Ishikawa, S., and Kaifu, N., 1992, Astrophys. J., 394, 539.
Hirahara, Y., Masuda, A., Kawaguchi, K., Ohishi, M., Ishikawa, S., Yamamoto, S., Takano, S., and Kaifu, N., 1995, Publ. Astron. Soc. Japan, in press.
Ho, P. T. P., Barrett, A. H., Myers, P. C., Matsakis, D. N., Cheung, A. C., Chui, M. F., Townes. C. H. and Yngvesson, K. S., 1979, Astrophys. J., 234, 912.
Ho, P. T. P., and Townes, C. H., 1983, Ann. Rev. Astron. Astrophys., 21, 239.
Hollenbach, D., and Salpeter, E. E., 1971, Astrophys. J., 163, 155.
Huntress, W. T. Jr., 1977, Astrophys. J. Suppl., 33, 495.
Irvine, W. M., and Schloeb, F. P., 1984, Astrophys. J., 282, 516.
Irvine, W. M., Schloerb, F. P., Hjalmarson, A., and Herbst, E., 1985, in "Protostars and Planets II", ed. by D. C. Black, and M. S. Matthews (Tuscon: University of Arizona Press), p. 579.
Jannuzi, B. T., and Black, J. H., Lada, C. J., and van Dishoeck, E. F., 1988, Astrophys. J., 332, 995.
Jenkins, E. B., Savage, B. D., Spitzer, Jr. L., 1986, Astrophys. J., 301, 355.
Jewell, P. R., Snyder, L. E., Walmsley, C. M., Wilson, T. L., and Gensheimer, P. D., 1991, Astron. Astrophys., 242, 211.
Johansson, L. E. B., Andersson, C., Ellder, J., Friberg, P., Hjalmarson, Å., Höglund, B., Irvine, W. M., Olofsson, H., and Rydbeck, G., 1984, Astron. Astrophys., 130, 227.
Jura, M., 1976, Astrophys. J., 204, 12.
Jura, M., and Meyer, D. M., 1985, Astrophys. J., 294, 238.
Kaifu, N., Morris, M., Palmer, P., and Zuckerman, B., 1973, Astrophys. J., 201, 98.
Kawaguchi, K., Ohishi, M., Ishikawa, S., and Kaifu, N., 1992a, Astrophys. J., 386, L51.
Kawaguchi, K., Takano, S., Ohishi, M., Ishikawa, S., Miyazawa, K., Kaifu, N., Yamashita, K., Yamamoto, S., Saito, S., Ohshima, Y., and Endo, Y., 1992b, Astrophys. J.,396, L49.
Keady, J. J., and Ridgway, S. T., 1993, Astrophys. J., 406, 199.
Knapp, G. R., and Bowers, P. F., 1988, Astrophys. J., 331, 974.
Knight, J. S., Freeman, C. G., McEwan, M. J., Smith, S. C., Adams, N. G., and Smith, D., 1986, Mon. Not. R. astr. Soc, 219, 89.
Kramers, H. A., and ter Haar, D., 1946, Bull. Astron. Inst. Neth., 10, nr. 371.
Kutner, M. L. and Ulich, B. L., 1981, Astrophys. J., 250, 341.
Lada, E. A., and Blitz, L., 1988, Astrophys. J., 326, L69.
Lang, K. R., and Wilson, R. F., 1978, Astrophys. J., 224, 125.

Langer, W. D., and Glassgold, A. E., 1990, Astrophys. J., 352, 123.
Lavendy, H., Gandara, G., and Robbe, J. M., 1984, J. Mol. Spectrosc., 106, 395.
Lavendy, H., Robbe, J. M., and Gandara, G., 1987, J. Phys. B., 20, 3067.
Lee, L. C., 1984, Astrophys. J., 282, 172.
Letzelter, C., Eidelsberg, M., Rostas, F., Breton, J, and Thiblemout, B., 1987, Chem. Phys., 114, 273.
Leung, C. M., Herbst, E., and Huebner, W. F., 1984, Astrophys. J. Suppl., 56, 231.
Levinson, F. H., and Brown, R. L., 1980, Astrophys. J., 242, 416.
Lichtin, D. A., and Lin, M. C., 1986, Chem. Phys., 104, 325.
Linke, R. A., and Goldsmith, P. F., 1980, Astrophys. J., 235, 437.
Linke, R. A., Stark, A. A., and Frerking, M. A. 1981, Astrophys, J., 243, 147.
Lis, D. C., 1989, Ph. D. Thesis.
Liszt, H. S., and Burton, W. B., 1978, Astrophys. J., 226, 790.
Liszt, H. S., and Burton, W. B., 1980, Astrophys. J., 236, 779.
Liszt, H. S., Burton, W. B., Sanders, R. H., and Scoville, N. Z., 1977, Astrophys. J., 213, 38.
Liszt, H. S., Sanders, R. H., and Burton, W. B., 1975, Astrophys. J., 198, 537.
Lovas, F. J., Lutz, H., and Dreizler, H., 1979, J. Phys. Chem. Ref. Data, 8, 1051.
Lugten, J. B., Stacey, G. J., and Genzel, R., 1995, in preparation
Macpherson, M. T., Philling, M. J., and Smith, M. J. C., 1985, J. Phys. Chem., 89, 2268.
Magnani, L., Blitz, L., and Mundy, L., 1985, Astrophys. J., 295, 402.
Magnani, L., Blitz, L., and Wouterloot, J. G. A., 1988, Astrophys. J., 326, 909.
Mann, A. P. C., and Williams, D. A., 1985, Mon. Not. R. astr. Soc, 214, 279.
Martin, A. H. M., and Downes, D., 1972, Astrophys. Lett., 11, 219.
Martin, R. N., Ho, P. T. P., and Ruf, K., 1982, Nature, 296, 632.
Martquette, J. B., Rowe, B. R., Dupeyrat, G., and Roueff, E., Astron. Astrophys., 1985, 147, 115.
Mathis, J. S., Metzger, P. G., and Panagia, N., 1983, Astron. Astrophys., 128, 212.
Matthews, H. E., and Irvine, W. M., 1985, Astrophys. J., 298, L61.
McKellar, A., 1940, Publ. Astron. Soc. Pacific., 52, 187.
Menon, T. K., and Ciotti, J. E., 1970, Nature, 227, 579.

Messing, I., Filseth, S. V., Sadowski, C. M., and Carrington, T., 1981, J. Chem. Phys., 74, 3874.

Mikami, H., T. Umemoto, S. Yamamoto, and S. Saito, 1992, Astrophys. J., 392, L87.
Millar, T. J., 1980, Ap. Space. Sci., 72, 509.
Millar, T. J., Adams, N. G., Smith, D., Lindinger, W., and Villinger, H., 1986, Mon. Not. R. astr. Soc, 221, 673.
Millar, T. J., and Herbst, E., 1990, Astron. Astrophys., 231, 466.
Millar, T. J., and Nejad, L. A. M., 1985, Mon. Not. R. astr. Soc, 217, 507.
Mitchell, G. F., 1984, Astrophys. J., 287, 665.
Mitchell, G. F., Ginsburg, J. L., Kuntz, P. J., 1978, Astrophys. J. Suppl., 38, 39.
Miyawaki, R., Hasegawa, T., and Hayashi, M., 1988, Publ. Astron. Soc. Japan, 40, 69.
Morimoto, M., et al., 1983, Astron. Soc. of Japan in Chofu, Tokyo, "Mapping Observations of The Sgr B2 using Molecular Lines".
Morimoto, M., Ohishi, M., and Kanzawa, T., 1985, Astrophys. J., 288, L11.
Morris, M., Gilmore, W., Palmer, P., Turner, B. E., and Zuckerman, B., 1975, Astrophys. J., 199, L47.
Morris, M., Snell, R. L., and Bout P. V., 1977, Astrophys. J., 216, 738.
Morris, M., and Yusef-Zadeh, F., 1987, in "The Galactic Center", ed. by Becker, D. C., (New York), p.127.
Morton, D. C., 1975, Astrophys. J., 197, 85.
Nadeu, D., and Geballe, T. R., 1979, Astrophys. J., 230, 169.
Nee, J. B., and Lee, L. C., 1985, Astrophys. J., 291, 202.
Nee, J. B., and Lee, L. C., 1986, J. Chem. Phys., 84, 5303.
Nercessian, E., Benayoun, J. J., and Viala, Y. P., 1988, Astron. Astrophys., 195, 245.
Neufeld, D. A., and Dalgarno, A., 1989, Astrophys. J., 340, 869.
Nyman, L-Å., 1983, Astron. Astrophys., 120, 307.
Nyman, L-Å., 1984, Astron. Astrophys., 141, 323.
Nyman, L-Å., and Millar, T. J., 1989, Astron. Astrophys., 222, 231.
Ogawa, M., and Cook, G. R., 1958, J. Chem. Phys., 28, 747.
Ogden, P. M., Roesler, F. L., Larson, H. P., Smith, H. A., Reynolds, R. J., and Scherb, F., 1979, Astrophys. J., 233, L21.
Ohishi, M., 1989, "Chemistry and Spectroscopy of Interstellar Matter", p.23.
Ohishi, M., 1991, in "Chemistry and Spectroscopy of Interstellar Molecules", ed. by Kaifu, N. (Tokyo: Univ. of Tokyo Press), p.23.
Ohishi et al., 1995, in preparation.

Ohishi, M., Irvine, W. M., and Kaifu, N., 1992, in IAU Symp. No.150, "Astrochemistry of Cosmic Phenomena", p.171.

Ohishi, M., Kaifu, N., Kawaguchi, K., Murakami, A., Saito, S., Yamamoto, S., Ishikawa, S., Fujita, Y., Shiratori, Y., and Irvine, W. M., 1989, Astrophys. J., 345, L83.

Oka, T., Shimizu, F. O., Shimizu, T., and Watson, J. K. G., 1971, Astrophys. J., 165, L15.

Olofsson, H., 1993, in IAU Coll. No. 146, "Molecular Opacities in the Stellar Environment".

Palmer, P., Zuckerman, B., Buhl, D., and Snyder, L. E., 1969, Astrophys. J., 156, L147.

Phillips, L. F., 1981, J. Phys. Chem., 85, 3994.

Prasad, S. S., and Huntress, W. T. Jr., 1980, Astrophys. J. Suppl., 43, 1.

Prasad, S. S., and Tarafdar, S. P., 1983, Astrophys. J., 267, 603.

Prasad, S. S., Tarafdar, S., P. Villere, K. R., and Huntress, Jr. W. T., 1987, in "Interstellar Processes", ed. D. J. Hollenbach, and Thronson, Jr., (Dordrecht: Reidel), p.631.

Pwa, T. H., and Pottasch, S. R., 1986, Astron. Astrophys., 164, 116.

Qi, T. Y., Pauzat, F., and Berthier, G., 1984, Astron. Astrophys., 135, L1.

Reid, M. J., Schneps, M. H., Moran, J. M, Gwinn, C. R., Genzel, R., Downes, D., and Rönnäng, B., 1988, Astrophys. J., 330, 809.

Righini, G., Simon, M., Joyce, R. R., 1976, Astrophys. J., 207, 119.

Roberge, W. G., 1981, Ph. D. Thesis.

Roberge, W. G., Jones, D., Lepp, S., and Dalgarno, A., 1991, Astrophys. J. Suppl., 77, 287.

Rouger, G. W., and Oort, J. H., 1960, Proc. Nat. Acad. Sci. USA, 46, 1.

Rydbeck, O. E. H., Kollberg, E., Hjalmarson, Å., Sume, A., Ellder, J., and Irvine, W. M., 1976, Astrophys. J. Suppl., 31, 333.

Salahub, D. R., and Sandorfy, C., 1971, Chem. Phys., 98, 147.

Salter, C. J., Emerson, D. T., Steppe, H., and Thum, C., 1989, Astron. Astrophys., 225, 167.

Sanders, D. B., Solomon, P. M., and Scoville, N. Z., 1984, Astrophys. J., 276, 182.

Scalo, J. M., and Slavsky, D. B., 1980, Astrophys. J., 239, L73.

Schinke, R., and Andresen, P., 1984, J. Chem. Phys., 81, 5644.

Scoville, N. Z., Hall, D. N. B., Kleinmann, S. G., and Ridgway, S. T., 1982, Astrophys. J., 253, 136.

Scoville, N. Z., and Solomon, P. M., 1974, Astrophys. J., 187, L67.
Scoville, N. Z., Solomon, P. M., and Jefferts, K. B., 1974, Astrophys. J., 187, L63.
Scoville, N. Z., Solomon, P. M., and Penzias, A. A., 1975, Astrophys. J., 201, 352.
Seab, C. G., and Shull, J. M., 1983, Astrophys. J., 275, 652.
Sharpless, S., 1959, Astrophys. J. Suppl., 4, 257.
Shiratori, Y., Morimoto, M., Kameya, O., Kawaguchi, K., Greaves, S. J., White, G. J., Ishikawa, S., 1995, in preparation.
Simon, M., Righini-Cohen, G., Joyce, R. R., and Simon, T., 1979, Astrophys. J., 230, L175.
Smith, D., and Adams, N. G., 1977, Astrophys. J., 217, 741.
Smith, D., Adams, N. G., Giles, K., and Herbst, E., 1988, Astron. Astrophys., 200, 191.
Snell, R. L., Langer, W. D., and Frerking, M. A., 1982, Astrophys. J., 255, 149.
Snow, T. P., 1980, in IAU symp. No.80, "Interstellar Molecules", ed. by Andrews, B. H., p.247.
Solomon, P. M., and Klemperer, W., 1972, Astrophys. J., 178, 389.
Stacey, G. J., Kurtz, N. T., Smyers, S. D., Harwit, M., Russell, R. W., and Melnick, G., 1982, Astrophys. J., 257, L37.
Stacey, G. J., Lugten, J. B., and Genzel, R., 1987, Astrophys. J., 313, 859.
Stark, G., Yoshino, K., and Smith, P. L., 1987, J. Mol. Spectrosc. 124, 420.
Stief, L. J., Donn, B., Glicker, S., Gentieu, E. P., and Mentall, J. E., 1972, Astrophys. J., 171, 21.
Storey, J. W. V., Watson, D. M., and Townes, C. H., 1981, Astrophys. J., 244, L27.
Storey, J. W. V., Watson, D. M., Townes, C. H., Haller, E. E., and Hansen, W. L., 1981, Astrophys. J., 247, 136.
Suzuki, H., 1979, Prog. Theor. Phys., 62, 18.
Suzuki, H., 1983, Astrophys. J., 272, 579.
Suzuki, H., Yamamoto, S., Ohishi, M., Kaifu, N., Ishikawa, S., Hirahara, Y., and Takano, S., 1992, Astrophys. J., 392, 551.
Swade, D. A., 1989, Astrophys. J., 345, 828.
Swings, P., and Rosenfeld, L., 1937, Astrophys. J., 86, 483.

Takano, S., Masuda, A., Hirahara, Y., Suzuki, H., Ishikawa, S., Kaifu, N., and Ohishi, M., 1991, in "Chemistry and Spectroscopy of Interstellar Molecules", ed. by Bohme, K., Herbst, E., Kaifu, N., Saito, S., (Tokyo: Univ. of Tokyo Press), p. 19.

Takano, T., 1986, Astrophys. J., 300, L85.

Tauber, J. A., Tielens, A. G. G. M., Meixner, M., and Goldsmith, P. F., 1994, Astrophys. J., 422, 136.

Thaddeus, P., Cummins, S. E., and Linke, R. A., 1984, Astrophys. J., 283, L45.

Thronson, H. A. Jr., and Harper, D. A., 1986, Astrophys. J., 300, 396.

Tieftrunk, A., Pineau des Forêts, G., Schilke, P., and Walmsley C. M., 1994, Astron. Astrophys., 289, 579.

Tielens, A. G. G. M., and Hollenbach, D., 1985, Astrophys. J., 291, 722.

Townes, C. H., and Schawlow, A. L., 1955, in "Microwave Spectroscopy", (New York; McGraw-Hill).

Turner, B. E., 1991, Astrophys. J. Suppl., 76, 617.

Turner, B. E., Rickard, L. J., and Xu, L., 1989, Astrophys. J., 344, 292.

Turner, B. E., and Steimle, T. C., 1985, Astrophys. J., 299, 956.

Turner, J. L., and Dalgarno, A., 1977, Astrophys. J., 213, 386.

Ulich, B. L., and Haas, R. W., 1976, Astrophys. J. Suppl., 30, 247.

Umemoto, T., Iwata, T., Fukui, Y., Mikami, H., Yamamoto, S., Kameya, O, and Hirano, N., 1992, Astrophys. J., 392, L83.

Ungerechets, H., Walmsley, C. M., and Winnewisser, G., 1986, Astron. Astrophys., 157, 207.

Urey, H. C., 1952, in " The Planets", chapter IV, Oxford. Univ. Press.

van Dishoeck, E. F., 1988, in "Rate Coefficients in Astrochemistry", ed. by Millar, T. J., and Williams, D. A., (Dordrecht: Kluwer), p.49.

van Dishoeck, E. F., and Black, J. H., 1986, Astrophys. J. Suppl., 62, 109.

van Dishoeck, E. F., and Black, J. H., 1988, Astrophys. J., 334, 771.

van Dishoeck, E. F., and Black, J. H., 1989, Astrophys. J., 340, 273.

van Hemert, M. C., Stehoumwr, A., and van Dishoeck, E. F., 1995, in preparation.

van Woerden, H., Rougoor, G. W., and Oort, J. H., 1957, J. H. Cr. Acad. Sci., 224, 1691.

Viala, Y. P., 1986, Astron. Astrophys. Suppl., 64, 391.

Viala, Y. P., Roueff, E., and Abgrall, H., 1988, Astron. Astrophys., 190, 215.

Vögel, S. N., Genzel, R., and Palmer, P., 1987, Astrophys. J., 316, 243.

Vrtilek, J. M., Gottlieb, C. A., and Thaddeus, P., 1987, Astrophys. J., 314, 716.

Walmsley, C. M., and Ungerechets, H., 1983, Astron. Astrophys., 122, 164.

Watson, W. D., 1973, Astrophys. J., 183, L17.
Watson, W. D., 1974, Astrophys. J., 188, 35.
Watson, D. M., Genzel, R., Townes, C. H., and Storey, J. W. V., 1985, Astrophys. J., 298, 316.
Watson, D. M., Storey, J. W. V., Townes, C. H., Haller, E. E., and Hansen, W. L., 1980, Astrophys. J., 239, L129.
Weinreb, S., Barret, A. H., Meeks, M. L., and Henry, J. C., 1963, Nature, 200, 829.
White, R. E., 1977, Astrophys. J., 211, 744.
Whiteoak, J. B., and Gardner, F. F., 1979, Mon. Not. R. astr. Soc, 188, 445.
Wilson, R. F., 1981, Astrophys. J., 247, 116.
Wilson, R. W., Jefferts, K. B., and Penzias, A. A., 1970, Astrophys. J., 161, L43.
Wilson, R. W., Penzias, A. A., Jefferts, K. B., Kutner, M., and Thaddeus, P., 1971, Astrophys. J., 167, L97.
Wlodek, S., and Bohme, D. K., 1988, J. Am. Chem. Soc., 110, 2396.
Wlodek, S., and Bohme, D. K., 1989, J. Am. Chem. Soc., 111, 61.
Wlodek, S., Fox, A., Bohme, D. K., 1987, J. Am. Chem. Soc., 109, 6663.
Wong, M. W., Gill, P. M. W., Nobes, R. H., and Random, L., 1988, J. Phys. Chem., 92, 4875.
Wooten, A., Snell, R., and Glassgold, A. E., 1979, Astrophys. J., 234, 876.
Wright, M. C. H., Plambeck, R. L., Vogel, S. N., Ho, R. T. P, Welch, W. J., 1983, Astrophys. J., 267, L41.
Wright, M. C. H., and Plambeck, R. L., 1980, Astrophys. J., 267, L115.
Yamamoto, S., Mikami, H., Saito, S., Kaifu, N., Ohishi, M., and Kawaguchi, K., 1992, Publ. Astron. Soc. Japan, 44, 459.
Yoshino, K., Stark, P. L., Smith, P. L., and Parkinson, W. H., 1995, J. de Physique, in press.
Ziurys, L. M., 1988, Astrophys. J., 324, 544.
Ziurys, L. M., and Friberg, P., 1987, Astrophys. J, 314, L49.
Ziurys, L. M., and Friberg, P., and Irvine, W. M., 1989, Astrophys. J., 343, 201.

Appendixes

A.1. Physical and Chemical Properties of Sagittarius B2

The Sagittarius B2 (Sgr B2) is situated at about 150 pc from the Galactic Center assuming the distance of 8.5 kpc to the Sgr B2 (Fig. 3). The Sgr B2 region is the most prominent and massive concentration of molecular gas and active star forming region in the vicinity of the galactic center. The gas mass is about $M \sim 3 \times 10^6 M_\odot$ over $d \sim 40$ pc diameter (Bally et al. 1987). The Sgr B2 region is known as one of the most luminous objects in millimeter-wavelength although it is not observed by optical because of high visual extinction in the line of sight. The Sgr B2 cloud has a complex chemistry and structure, with gas densities ranging from $n(H_2) > 10^2$ cm^{-3} ($M = 3 \times 10^6 M_\odot$) in the 40 pc "envelope" (sampled by the mm transitions of CO; Scoville, Solomon and Penzias 1975) to $n(H_2) \geqq 10^7$ cm^{-3} in small ($d \sim 0.1$ pc) condensations associated with newly-formed stars and H_2O masers near the cloud core.

Many molecular species are discovered in this region (Cummies et al. 1986), and the region is one of the four objects (OMC-1, TMC-1, IRC+10216, Sgr B2) which line surveys are conformed.

Lower density gas in the envelope of the cloud can be sampled in the far-infrared through absorption in the lowest rotational transitions of light hydrides like OH and CH. The 119 μm $^2\Pi_{3/2}$ J=3/2-5/2 transitions of ^{16}OH, which was first detected in absorption toward the far-infrared continuum peak by Storey et al. (1981), and was very large optical depths ($\tau > 50$). Absorption of CH was detected by Stacey et al. (1987) and of ^{18}OH by Lugten, Stacey and Genzel (1995). The far-infrared absorption lines of the latter two molecules are optically thin and can be used to investigate abundance and excitation of CH and OH by comparison of their radio and far-infrared lines. In the case of ^{18}OH, the measurements indicate a very low ($T_{ex} = 4$ K) excitation temperature of the ground state Λ doublet. Lugten et al. (1995) conclude that the low excitation temperature is the result of excitation of the molecular states at moderate densities ($n(H_2) = 10^2$ to a few 10^3 cm^{-3}), to give the strong parity dependence of the collisional cross sections of OH with H_2 (Schinke and Andresen 1984). In the case of CH, the measurements by Stacey et al. (1987) show that the ground state Λ doublet is definitely inverted with $T_{ex} = -5$ to -15 K, thus confirming earlier measurements in the radio and UV region (Rydbeck et al. 1976, Genzel et al. 1979, Jura and Meyer 1985).

From the millimeter/submillimeter continuum observation by Lis (1989), the central 5-10 pc diameter core of Sgr B2 is an active region of star formation with a total luminosity of $L = 10^7 L_\odot$ and a total mass of $M = 10^5 M_\odot$. Within this region, Benson and Johnston (1984) find about a dozen HII regions with exciting stars earlier than O6. These compact HII regions distribute in three groups (Sgr B2 north(N), Sgr B2 middle(M), and Sgr B2 south(S)). Of these, northern two groups are known as strong continuum sources by Martin and Downes (1972)(11" at 2.7 GHz; 6" at 5 GHz). Each is named MD4 (Sgr B2(N)) and MD5 (Sgr B2(M)) after the results of Martin and Downes (1972). Both MD4 and MD5 have a total mass of $M = 10^5 M_\odot$ spacing about 2 pc (Fig. 4).

Sgr B2 is also a strong source of infrared emission ($L \sim 5 \times 10^5 L_\odot$; Harvey, Campbell and Hoffman 1977; Righini, Simon and Joyce 1976). This is powered by massive young stars which also maintain ionized regions.

One of the most interesting results of the high resolution continuum studies of Sgr B2 is a striking difference between distribution of the 350 μm and the 1100 μm continuum emission (Goldsmith et al. 1990). The 1100 μm emission peaks at the position of Sgr B2 north(N), where no excess 350 μm emission is observed. It has been suggested that the observed change in the middle-to-north peak flux ratio is caused by the facts that the northern source is situated behind the dust cloud associated with Sgr B2(M), and its emission is attenuated by cold foreground dust (Thronson and Harper 1986, Goldsmith, Snell, and Lis 1987). Also at the position of Sgr B2(N), the column density of H_2 is very high ($N(H_2) = 3 \times 10^{24}$ cm^{-2}, $A_V = 10^3$ mag; Goldsmith et al. 1990).

Various chemical species show different spatial distribution. Goldsmith et al. (1987) show that the SO line peaks at the position of MD5, but other species peak at that of MD4. Goldsmith et al. (1987) conclude that the differences in spatial distributions of the various chemical species cannot be attributed to excitation or radiative transport effects but must be a consequence of spatial variation in chemical abundance.

MD4 and MD5 are associated with many maser sources (H_2O, H_2CO, CH_3OH, SiO, and OH; Garay, Reid and Moran 1985; Benson and Johnston 1984; Genzel, Downes, and Bieging 1976; Hasegawa et al. 1985; Morimoto, Ohishi, and Kanzawa 1985; Gardner et al. 1986).

Denser, compact regions have been found in recent interferometric observations. By the observations of metastable and non-metastable NH_3 inversion lines with the VLA (Vogel et al. 1987), found two compact regions (d = 0.2 pc) of NH_3 emission and absorption associated with the strong H_2O masers

Sgr B2(N) and Sgr B2(M). Carlstrom and Vogel (1987) found the same condensations in SO 3 mm emission from Hat Creek interferometer observations. The northern NH_3 and SO knot is also a strong 3 mm continuum source, indicating the presence of either an extremely small and dense (d = 0.006 pc, $\langle n_e \rangle = 3 \times 10^6$ cm^{-3}) HII region or, more likely, of a large concentration of dust. The latter interpretation also fits well the NH_3 data which indicate high hydrogen column densities of $N(H_2) = 10^{25}$ cm^{-2}. From the excitation of different NH_3 lines, Vogel et al. (1987) derive molecular hydrogen densities $n(H_2) > 10^7$ cm^{-3} and gas kinetic temperatures of 200 K. In the dense molecular condensations, Goldsmith et al. (1987) find vibrationally excited HC_3N in Sgr B2 (N), further supporting the existence of highly excited molecular material near the maser. The NH_3 and SO data as well as the proper motion measurements of the H_2O masers in Sgr B2 (N) by Reide et al. (1988) show that the dense molecular gas is expanding.

A.2. Chopper-Wheel Method

The Chopper-Wheel method is currently used to calibrate the intensity of millimeter-wavelength spectral lines (Ulich and Hass 1976). A rotating chopper-wheel is used in this calibration. A microwave absorber at ambient temperature (usually 293 K) is alternatively introduced and removed at a point just in front of the antenna feed horn, resulting in a calibration signal equal to the temperature difference between the absorber and the antenna. This method produces a thermal scale (the antenna temperature; T_A^*) corrected by the atmospheric extinction.

When the absorbing material, of which optical depth τ is constant, on the chopper-wheel at ambient temperature T_{atm} covers the feed horn aperture, the antenna temperature looking at the ON point T_{on} , that looking at the OFF point T_{off}, and that looking at the Dummy Load, T_{load} are given by

$$T_{on} = G\,[T_{rx} + T_{atm}\,\{1-\exp(-\tau \sec Z)\} + T_A^* \exp(-\tau \sec Z)\}], \qquad (A.2.1)$$

$$T_{off} = G\,[T_{rx} + T_{atm}\,\{1-\exp(-\tau \sec Z)\}], \qquad (A.2.2)$$

$$T_{load} = G\,(T_{rx} + T_l), \qquad (A.2.3)$$

respectively, where T_l and T_{rx} are the temperature of the dummy load and the receiver temperature, and G and Z are the receiver power gain and the zenith distance.

When the ambient temperature T_{atm} and the temperature of the dummy load T_l are equal, the antenna temperature T_A^* is given by,

$$T_A^* = T_{atm}\,(T_{on} - T_{off}) / (T_{load} - T_{off}). \qquad (A.2.4)$$

The uncertainty in the determination of antenna temperature is believed to be less than 10 %.

A.3. Determination of Rotational Temperature Using NH_3 lines

The rotational energy of NH_3 is a function of the two principal quantum numbers (J, K), corresponding to the total angular momentum and its projection along the molecular axis. The molecules has an electric dipole moment only the molecular axis, and the dipole selection rules are $\Delta K = 0$, $\Delta J = 0, \pm 1$. Interaction between rotational and vibrational motions, even in the lowest vibrational state, induces a small dipole moment perpendicular to the rotational axis, giving rise to very slow $\Delta k = \pm 3$ ($K = |k|$) transition moment (Oka et al. 1971) except for this, the K-ladders are essentially independent one another. Normal intermolecular collisions (not involving weak magnetic effects) also produce only transitions in which Δk is a multiple of 3 (including 0). Within each K-ladder, the levels with $J > K$ are called nonmetastable state because they can decay rapidly (10-100 s) via the far-infrared $\Delta J = 1$ transitions and the levels with $J = K$ are called metastable state. The brightness temperature Tmb is given by the radiative transfer equation

$$Tmb = \{J(Tex)-Tc^{BG}-J(Tbg)\}\ \{1-\exp(-\tau_m)\}, \qquad (A.3.1)$$

where η is the beam efficiency (0.67), $\tau_m(J,K)$ is the optical depth of the main component (J,K), Tex is the excitation temperature, Tbg is the brightness temperature of the cosmic background radiation, $Tc^{BG} = Tcont/\eta$ is the continuum brightness temperature, J(T) is the Planck function $(J(T) = (h\nu/k) / [\exp(h\nu / kT)-1])$.

h : Planck constant
k : Boltzmann constant
ν : Transition frequency

Assuming the excitation temperature of the $NH_3(1,1)$ line is equal to that of the $NH_3(2,2)$ lines ($Tex(1,1) = Tex(2,2)$), and Tc^{BG} and J(Tbg) at the frequencies of $NH_3(1,1)$ and $NH_3(2,2)$ are assumed to be equal, we find the following formula,

$$\frac{Tmb(2,2)}{Tmb(1,1)} = \frac{1-\exp(-\tau_m(2,2))}{1-\exp(-\tau_m(1,1))}. \qquad (A.3.2)$$

From (A.3.2), the optical depth is given by

$$\tau_m(2,2) = -\ln[1-\{1-\exp(\tau_m(1,1))\frac{T_{mb}(2,2)}{T_{mb}(1,1)}\}]. \quad (A.3.3)$$

According to Ho et al. (1983), the rotational temperature $T_R(2,2;1,1)$ is given by

$$\frac{\tau_m(2,2)}{\tau_m(1,1)} = \frac{\nu^2(2,2)\,\Delta\nu(1,1)\,Tex(1,1)\,|\mu(2,2)^2|\,g(2,2)}{\nu^2(1,1)\,\Delta\nu(2,2)\,Tex(2,2)\,|\mu(1,1)^2|\,g(1,1)}\exp\left(\frac{-\Delta E}{kT_R}\right). \quad (A.3.4)$$

From the equation (A.3.4), we obtain the following relation,

$$\exp\left(\frac{-\Delta E}{kT_R}\right) = \frac{9}{20}\left(\frac{\nu_{11}}{\nu_{22}}\right)\left(\frac{\tau_m(J,K)}{\tau_m(J,K)}\right), \quad (A.3.5)$$

where ΔE is the energy difference between (J,K) = (1,1) and (2,2) levels, and corresponds to 41.5 K.

When (A.3.3) is substituted into (A.3.5), we obtain,

$$\exp\left(\frac{-41.5}{kT_R}\right) = \frac{9}{20}\left(\frac{\nu_{11}}{\nu_{22}}\right)\ln[1-\{1-\exp(\tau_m(1,1))\}]\left(\frac{T_{mb}(2,2)}{T_{mb}(1,1)}\right). \quad (A.3.6)$$

Then, the rotational temperature $T_R(2,2;1,1)$ is given by,

$$T_R(2,2;1,1) = \frac{-41.5}{\ln\left(\frac{-0.282}{\tau_m(1,1)}\ln[1-\frac{T_{mb}(1,1)}{T_{mb}(2,2)}\{1-\exp(-\tau_m(1,1))\}]\right)}. \quad (A.3.7)$$

A.4. LVG (Large Velocity Gradient) Model Calculation

The rotational levels of the diatomic molecule are indexed by the rotational angular-momentum quantum number J. The J level has energy

$$E_J = hBJ(J+1), \tag{A.4.1}$$

where h is Planck's constant and B is the rotational constant. The fraction of molecules in the J rotational state divided by the degeneracy 2J+1 is represented by the symbol n_J,

$$\sum_{J=0}^{\infty}(2J+1)n_J = 1, \tag{A.4.2}$$

The rate coefficients of the spontaneous and stimulated emission from the J+1 to the J level are denoted by their conventional symbols $A_{J+1,J}$ and $B_{J+1,J}$. Note that the Einstein coefficient should not be confused with the unsubscribed molecular rotation constant B:

$$A_{J+1,J} = \frac{16hB^3}{c^2}(J+1)^3 B_{J+1,J}, \tag{A.4.3}$$

$$B_{J+1,J} = \frac{32\pi^4\mu^2}{3hc^2}\frac{(J+1)}{(2J+3)}, \tag{A.4.4}$$

where μ is the molecular electronic dipole moment and c is the velocity of light.

Radiative transition with $\Delta J \neq 0, \pm 1$ are forbidden by selection rules. This numerical calculations are based on a large velocity gradient (LVG) approximation. This simple analysis is used in general because it gives similar results with complicated analysis based on more realistic assumption (e.g., White 1977; Castets et al. 1990). Also strictly speaking, this approximation lies in the assumption of uniform density in a cloud. However it is adopted to the cloud with a density gradient in this thesis.

The equation of statistical equilibrium of the J-level is given by

$$(2J+1)\frac{dn_J}{dT} = \beta_{J+1,J}A_{J+1,J}(2J+3)n_{J+1}$$

$$- \beta_{J,J-1}A_{J,J-1}(2J+1)n_J$$

$$+ \frac{\beta_{J+1,J}A_{J+1,J}(2J+3)(n_{J+1}-n_J)}{[\exp\{2hB(J+1)/kT_{bg}\}-1]}$$

$$- \frac{\beta_{J,J-1}A_{J,J-1}(2J+1)(n_J-n_{J-1})}{[\exp\{2hBJ/kT_{bg}\}-1]}$$

$$+ \sum_{L=J+1}^{\infty} C[(2L+1)n_L-(2J+1)n_J]$$

$$- \sum_{L=0}^{J} C[(2L+1)nJ-(2J+1)n_L]. \qquad (A.4.5)$$

In the right side of this formula, the first and second terms denote transitions of the spontaneous emission, the third and forth terms denote transitions induced by background radiation, and the fifth and sixth terms denote transitions induced by collisional process.

The average escape probability of a photon emitted in a transition from the J+1 to the J rotational level is expressed as follows, by using a simple modification of Castor's results

$$\beta_{J+1,J} = \frac{[1-\exp(-\tau_{J+1,J})]}{\tau_{J+1,J}}, \qquad (A.4.6)$$

(Castor 1970), where $\tau_{J+1,J}$ is the optical depth.

$$(2J+1)\frac{dn_J}{dT} = \beta_{J+1,J}A_{J+1,J}(2J+3)n_{J+1}. \qquad (A.4.7)$$

If the system is in thermal equilibrium, we can assume $dn_J/dT=0$ in the all J-levels.

$$
\begin{aligned}
0 = {} & \beta_{J+1,J}A_{J+1,J}(2J+3)n_{J+1} \\
& - \beta_{J,J-1}A_{J,J-1}(2J+1)n_J \\
& + \frac{\beta_{J+1,J}A_{J+1,J}(2J+3)(n_{J+1}-n_J)}{[\exp\{2hB(J+1)/kT_{bg}\}-1]} \\
& - \frac{\beta_{J,J-1}A_{J,J-1}(2J+1)(n_J-n_{J-1})}{[\exp\{2hBJ/kTbg\}-1]} \\
& + \sum_{L=J+1}^{20} C[(2L+1)n_L-(2J+1)n_J] \\
& - \sum_{L=0}^{J-1} C[(2L+1)n_J-(2J+1)n_L]. \qquad \text{(A.4.8)}
\end{aligned}
$$

The collisional coefficients calculated by Green and Chapman(1978) are used in the H_2-CS collision and H_2-SiO collision in this thesis.

Then, kinetic temperature (Tk), molecular hydrogen density ($n(H_2)$), and the relative abundance divided by velocity gradient ($X(x)/(\Delta v/\Delta r)$) are changed as parameters, non-linear simultaneous equations of (A.4.2), (A.4.3) and (A.4.6) are solved to get the excitation temperatures and optical depths.

A.5. Determination Method of Molecular Column Densities

The equation of radiative transfer, which relates the observed excess brightness temperatures Tmb and the excitation temperature Tex is given by

$$Tmb = \{J(Tex)-T_C^{BG}-J(Tbg)\}\{1-\exp(-\tau)\}, \quad (A.5.1)$$

where J(T)is the source function , Tex is the excitation temperature of the observed transition, and Tbg is the background temperature, respectively. At line center the opacity is given by

$$\tau = \frac{\lambda^2 A\, g_u}{8\pi\delta\nu\, g_l} N_l \left[1-\exp\left(-\frac{h\nu}{kTex}\right)\right]. \quad (A.5.2)$$

If $\tau \ll 1$, then the brightness temperature is transformed to

$$Tmb = \{J(Tex)-T_C^{BG}-J(Tbg)\}\,\tau. \quad (A.5.3)$$

And then, (A.5.2) and (A.5.3) yield the following formula

$$W = \{J(Tex)-T_C^{BG}-J(Tbg)\}\Delta V \frac{\lambda^2 A g_u}{8\pi\delta\nu g_l} N_l \left[1-\exp\left(-\frac{h\nu}{kTex}\right)\right], \quad (A.5.4)$$

where W is an integrated brightness temperature given by $W = \int Tmb\,\Delta V$.

Next, when the Rayleigh-Jeans approximation ($h\nu/kT \ll 1$) has been used, eq. (A.5.4) is transformed to

$$W = \frac{Tex-T_C^{BG}-Tbg}{Tex}\Delta V \frac{\lambda^2 A g_u}{8\pi\delta\nu g_l} Nu \frac{h\nu}{k}. \quad (A.5.5)$$

Then the upper state column density of a specie is given by

$$Nu = \frac{Tex}{(Tex-T_C^{BG}-Tbg)} \frac{8\pi\delta\nu g_l k}{\lambda^2 A g_u h\nu} W. \quad (A.6.6)$$

Finally, the assumption of LTE is made by taking all Tex to equal a fixed value, then

$$\frac{Nu}{N} = \frac{g_u g_k g_l}{Q_{rot}} \exp\left(\frac{E_u}{kTex}\right). \qquad (A.5.7)$$

where Eu is the upper energy level, T_{ex} is the rotational temperature, k is the Boltzmann constant(1.3807×10^{-23} J•K^{-1}), v is the frequency of the molecule, c is the light velocity, g_u is the rotational degeneracy of the upper level, g_k is the k-level degeneracy, g_l is the reduced nuclear spin degeneracy, Q_{rot} is the rotational partition function, (A.5.6) and (A.5.7) yield the total column density of a specie,

$$N = \frac{\tau}{A} \exp(-E_u / kTex)\, Tex \frac{8\pi k v^2}{hc^2 g_u g_k g_l} Q_{rot} \Delta V, \qquad (A.5.8)$$

where A is the Einsein coefficient, Tc the brightness temperature of the continuum source Sgr B2, and τ the optical depth. The Tc value was calculated from the results of continuum observations by Lis (1989), Salter et al. (1989) and Akabane et al. (1988) as listed in Table 5.

We note that the correct energy on the right-hand side is E_u (as used by Cummins et al. 1986 and Blake et al. 1987) and not E_l (as used by Johansson et al. 1984), although the effect of this difference is small, commensurate with the Rayleigh-Jeans approximation and is not important at $\lambda = 3$ mm.

The rotational partition function Qrot is defined as

$$Q_{rot} = \sum_{\text{all Ei}} g_j \exp\left(-\frac{E_i}{kTex}\right), \qquad (A.5.9)$$

where $g_j = 2J + 1$ is the rotational degeneracy. Qrot may be evaluated numerically, provided a sufficient number of energy levels are used. A sufficient number may in fact be very large when the molecular rotation constants are small and Tex is high. However, in the case of this thesis, only Tex is small. Therefore, only a small number of energy levels are used in the calculation.

A.6. Determination Method of Correlation Coefficients

Correlation coefficients are used in order to describe the degree of the correlation between the variances.

If the two variance $\{(x_i, y_i)\}$ $(i = 1, \ldots\ldots, n)$ are given, covariance between x and y are given by

$$S_{xy} = \sum_{i=1}^{n} (x_i - x)(y_i - y)$$

$$= \sum_{i=1}^{n} x_i y_i - \frac{T_x T_y}{n}, \qquad \text{(A.6.1)}$$

where T_x, T_y are the sum, x, y is the average, and S_{xy} is the change of variances xy, respectively. And T_y, y, and S_y is the similar as the former.

Then, the correlation coefficients are given by

$$r_{xy} = \frac{S_{xy}}{\sqrt{S_x S_y}}. \qquad \text{(A.6.2)}$$

This correlation coefficients are in the range between -1 and +1 ($-1 \leqq r_{xy} \leqq +1$). The characteristic of the correlation coefficients is as follows:

If $r_{xy} > 0$, the correlation has a positive correlation. When the values of xi become larger, the values of yi become larger. When the values of xi become smaller, the values of yi become smaller. If $r_{xy} < 0$, the correlation has a negative correlation. If $r_{xy} = 0$, the correlation between xi and yi has no apparent correlation. Then, the values of xi and those of yi are irrelevance.

In summary, the correlation relation is linearly stronger, $|r_{xy}|$ becomes nearer to one. On the other hand, it is weaker, $|r_{xy}|$ becomes nearer to zero.

Tables

Table 1; Identified Interstellar Molecules (1994, July)

Simple Hydrides, Oxides, Sulfides, Halides, and Related Molecules

H_2	CO	NH_3	CS	NaCl[a]
HCl	SiO	SiH_4 [IR][ab]	SiS	AlCl[a]
H_2O	SO_2	C_2	H_2S	KCl[a]
HNO	OCS	CH_4 [IR][ab]	PN	AlF[a]
NNO	NaCl[a]			

Nitrides, Acetylene Derivatives, and Related Molecules

C_3 [IR][ab]	HCN	CH_3NC	CH_3CH_2CN	C_2H_4 [IR][ab]
C_5 [IR][ab]	HC_3N	CH_3CN	CH_2CHCN	C_2H_2 [IR][ab]
C_2O	HC_5N	CH_3C_3N	HNC	HCCNC
C_3O	HC_7N	CH_3C_2H	HNCO	HNCCC
C_3S	HC_9N	CH_3C_4H	HNCS	CH_3NC
C_4Si	$HC_{11}N$	CH_3C_3N?[c]	H_2C_3	HC_2CHO
H_2C_4				

Aldehydes, Alchols, Eters, Ketons, Amides, and Related Molecules

H_2CO	CH_3OH	HCOOH	CH_2NH
H_2CS	CH_3CH_2OH	$HCOOCH_3$	CH_3NH_2
CH_3CHO	CH_3SH	$(CH_3)_2O$	NH_2CN
NH_2CHO	$(CH_3)_2CO$?[c]	H_2CCO	CH_2CC
CH_2CCC			

Cyclic Molecules

c-C_3H_2	SiC_2[a]	c-C_3H

(Table 1, continued)

Ions

HCS^+	HCO^+	$HCNH^+$	H_3O^+
HN_2^+	$HOCO^+$	SO^+	H_2D^+?[c]
HOC^+	H_2COH^+	HC_3NH^+	
CH^+ [OPT][d]			

Radicals

OH	C_3H	CN	HCO	C_2S
CH	C_4H	C_3N	NO	NS
C_2H	C_5H	H_2CCN	SO	SiC[a]
CH_2N	C_6H	CP[a]	SiN[a]	NH [UV][e]
HCCN[a]	C_2O	MgNC[a]	MgCN[a]	HCO
CH_2CN				

[a] ; Detected only in the envelope around the evolved star IRC+10216

[b] IR; Detected by infrared observation

[c] ?; Claimed but not yet confirmed

[d] OPT; Detected by optical observation

[e] UV; Detected by UV observation

Table 2; Molecular Transitions Used in This Thesis

Species	Transition	Frequency (GHz)	R.m.s.[a] (K)	HPBW[b]	Ref.
^{12}CO	J = 1-0	115.27	0.10	42"	c
^{13}CO	J = 1-0	110.20	0.15	42"	c
^{13}CO	J = 1-0	110.20	0.15	15"	d
$C^{18}O$	J = 1-0	109.78	0.04	15"	d
^{12}CN	N = 1-0	113.49	0.04	14"	d
^{13}CN	N = 1-0	108.78	0.04	15"	d
$C^{32}S$	J = 1-0	48.99	0.05	33"	e
$C^{32}S$	J = 2-1	97.98	0.07	17"	e
$C^{34}S$	J = 1-0	48.20	0.03	34"	e
$C^{34}S$	J = 2-1	96.41	0.07	17"	d
SO	$J_N = 3_2$-2_1	99.29	0.02	16"	d
^{28}SiO	J = 1-0	43.42	0.02	38"	f
^{28}SiO	J = 2-1	86.84	0.07	19"	f
^{29}SiO	J = 1-0	42.87	0.02	38"	f
$H^{12}CN$	J = 1-0	88.63	0.04	18"	d
$H^{13}CN$	J = 1-0	86.34	0.04	19"	e
$HN^{12}C$	J = 1-0	90.66	0.03	18"	d
$HN^{13}C$	J = 1-0	87.09	0.07	19"	d
$H^{12}CO^+$	J = 1-0	89.18	0.07	18"	g
$H^{13}CO^+$	J = 1-0	86.75	0.07	19"	f
NH_3	(1,1)-(1,1)	23.69	0.03	80"	d
NH_3	(2,2)-(2,2)	23.72	0.03	80"	d
NH_3	(3,3)-(3,3)	23.87	0.03	80"	d
NH_3	(4,4)-(4,4)	24.13	0.04	80"	d
NH_3	(5,5)-(5,5)	24.53	0.03	80"	d
NH_3	(6,6)-(6,6)	25.56	0.04	80"	d
NH_3	(7,7)-(7,7)	25.71	0.03	80"	d
HC_3N	J = 1-0	9.09	0.03	180"	d
HC_3N	J = 2-1	18.19	0.05	90"	d
HC_3N	J = 4-3	36.39	0.02	45"	d
HC_3N	J = 5-4	45.49	0.03	36"	d

(Table 2, continued)

C_3H_2	$1_{1,0}$-$1_{0,1}$	18.34	0.05	90"	d
C_3H_2	$2_{2,0}$-$2_{1,1}$	21.58	0.03	77"	d
C_3H_2	$2_{0,2}$-$1_{1,1}$	82.09	0.04	20"	d
C_3H_2	$2_{1,2}$-$1_{0,1}$	85.33	0.02	19"	e
CH_3OH	0_2-1_{-1} E	108.89	0.10	15"	d

[a] R.m.s. noise temperature of the brightness temperature, in unit K.

[b] Half-Power Beam Width of the telescope used for the observation.

[c] Observed by Lis (1989) with FCRAO 14m telescope.

[d] Observed by Ohishi et al. (1995; line survey) with NRO 45m telescope.

[e] Observed by Greaves et al. (1992) with NRO 45m telescope.

[f] Observation by us with NRO 45m telescope.

[g] Observed by Morimoto et al. (1983) with NRO 45m telescope.

Table 3; Brightness Temperatures of the Molecular Absorption Lines[a]

Velocity Component (km/s)	^{12}CO J = 1-0 (Lis)[b]	^{13}CO J = 1-0 (Lis)[b]	^{13}CO J = 1-0 (Ohishi)[c]	$C^{18}O$ J = 1-0	^{12}CN N = 1-0	^{13}CN N = 1-0
+22	-	1.0 (0.2)	≦0.16	≦0.12	0.40 (0.04)	0.51 (0.02)
+3	1.2 (0.1)	0.4 (0.1)	≦0.16	≦0.12	0.42 (0.04)	0.24 (0.02)
-20	1.4 (0.1)	0.1 (0.1)	1.43 (0.13)	0.38 (0.04)	0.60 (0.04)	0.15 (0.03)
-28	1.6 (0.1)	0.4 (0.2)	1.06 (0.15)	0.32 (0.04)	0.56 (0.04)	0.15 (0.03)
-42	0.9 (0.1)	0.9 (0.2)	1.51 (0.15)	1.28 (0.03)	0.60 (0.04)	0.19 (0.03)
-46	0.8 (0.1)	0.5 (0.2)	1.36 (0.15)	0.84 (0.04)	0.60 (0.04)	0.08 (0.02)
-76	1.1 (0.1)	-	0.91 (0.16)	≦0.12	0.44 (0.04)	0.13 (0.02)
-92	1.6 (0.1)	-	0.42 (0.02)	≦0.12	0.42 (0.08)	0.13 (0.02)
-105	0.6 (0.1)	-	0.57 (0.04)	≦0.12	0.51 (0.04)	0.33 (0.02)

(Table 3, continued)

Velocity Component (km/s)	$C^{32}S$ J = 1-0	$C^{32}S$ J = 2-1	$C^{34}S$ J = 1-0	$C^{34}S$ J = 2-1	SO $J_N = 3_2$-2_1	^{28}SiO J = 1-0
+22	≦0.38	≦0.83	0.11 (0.03)	0.29 (0.03)	≦0.28	≦0.07
+3	1.42 (0.03)	2.04 (0.11)	0.25 (0.03)	0.72 (0.03)	0.53 (0.04)	0.57 (0.01)
-20	0.62 (0.03)	1.01 (0.15)	0.18 (0.03)	-	≦0.06	0.10 (0.02)
-28	0.54 (0.03)	1.02 (0.11)	0.16 (0.03)	-	≦0.06	0.10 (0.02)
-42	1.60 (0.03)	2.48 (0.06)	0.39 (0.03)	-	0.50 (0.02)	0.10 (0.02)
-46	0.59 (0.03)	1.36 (0.07)	0.24 (0.03)	-	0.38 (0.02)	0.10 (0.02)
-76	0.54 (0.03)	1.38 (0.07)	≦0.10	-	≦0.06	≦0.07
-92	0.42 (0.03)	1.32 (0.07)	≦0.10	-	≦0.06	0.40 (0.01)
-105	1.34 (0.03)	2.07 (0.07)	≦0.10	-	≦0.06	0.36 (0.01)

(Table 3, continued)

Velocity Component (km/s)	^{28}SiO J = 2-1	^{29}SiO J = 1-0	H^{12}CN J = 1-0	H^{13}CN J = 1-0	HN^{12}C J = 1-0	HN^{13}C J = 1-0
+22	≦0.21	≦0.07	≦0.44	0.38 (0.03)	≦0.09	0.23 (0.07)
+3	0.62 (0.09)	0.19 (0.05)	0.94 (0.04)	1.58 (0.03)	0.50 (0.04)	0.38 (0.07)
-20	≦0.21	≦0.07	1.29 (0.04)	0.22 (0.03)	-	≦0.21
-28	≦0.21	≦0.07	1.32 (0.08)	0.22 (0.03)	-	≦0.21
-42	≦0.21	≦0.07	1.38 (0.12)	0.30 (0.03)	-	≦0.21
-46	≦0.21	≦0.07	1.31 (0.12)	0.22 (0.03)	-	≦0.21
-76	≦0.21	≦0.07	0.75 (0.04)	≦0.09	-	≦0.21
-92	0.48 (0.07)	≦0.07	1.04 (0.04)	0.28 (0.03)	-	≦0.21
-105	0.44 (0.07)	≦0.07	1.22 (0.04)	0.64 (0.03)	-	0.31 (0.05)

(Table 3, continued)

Velocity Component (km/s)	$H^{12}CO^+$ J = 1-0	$H^{13}CO^+$ J = 1-0	NH_3 (1,1)-(1,1)	NH_3 (2,2)-(2,2)	NH_3 (3,3)-(3,3)	NH_3 (4,4)-(4,4)
+22	0.25 (0.10)	1.00 (0.07)	≦0.09	≦0.09	≦0.09	≦0.12
+3	0.60 (0.10)	1.04 (0.07)	0.58 (0.03)	0.51 (0.02)	0.48 (0.02)	0.44 (0.04)
-20	0.45 (0.10)	0.22 (0.06)	0.16 (0.03)	0.11 (0.02)	≦0.09	≦0.12
-28	0.35 (0.09)	≦0.21	0.14 (0.03)	0.11 (0.02)	≦0.09	≦0.12
-42	0.50 (0.09)	0.75 (0.06)	0.21 (0.03)	≦0.09	≦0.09	≦0.12
-46	0.46 (0.10)	0.22 (0.06)	0.20 (0.03)	≦0.09	≦0.09	≦0.12
-76	≦0.30	≦0.21	0.13 (0.03)	≦0.09	0.13 (0.03)	≦0.12
-92	-	≦0.21	0.19 (0.03)	0.14 (0.02)	0.15 (0.03)	≦0.12
-105	-	0.83 (0.09)	0.34 (0.03)	0.26 (0.02)	0.26 (0.02)	0.16 (0.04)

(Table 3, continued)

Velocity Component (km/s)	NH_3 (5,5)-(5,5)	NH_3 (6,6)-(6,6)	NH_3 (7,7)-(7,7)	HC_3N J = 1-0	HC_3N J = 2-1	HC_3N J = 4-3
+22	≦0.09	≦0.12	≦0.09	≦0.10	≦0.15	≦0.03
+3	0.26 (0.03)	0.31 (0.04)	0.13 (0.03)	≦0.10	≦0.15	0.28 (0.01)
-20	≦0.09	≦0.12	≦0.09	≦0.10	≦0.15	0.06 (0.01)
-28	≦0.09	≦0.12	≦0.09	≦0.10	≦0.15	0.06 (0.01)
-42	≦0.09	≦0.12	≦0.09	≦0.10	≦0.15	≦0.03
-46	≦0.09	≦0.12	≦0.09	≦0.10	≦0.15	≦0.03
-76	≦0.09	≦0.12	≦0.09	≦0.10	≦0.15	≦0.03
-92	≦0.09	≦0.12	≦0.09	≦0.10	≦0.15	≦0.03
-105	0.10 (0.03)	≦0.12	≦0.09	≦0.10	≦0.15	0.15 (0.02)

(Table 3, continued)

Velocity Component (km/s)	HC_3N J = 5-4	C_3H_2 $1_{1,0}$-$1_{0,1}$	C_3H_2 $2_{2,0}$-$2_{1,1}$	C_3H_2 $2_{0,2}$-$1_{1,1}$	C_3H_2 $2_{1,2}$-$1_{0,1}$	CH_3OH 0_2-1_{-1} E
+22	≦0.09	≦0.15	≦0.09	≦0.12	0.16 (0.04)	≦0.09
+3	0.36 (0.03)	0.40 (0.05)	≦0.09	0.32 (0.04)	0.91 (0.04)	0.62 (0.03)
-20	≦0.09	≦0.15	≦0.09	≦0.12	0.36 (0.04)	≦0.09
-28	≦0.09	≦0.15	≦0.09	≦0.12	0.33 (0.04)	≦0.09
-42	≦0.09	0.26 (0.05)	≦0.09	≦0.12	1.03 (0.04)	0.33 (0.03)
-46	0.10 (0.03)	≦0.15	≦0.09	≦0.12	0.67 (0.04)	0.29 (0.03)
-76	≦0.09	0.19 (0.05)	≦0.09	≦0.12	0.33 (0.04)	≦0.09
-92	0.10 (0.03)	0.24 (0.05)	≦0.09	≦0.12	0.20 (0.05)	≦0.09
-105	0.11 (0.03)	0.44 (0.05)	≦0.09	≦0.12	0.48 (0.04)	≦0.09

[a] In unit K. The numbers in parentheses represent one standard deviation.

[b] Observed by Lis (1989).

[c] Observed by Ohishi et al. (1995).

Table 4; Velocity Widths of the Molecular Absorption Lines[a]

Velocity Component (km/s)	^{12}CO J = 1-0 (Lis)[b]	^{13}CO J = 1-0 (Lis)[b]	^{13}CO J = 1-0 (Ohishi)[c]	$C^{18}O$ J = 1-0	^{12}CN N = 1-0	^{13}CN N = 1-0
+22	-	0.8 (0.5)	-	-	-	17.1 (1.5)
+3	-	3.1 (0.8)	-	-	-	3.4 (0.3)
-20	-	3.7 (0.8)	2.6 (0.5)	2.7 (0.5)	-	3.7 (0.3)
-28	-	2.5 (0.8)	3.8 (0.3)	1.7 (0.3)	-	3.7 (0.3)
-42	-	2.5 (0.8)	3.8 (0.2)	3.3 (0.3)	-	1.8 (0.3)
-46	-	1.5 (0.6)	4.0 (0.2)	2.2 (0.3)	-	3.4 (0.3)
-76	-	-	4.3 (0.2)	-	-	3.4 (0.3)
-92	-	-	3.9 (0.1)	-	-	3.4 (0.3)
-105	-	-	3.5 (0.1)	-	-	3.8 (0.3)

(Table 4, continued)

Velocity Component (km/s)	$C^{32}S$ J = 1-0	$C^{32}S$ J = 2-1	$C^{34}S$ J = 1-0	$C^{34}S$ J = 2-1	SO $J_N = 3_2$-2_1	^{28}SiO J = 1-0
+22	-	-	4.5 (0.3)	3.5 (0.3)	-	-
+3	14.1 (1.8)	13.1 (2.5)	12.8 (0.3)	12.0 (1.5)	7.5 (1.3)	9.5 (1.8)
-20	6.8 (0.8)	7.5 (0.9)	3.5 (0.3)	-	-	1.7 (0.3)
-28	6.5 (0.7)	7.2 (0.9)	3.5 (0.3)	-	-	1.7 (0.3)
-42	4.1 (0.5)	4.5 (0.6)	2.1 (0.3)	-	1.5 (0.2)	1.7 (0.3)
-46	6.6 (0.7)	7.6 (0.9)	2.5 (0.3)	-	1.0 (0.2)	1.7 (0.3)
-76	6.2 (0.7)	7.1 (0.9)	-	-	-	-
-92	8.7 (0.9)	10.4 (0.9)	-	-	-	9.5 (0.5)
-105	11.2 (1.2)	9.4 (1.5)	-	-	-	6.5 (1.2)

(Table 4, continued)

Velocity Component (km/s)	^{28}SiO J = 2-1	^{29}SiO J = 1-0	$H^{12}CN^{c}$ J = 1-0	$H^{13}CN$ J = 1-0	$HN^{12}C$ J = 1-0	$HN^{13}C$ J = 1-0
+22	-	-	-	1.7 (0.2)	-	6.5 (0.3)
+3	12.2 (1.4)	9.1 (1.8)	-	14.9 (1.3)	13.4 (0.4)	7.0 (0.3)
-20	-	-	-	5.2 (0.3)	-	-
-28	-	-	-	3.1 (0.3)	-	-
-42	-	-	-	1.8 (0.2)	-	-
-46	-	-	-	1.9 (0.2)	-	-
-76	-	-	-	-	-	-
-92	0.3 (0.1)	-	-	7.3 (0.4)	-	-
-105	0.3 (0.1)	-	-	8.7 (0.4)	-	6.4 (0.3)

(Table 4, continued)

Velocity Component (km/s)	$H^{12}CO^+$ J = 1-0	$H^{13}CO^+$ J = 1-0	NH_3 (1,1)-(1,1)	NH_3 (2,2)-(2,2)	NH_3 (3,3)-(3,3)	NH_3 (4,4)-(4,4)
+22	-	13.4 (0.6)	-	-	-	-
+3	-	5.8 (0.3)	13.7 (1.6)	6.5 (0.4)	14.0 (0.6)	13.7 (0.6)
-20	-	2.1 (0.2)	6.8 (0.4)	6.5 (0.4)	-	-
-28	-	-	6.8 (0.4)	6.5 (0.4)	-	-
-42	-	2.1 (0.2)	6.8 (0.4)	-	-	-
-46	-	2.0 (0.2)	6.8 (0.4)	-	-	-
-76	-	-	6.8 (0.4)	-	7.8 (0.4)	-
-92	-	-	6.8 (0.4)	6.5 (0.4)	10.6 (0.6)	-
-105	-	2.1 (0.2)	9.5 (0.5)	14.0 (0.6)	18.8 (0.6)	7.7 (0.4)

(Table 4, continued)

Velocity Component (km/s)	NH_3 (5,5)-(5,5)	NH_3 (6,6)-(6,6)	NH_3 (7,7)-(7,7)	HC_3N J = 1-0	HC_3N J = 2-1	HC_3N J = 4-3
+22	-	-	-	-	-	-
+3	14.0 (0.6)	18.8 (0.9)	25.6 (1.3)	-	-	9.4 (0.5)
-20	-	-	-	-	-	5.1 (0.3)
-28	-	-	-	-	-	5.1 (0.3)
-42	-	-	-	-	-	-
-46	-	-	-	-	-	-
-76	-	-	-	-	-	-
-92	-	-	-	-	-	-
-105	7.7 (0.4)	-	-	-	-	7.2 (0.4)

(Table 4, continued)

Velocity Component (km/s)	HC_3N J = 5-4	C_3H_2 $1_{1,0}$-$1_{0,1}$	C_3H_2 $2_{2,0}$-$2_{1,1}$	C_3H_2 $2_{0,2}$-$1_{1,1}$	C_3H_2 $2_{1,2}$-$1_{0,1}$	CH_3OH 0_2-1_{-1} E
+22	-	-	-	-	8.3 (0.4)	-
+3	6.8 (0.3)	18.8 (1.5)	-	8.5 (0.6)	16.7 (1.3)	7.2 (0.6)
-20	-	-	-	-	6.3 (0.4)	-
-28	-	-	-	-	6.3 (0.4)	-
-42	-	6.5 (0.3)	-	-	2.3 (0.2)	6.8 (0.6)
-46	6.8 (0.3)	-	-	-	3.0 (0.2)	6.8 (0.6)
-76	-	10.2 (0.9)	-	-	2.7 (0.2)	-
-92	6.8 (0.3)	8.5 (0.9)	-	-	6.3 (0.4)	-
-105	6.8 (0.3)	10.2 (0.9)	-	-	7.9 (0.5)	-

[a] In km/s unit. The numbers in parentheses represent three standard deviation

[b] Observed by Lis (1989)

[c] Observed by Ohishi et al. (1995).

Table 5; Continuum Brightness Temperatures of Sgr B2 MD5[a]

Frequency	T_B (K)	HPBW (arcsec)	Ref.
23 GHz	11.0 (0.3)	80[b]	c
43 GHz	4.5 (0.8)	40	c
91 GHz	5.8 (0.5)	30	d
115 GHz	12.1 (2.3)	42[e]	

[a] The numbers in parentheses represent the root mean square noise temperature.

[b] Deconvolved from the data of Akabane et al. (1988) observed with beam size 40" to the beam size 80".

[c] Akabane et al. (1988).

[d] Salter et al. (1989).

[e] Interpolated using 105 ± 26 Jy at beam size 30" (231 GHz; Lis 1989) and 15.1 ± 1.2 Jy at beam size 30" (90.9 GHz; Salter et al. 1989), and deconvolved to the beam size 42".

Table 6; Observed Data of the $NH_3(1,1)$ and $NH_3(2,2)$ transitions and Derived Physical Properties[a]

Velocity Component (km/s)	$T_{mb}(1,1)$[b] (K)	$T_{mb}(2,2)$[b] (K)	$\tau_m(1,1)$	$T_R(2,1)$[c] (K)
+22	≦0.09	≦0.09	≦0.008	-
+3	0.58 (0.03)	0.51 (0.02)	0.054 (0.003)	30.1 (4.8)
-20	0.16 (0.03)	0.11 (0.02)	0.015 (0.002)	29.4 (5.2)
-28	0.14 (0.03)	0.11 (0.02)	0.013 (0.002)	28.2 (5.2)
-42	0.21 (0.03)	≦0.09	0.019 (0.003)	-
-46	0.20 (0.03)	≦0.09	0.018 (0.003)	-
-76	0.13 (0.03)	≦0.09	0.012 (0.003)	-
-92	0.19 (0.03)	0.14 (0.02)	0.017 (0.003)	26.4 (4.6)
-105	0.34 (0.03)	0.26 (0.02)	0.031 (0.003)	27.4 (4.9)
Average				28.3 (4.9)

[a] The numbers in parentheses represent the standard deviation for the value.

[b] Observed brightness temperature.

[c] Rotational temperature derived from the NH_3 (1,1) and NH_3 (2,2) lines.

Table 7; Observed Data of ^{12}CO, ^{13}CO and Derived Physical Properties[a]

Velocity Component (km/s)	$T_{mb}(^{12}CO)$ (K)	$T_{mb}(^{13}CO)$ (K)	$\tau_m(^{12}CO)$[b]	T_k (K)
+22	-	1.0 (0.2)	-	-
+3	1.2 (0.1)	0.4 (0.1)	19 (1)	13.3 (2.4)
-20	1.4 (0.1)	0.4 (0.1)	11 (2)	13.5 (2.4)
-28	1.6 (0.1)	0.4 (0.2)	20 (1)	13.7 (2.4)
-42	0.9 (0.1)	0.9 (0.2)	19 (1)	13.0 (2.4)
-46	0.8 (0.1)	0.5 (0.2)	14 (2)	12.9 (2.4)
-76	1.1 (0.1)	-	-	13.2 (2.4)
-92	1.6 (0.1)	-	-	13.7 (2.4)
-105	0.6 (0.1)	-	-	12.7 (2.4)
Average				13.3 (2.4)

[a] The numbers in parentheses represent the standard deviation for the values.

[b] The optical depth derived from the data of ^{12}CO and the ^{13}CO by assuming the terrestrial isotopic ratio of $[^{12}C]/[^{13}C] = 90$.

Table 8; Results of LVG Analysis for the CS J = 1-0 and J = 2-1 lines[a]

Velocity Component (km/s)	$T_{ex}(1\text{-}0)$[b] (K)	$\tau(1\text{-}0)$	$T_{ex}(2\text{-}1)$[b] (K)	$\tau(2\text{-}1)$	$\log(n(H_2))$[c]	$\log(N(CS)/\Delta V)$[d]
+22	-	-	-	-	-	-
+3	4.8 (0.3)	0.4 (0.2)	3.9 (0.3)	0.53 (0.2)	2.4 (0.4)	13.26 (0.38)
-20	3.5 (0.4)	0.2 (0.2)	3.1 (0.4)	0.21 (0.2)	2.0 (0.4)	12.51 (0.35)
-28	3.5 (0.3)	0.2 (0.2)	3.1 (0.3)	0.21 (0.2)	2.0 (0.4)	12.50 (0.35)
-42	3.7 (0.2)	0.4 (0.2)	3.3 (0.1)	0.49 (0.1)	2.1 (0.3)	13.11 (0.33)
-46	3.7 (0.1)	0.2 (0.1)	3.3 (0.1)	0.25 (0.1)	2.1 (0.3)	12.52 (0.25)
-76	3.7 (0.1)	0.2 (0.1)	3.3 (0.1)	0.25 (0.1)	2.1 (0.3)	12.52 (0.25)
-92	3.9 (0.1)	0.2 (0.1)	3.5 (0.1)	0.25 (0.1)	2.2 (0.3)	12.72 (0.26)
-105	4.3 (0.1)	0.4 (0.1)	3.8 (0.1)	0.51 (0.1)	2.4 (0.3)	13.20 (0.33)

[a] The numbers in parentheses represent the one standard deviation for the values. The average rotational temperature (28 K) derived from NH_3 is used for the kinetic temperature.

[b] Excitation temperature.

[c] In cm^{-3} unit.

[d] In $(cm^{-2}/km/s)$.

Table 9; Results of LVG Analysis for the SiO J = 1-0 and J = 2-1 lines[a]

Velocity Component (km/s)	$T_{ex}(1\text{-}0)$[b] (K)	$\tau(1\text{-}0)$	$T_{ex}(2\text{-}1)$[b] (K)	$\tau(2\text{-}1)$	$\log(n(H_2))$[c]	$\log(N(SiO)/\Delta V)$[d]
+22	-		-	-	-	-
+3	4.3 (0.4)	0.13 (0.04)	3.5 (0.4)	0.08 (0.02)	2.4 (0.4)	11.57 (0.38)
-20	-	-	-	-	-	-
-28	-	-	-	-	-	-
-42	-	-	-	-	-	-
-46	-	-	-	-	-	-
-76	-	-	-	-	-	-
-92	3.8 (0.3)	0.11 (0.04)	3.3 (0.3)	0.07 (0.02)	2.2 (0.4)	11.30 (0.35)
-105	3.8 (0.3)	0.11 (0.04)	3.3 (0.3)	0.07 (0.02)	2.3 (0.4)	11.36 (0.35)

[a-d] See the footnotes of Table 8.

Table 10a; Optical Depths of the Molecular Absorption Lines Derived from LTE Calculations[a]

Velocity Component (km/s)	^{13}CO J = 1-0 (Ohishi)[c]	$C^{18}O$ J = 1-0	^{12}CN N = 1-0	^{13}CN N = 1-0	$C^{32}S$ J = 1-0	$C^{32}S$ J = 2-1
+22	≦0.013	≦0.010	0.034 (0.004)	0.043 (0.002)	≦0.089	≦0.154
+3	≦0.013	≦0.010	0.035 (0.003)	0.020 (0.002)	0.379 (0.010)	0.433 (0.030)
-20	0.126 (0.012)	0.032 (0.003)	0.051 (0.004)	0.014 (0.002)	0.148 (0.007)	0.191 (0.032)
-28	0.092 (0.013)	0.027 (0.004)	0.047 (0.003)	0.0014 (0.002)	0.128 (0.008)	0.193 (0.024)
-42	0.133 (0.014)	0.112 (0.003)	0.051 (0.004)	0.016 (0.003)	0.549 (0.012)	0.558 (0.018)
-46	0.119 (0.014)	0.072 (0.004)	0.051 (0.004)	0.011 (0.002)	0.141 (0.008)	0.267 (0.015)
-76	0.078 (0.014)	≦0.010	0.037 (0.003)	0.011 (0.002)	0.128 (0.008)	0.272 (0.016)
-92	0.035 (0.001)	≦0.010	0.035 (0.003)	0.011 (0.002)	0.098 (0.007)	0.258 (0.015)
-105	0.048 (0.004)	≦0.010	0.043 (0.003)	0.028 (0.002)	0.354 (0.010)	0.441 (0.018)

(Table 10a, continued)

Velocity Component (km/s)	$C^{34}S$ J = 1-0	$C^{34}S$ J = 2-1	SO $J_N = 3_2$-2_1	^{28}SiO J = 1-0	^{28}SiO J = 2-1	^{29}SiO J = 1-0
+22	0.024 (0.006)	0.050 (0.004)	≦0.049	≦0.016	≦0.037	≦0.016
+3	0.057 (0.007)	0.133 (0.006)	0.096 (0.008)	0.135 (0.002)	0.113 (0.013)	0.043 (0.011)
-20	0.040 (0.006)	-	≦0.010	0.022 (0.004)	≦0.037	≦0.016
-28	0.036 (0.007)	-	≦0.010	0.022 (0.004)	≦0.037	≦0.016
-42	0.089 (0.006)	-	0.090 (0.004)	0.022 (0.004)	≦0.037	≦0.016
-46	0.054 (0.006)	-	0.068 (0.004)	0.022 (0.004)	≦0.037	≦0.016
-76	≦0.010	-	≦0.010	≦0.016	≦0.037	≦0.016
-92	≦0.010	-	≦0.010	0.093 (0.002)	0.086 (0.013)	≦0.016
-105	≦0.010	-	≦0.010	0.083 (0.002)	0.079 (0.013)	≦0.016

(Table 10a, continued)

Velocity Component (km/s)	$H^{12}CN$ J = 1-0	$H^{13}CN$ J = 1-0	$HN^{12}C$ J = 1-0	$HN^{13}C$ J = 1-0	$H^{12}CO^+$ J = 1-0	$H^{13}CO^+$ J = 1-0
+22	≦0.079	0.068 (0.006)	≦0.016	0.040 (0.012)	0.044 (0.018)	0.189 (0.014)
+3	0.177 (0.008)	0.318 (0.007)	0.090 (0.007)	0.068 (0.013)	0.109 (0.019)	0.197 (0.014)
-20	0.252 (0.009)	0.041 (0.006)	-	≦0.037	0.081 (0.019)	0.038 (0.011)
-28	0.258 (0.017)	0.039 (0.006)	-	≦0.037	0.062 (0.016)	≦0.037
-42	0.272 (0.027)	0.040 (0.006)	-	≦0.037	0.090 (0.017)	0.158 (0.013)
-46	0.256 (0.026)	0.039 (0.006)	-	≦0.037	0.083 (0.019)	0.038 (0.011)
-76	0.138 (0.007)	≦0.016	-	≦0.037	≦0.053	≦0.037
-92	0.198 (0.009)	0.049 (0.005)	-	≦0.037	-	≦0.037
-105	0.236 (0.009)	0.117 (0.006)	-	0.055 (0.009)	-	0.154 (0.018)

(Table 10a, continued)

Velocity Component (km/s)	NH_3 (1,1)-(1,1)	NH_3 (2,2)-(2,2)	NH_3 (3,3)-(3,3)	NH_3 (4,4)-(4,4)	NH_3 (5,5)-(5,5)	NH_3 (6,6)-(6,6)
+22	≦0.008	≦0.008	≦0.008	≦0.011	≦0.008	≦0.011
+3	0.054 (0.003)	0.047 (0.003)	0.045 (0.003)	0.041 (0.004)	0.024 (0.003)	0.029 (0.004)
-20	0.015 (0.002)	0.010 (0.002)	≦0.008	≦0.011	≦0.008	≦0.011
-28	0.013 (0.002)	0.010 (0.002)	≦0.008	≦0.011	≦0.008	≦0.011
-42	0.019 (0.003)	≦0.008	≦0.008	≦0.011	≦0.008	≦0.011
-46	0.018 (0.003)	≦0.008	≦0.008	≦0.011	≦0.008	≦0.011
-76	0.012 (0.003)	≦0.008	0.012 (0.003)	≦0.011	≦0.008	≦0.011
-92	0.017 (0.003)	0.013 (0.003)	0.014 (0.003)	≦0.011	≦0.008	≦0.011
-105	0.031 (0.003)	0.024 (0.003)	0.024 (0.003)	0.015 (0.004)	0.009 (0.003)	≦0.011

(Table 10a, continued)

Velocity Component (km/s)	NH_3 (7,7)-(7,7)	HC_3N J = 1-0	HC_3N J = 2-1	HC_3N J = 4-3	HC_3N J = 5-4	C_3H_2 $1_{1,0}$-$1_{0,1}$
+22	≦0.008	≦0.009	≦0.014	≦0.007	≦0.020	≦0.014
+3	0.012 (0.003)	≦0.009	≦0.014	0.064 (0.003)	0.083 (0.007)	0.037 (0.005)
-20	≦0.008	≦0.009	≦0.014	0.013 (0.002)	≦0.020	≦0.014
-28	≦0.008	≦0.009	≦0.014	0.013 (0.002)	≦0.020	≦0.014
-42	≦0.008	≦0.009	≦0.014	≦0.007	≦0.020	0.024 (0.005)
-46	≦0.008	≦0.009	≦0.014	≦0.007	0.022 (0.006)	≦0.014
-76	≦0.008	≦0.009	≦0.014	≦0.007	≦0.020	0.017 (0.004)
-92	≦0.008	≦0.009	≦0.014	≦0.007	0.022 (0.006)	0.022 (0.005)
-105	≦0.008	≦0.009	≦0.014	0.034 (0.005)	0.025 (0.006)	0.041 (0.005)

(Table 10a, continued)

Velocity Component (km/s)	C_3H_2 $2_{2,0}$-$2_{1,1}$	C_3H_2 $2_{0,2}$-$1_{1,1}$	C_3H_2 $2_{1,2}$-$1_{0,1}$	CH_3OH 0_2-1_{-1} E
+22	≦0.008	≦0.021	0.028 (0.007)	≦0.007
+3	≦0.008	0.057 (0.008)	0.171 (0.008)	0.053 (0.003)
-20	≦0.008	≦0.021	0.064 (0.007)	≦0.007
-28	≦0.008	≦0.021	0.059 (0.008)	≦0.007
-42	≦0.008	≦0.021	0.196 (0.009)	0.028 (0.003)
-46	≦0.008	≦0.021	0.123 (0.008)	0.024 (0.002)
-76	≦0.008	≦0.021	0.059 (0.008)	≦0.007
-92	≦0.008	≦0.021	0.035 (0.009)	≦0.007
-105	≦0.008	≦0.021	0.086	≦0.007 (0.007)

[a] The numbers in parentheses represent three times of the standard deviation.

[b] Observed by Lis (1989).

[c] Observed by Ohishi et al. (1995).

Table 10b; Determined Optical Depths Using Main and Isotopic Species[a]

Velocity Component (km/s)	^{12}CO J = 1-0	^{13}CO J = 1-0	^{13}CO J = 1-0	$C^{18}O$ J = 1-0	^{12}CN N = 1-0	^{13}CN N = 1-0
+22	-	-	-	-	-	-
+3	19	0.2	-	-	75.5	0.8
	(1)	(0.02)			(10.2)	(0.1)
-20	11	0.1	1.1	0.2	32.2	0.4
	(2)	(0.01)	(0.5)	(0.1)	(7.5)	(0.1)
-28	20	0.2	1.4	0.3	32.2	0.4
	(1)	(0.02)	(0.6)	(0.1)	(7.5)	(0.1)
-42	19	0.2	12.1	2.2	34.3	0.4
	(1)	(0.02)	(1.3)	(0.2)	(8.3)	(0.1)
-46	14	0.2	6.3	1.2	13.2	0.1
	(2)	(0.02)	(0.8)	(0.1)	(4.8)	(0.1)
-76	-	-	-	-	32.3	0.4
					(8.3)	(0.1)
-92	-	-	-	-	33.5	0.4
					(9.0)	(0.1)
-105	-	-	-	-	90.2	1.0
					(4.9)	(0.1)

(Table 10b, continued)

Velocity Component (km/s)	$C^{32}S$ J = 1-0	$C^{34}S$ J = 1-0	$C^{32}S$ J = 2-1	$C^{34}S$ J = 2-1	^{28}SiO J = 1-0	^{29}SiO J = 1-0
+22	-	-	-	-	-	-
+3	4.5 (0.7)	0.2 (0.03)	9.8 (1.0)	0.4 (0.04)	8.0 (0.5)	0.2 (0.03)
-20	7.5 (1.6)	0.3 (0.07)	-	-	-	-
-28	7.9 (2.0)	0.3 (0.09)	-	-	-	-
-42	5.1 (0.4)	0.2 (0.02)	-	-	-	-
-46	11.3 (1.8)	0.5 (0.08)	-	-	-	-
-76	-	-	-	-	-	-
-92	-	-	-	-	-	-
-105	-	-	-	-	-	-

(Table 10b, continued)

Velocity Component (km/s)	$H^{12}CN$ J = 2-1	$H^{13}CN$ J = 1-0	$HN^{12}C$ J = 1-0	$HN^{13}C$ J = 1-0	$H^{12}CO^+$ J = 1-0	$H^{13}CO^+$ J = 1-0
+22	-	-	-	-	-	-
+3	-	-	102.5 (7.5)	1.1 (0.08)	-	-
-20	17.0 (3.0)	0.2 (0.03)	-	-	55.0 (15.1)	0.7 (0.2)
-28	16.5 (3.3)	0.2 (0.04)	-	-	-	-
-42	82.3 (8.5)	0.9 (0.09)	-	-	-	-
-46	16.7 (3.7)	0.2 (0.04)	-		81.9 (20.5)	0.9 (0.2)
-76	-	-	-	-	-	-
-92	27.2 (4.2)	1.7 (0.05)	-	-	-	-
-105	30.2 (2.5)	0.3 (0.03)	-	-	-	-

[a] The numbers in parentheses represent three times of the standard deviation. The terrestrial isotope ratio is assumed for the main and isotope abundance ratio.

Table 10c; Optical Depths of the Molecular Absorption Lines Derived from Large Velocity-Gradient Calculations[a]

Velocity Component (km/s)	$C^{32}S$[b] J = 1-0	$C^{32}S$[c] J = 1-0	$C^{32}S$[b] J = 2-1	$C^{32}S$[c] J = 2-1
+22	≦0.080	-	≦0.154	-
+3	0.379 (0.010)	0.4 (0.2)	0.433 (0.030)	0.53 (0.2)
-20	0.148 (0.007)	0.2 (0.2)	0.191 (0.032)	0.21 (0.2)
-28	0.128 (0.008)	0.2 (0.2)	0.193 (0.024)	0.21 (0.2)
-42	0.549 (0.012)	0.4 (0.2)	0.558 (0.018)	0.49 (0.1)
-46	0.141 (0.008)	0.2 (0.2)	0.267 (0.015)	0.25 (0.1)
-76	0.128 (0.008)	0.2 (0.1)	0.272 (0.016)	0.25 (0.1)
-92	0.098 (0.007)	0.2 (0.1)	0.258 (0.015)	0.25 (0.1)
-105	0.354 (0.010)	0.4 (0.1)	0.441 (0.018)	0.51 (0.1)

[a] The numbers in parentheses represent three times of the standard deviation.

[b] Results derived from LTE calculations.

[c] Results of Large Velocity-Gradient Calculations.

Table 11; Molecular Data Used in This Thesis

Species	Transition	A[a]	Eu (K)	Q_{rot}[b]
$C^{18}O$	J = 1-0	7.2×10^{-8}	5.53	1.87
^{13}CN	N = 1-0	1.2×10^{-5}	5.45	3.65
$C^{32}S$	J = 1-0	2.0×10^{-6}	2.35	3.68
$C^{32}S$	J = 2-1	1.6×10^{-5}	7.05	3.68
$C^{34}S$	J = 1-0	1.9×10^{-6}	2.31	3.73
$C^{34}S$	J = 2-1	1.6×10^{-5}	6.94	3.73
SO	$J_N = 3_2$-2_1	1.0×10^{-5}	9.23	10.42
^{28}SiO	J = 1-0	3.4×10^{-6}	2.35	4.09
^{28}SiO	J = 2-1	2.7×10^{-5}	6.25	4.09
$H^{13}CN$	J = 1-0	2.5×10^{-5}	4.14	2.27
$HN^{13}C$	J = 1-0	2.6×10^{-5}	4.18	2.25
$H^{13}CO^+$	J = 1-0	3.1×10^{-5}	4.16	2.20
HC_3N	J = 4-3	2.9×10^{-6}	4.37	18.25
HC_3N	J = 5-4	5.7×10^{-6}	6.55	18.25
C_3H_2	$1_{1,0}$-$1_{0,1}$	3.2×10^{-7}	0.9	10.23
C_3H_2	$2_{0,2}$-$1_{1,1}$	2.8×10^{-5}	6.43	10.23
C_3H_2	$2_{1,2}$-$1_{0,1}$	3.2×10^{-5}	4.10	10.23
CH_3OH	0_2-1_{-1} E	1.2×10^{-5}	5.23	14.86

[a] Einstein A coefficient is s^{-1} unit.

[b] Rotational partition function calculated by using Tex, where the average excitation temperature (3.9 K) derived from the CS lines is assumed for all species.

Table 12; Column Densities of the Observed Molecules and Visual Extinction[a]

Velocity Component (km/s)	$C^{18}O$	^{13}CN	$C^{32}S$	$C^{34}S$	SO	^{28}SiO
+22	≦13.82	13.66 (0.50)	≦12.53	11.97 (0.12)	≦11.81	≦12.87
+3	≦13.82	12.62 (0.09)	13.70 (0.18)	12.87 (0.18)	12.73 (0.14)	13.08 (0.05)
-20	14.25 (0.06)	12.50 (0.09)	12.97 (0.02)	12.12 (0.14)	≦11.12	12.65 (0.03)
-28	13.98 (0.02)	12.50 (0.09)	12.89 (0.02)	12.07 (0.14)	≦11.12	12.65 (0.03)
-42	14.88 (0.06)	12.32 (0.09)	12.82 (0.02)	12.24 (0.15)	12.00 (0.11)	12.65 (0.03)
-46	14.51 (0.04)	12.16 (0.07)	12.95 (0.04)	12.10 (0.14)	11.70 (0.08)	12.65 (0.03)
-76	≦13.82	12.37 (0.09)	12.88 (0.02)	≦11.47	≦11.12	≦12.87
-92	≦13.82	12.37 (0.09)	13.13 (0.12)	≦11.47	≦11.12	12.93 (0.03)
-105	≦13.82	12.72 (0.10)	13.56 (0.18)	≦11.47	≦11.12	12.73 (0.02)

(Table 12, continued)

Velocity Component (km/s)	$H^{13}CN$	$HN^{13}C$	$H^{13}CO^+$	NH_3	HC_3N	C_3H_2
+22	11.93 (0.02)	11.90 (0.02)	13.17 (0.11)	-	≦11.76	12.43 (0.04)
+3	13.54 (0.14)	12.52 (0.06)	12.82 (0.07)	13.77 (0.03)	12.93 (0.10)	13.51 (0.12)
-20	12.17 (0.04)	≦11.87	11.73 (0.02)	12.91 (0.04)	11.97 (0.05)	12.67 (0.05)
-28	11.95 (0.02)	≦11.87	≦11.65	12.84 (0.05)	11.97 (0.05)	12.58 (0.05)
-42	11.86 (0.02)	≦11.87	11.95 (0.04)	13.01 (0.04)	≦11.76	12.72 (0.05)
-46	11.74 (0.01)	≦11.87	11.68 (0.02)	12.81 (0.04)	11.79 (0.03)	12.63 (0.05)
-76	≦11.73	≦11.87	≦11.65	12.81 (0.04)	≦11.76	12.27 (0.04)
-92	12.42 (0.06)	≦11.87	≦11.65	12.96 (0.04)	11.79 (0.03)	12.41 (0.04)
-105	12.87 (0.09)	12.39 (0.05)	12.27 (0.04)	13.37 (0.04)	12.54 (0.08)	12.90 (0.07)

(Table 12, continued)

Velocity Component (km/s)	CH_3OH	A_V[b] (mag)
+22	≦11.86	≦1.4
+3	12.77 (0.05)	≦1.4
-20	≦11.86	1.8 (1.1)
-28	≦11.86	1.5 (0.8)
-42	12.47 (0.03)	4.1 (1.3)
-46	12.40 (0.03)	2.4 (1.3)
-76	≦11.86	1.4 (1.2)
-92	≦11.86	1.3 (1.2)
-105	≦11.86	1.3 (1.2)

[a] log N value, where column density N is given by cm^{-2} unit. The numbers in parentheses represent three times of the standard deviation.

[b] The visual extinction derived using the data of $C^{18}O$ for the +22 ~ -46 km/s velocity components and from the data of ^{13}CO for the -76, -92, and -105 km/s velocity components.

Table 13; Brightness Temperatures Multiplied by Velocity Widths (Tmb×ΔV) of the Molecular Absorption Lines[a]

Velocity Component (km/s)	$C^{18}O$ J = 1-0	^{13}CN N = 1-0	$C^{34}S$ J = 1-0	SO $J_N = 3_2$-2_1	^{28}SiO J = 1-0	$H^{13}CN$ J = 1-0
+22	-	8.72 (1.11)	0.50 (0.17)	-	-	0.65 (0.13)
+3	-	0.82 (0.14)	3.20 (0.46)	3.98 (0.99)	5.42 (1.12)	23.54 (2.50)
-20	1.03 (0.30)	0.55 (0.12)	0.63 (0.16)	-	0.17 (0.06)	1.14 (0.22)
-28	0.54 (0.16)	0.55 (0.12)	0.56 (0.15)	-	0.17 (0.06)	0.68 (0.16)
-42	4.22 (0.48)	0.34 (0.11)	0.82 (0.18)	0.75 (0.13)	0.17 (0.06)	0.55 (0.12)
-46	1.85 (0.34)	0.27 (0.09)	0.60 (0.15)	0.38 (0.10)	0.17 (0.06)	0.42 (0.10)
-76	-	0.44 (0.11)	-	-	-	-
-92	-	0.44 (0.11)	-	-	3.80 (0.30)	2.05 (0.33)
-105	-	1.25 (0.18)	-	-	2.34 (0.50)	5.57 (0.52)

(Table 13, continued)

Velocity Component (km/s)	$HN^{13}C$ J = 1-0	$H^{13}CO^+$ J = 1-0	NH_3 (1,1)-(1,1)	HC_3N J = 4-3	C_3H_2 $2_{1,2}$-$1_{0,1}$	CH_3OH 0_2-1_{-1} E
+22	1.50 (0.52)	13.40 (1.54)	-	-	1.33 (0.40)	-
+3	2.66 (0.60)	6.03 (0.72)	7.95 (1.34)	2.63 (0.23)	15.20 (1.85)	4.46 (0.59)
-20	-	0.50 (0.16)	1.09 (0.27)	0.31 (0.07)	2.27 (0.38)	-
-28	-	-	0.95 (0.26)	0.31 (0.07)	2.08 (0.38)	-
-42	-	0.83 (0.18)	1.43 (0.29)	-	2.37 (0.30)	2.24 (0.40)
-46	-	0.45 (0.16)	1.36 (0.28)	-	2.01 (0.25)	1.97 (0.38)
-76	-	-	0.89 (0.26)	-	0.89 (0.17)	-
-92	-	-	1.29 (0.28)	-	1.26 (0.40)	-
-105	1.98 (0.41)	1.74 (0.36)	3.23 (0.46)	1.08 (0.20)	2.70 (0.56)	-

[a] In K km/s unit. The numbers in parentheses denote one standard deviation.

Table 14; Summary of Physical Properties of the Diffuse Molecular Cloud and Comparison with Other Clouds

Velocity Component (km/s)	log[n(H_2)] (cm^{-3})	Tk (K)	Av[a] (mag)	size (pc)	log[N(H_2)] (cm^{-2})
+22	-	-	≦1.4	0.08	-
+3	2.4	30.1	≦1.4	0.21	-
-20	2.0	29.4	1.8	0.05	20.95
-28	2.0	28.2	1.5	0.06	20.68
-42	2.1	-	4.1	0.11	21.58
-46	2.1	-	2.4	0.20	21.21
-76	2.1	-	1.4	0.09	20.52
-92	2.2	26.4	1.3	0.16	20.41
-105	2.4	27.4	1.3	0.07	20.41
Diffuse Cloud (ζOph)	2	20 ~ 100	<1	1 ~ 3	<15
Dense Molecular Cloud (TMC-1)	4 ~ 6	10	>10	0.05 ~ 0.2	22

[a] The visual extinction derived using the data of $C^{18}O$ for the +22 ~ -46 km/s velocity components and from the data of ^{13}CO for the -76, -92, and -105 km/s velocity components.

Table 15; Correlation Coefficients for values of Brightness Temperatures Multiplied by Velocity Widths ($Tmb \times \Delta V$)[a]

	^{13}CN	$H^{13}CN$	^{28}SiO	NH_3	$H^{13}CO^+$	$C^{34}S$	C_3H_2	$C^{18}O$
^{13}CN	1.00	0.93 (0.02)	0.85 (0.02)	0.93 (0.01)	0.82 (0.01)	-	0.34 (0.02)	-
$H^{13}CN$		1.00	0.80 (0.03)	0.92 (0.01)	0.84 (0.01)	0.35 (0.01)	0.37 (0.01)	0.55 (0.02)
^{28}SiO			1.00	0.62 (0.01)	0.78 (0.01)	-	0.54 (0.01)	-
NH_3				1.00	0.75 (0.02)	0.52 (0.02)	0.60 (0.01)	0.70 (0.02)
$H^{13}CO^+$					1.00	-	0.50 (0.02)	-
$C^{34}S$						1.00	0.83 (0.02)	0.91 (0.02)
C_3H_2							1.00	0.80 (0.02)
$C^{18}O$								1.00

[a] The numbers in parentheses represent three times of the standard deviation.

Table 16; Correlation Coefficients for Column Densities of the Observed Molecules[a]

	^{13}CN	$H^{13}CN$	^{28}SiO	NH_3	$H^{13}CO^+$	$C^{34}S$	C_3H_2	$C^{18}O$
^{13}CN	1.00	0.80 (0.02)	0.78 (0.02)	0.90 (0.01)	0.75 (0.01)	-	0.46 (0.02)	-
$H^{13}CN$		1.00	0.72 (0.03)	0.91 (0.01)	0.78 (0.01)	0.42 (0.01)	0.40 (0.01)	0.58 (0.02)
^{28}SiO			1.00	0.58 (0.01)	0.75 (0.01)	-	0.42 (0.01)	-
NH_3				1.00	0.64 (0.02)	0.55 (0.02)	0.68 (0.01)	0.64 (0.02)
$H^{13}CO^+$					1.00	-	0.61 (0.02)	-
$C^{34}S$						1.00	0.81 (0.02)	0.89 (0.02)
C_3H_2							1.00	0.74 (0.02)
$C^{18}O$								1.00

[a] See the footnotes of Table 15.

Table 17; Photodissociation Energies and Rates of the Observed Molecules

	D[a]	Rate(s^{-1})[b]	Ref.
SO	4.07	$2.4\times10^{-9}\exp(-1.95Av)$	Nee and Lee (1986) Phillips (1981)
CH_3OH	5.36	$9.4\times10^{-10}\exp(-1.76Av)$	Salahub and Sandorfy (1971) Nee and Lee (1985) Ogawa and Cook (1958)
c-C_3H_2	-	$1.2\times10^{-9}\exp(-1.79Av)$	van Hemert, Stehoumwr, and van Dishoeck (1995)
CS	7.36	$2\times10^{-10} \sim 1\times10^{-9}$	Drdla et al. (1989)
HCN	5.48	$1.1\times10^{-9}\exp(-2.08Av)$	Lee (1984)
HNC	-	-	-
CN	7.48	$5.8\times10^{-10}\exp(-7.04Av)$	Roberge et al. (1991)
HC_3N	-	-	-
NH_3	-	$6.0\times10^{-10}\exp(-4.54Av)$	Roberge et al. (1991)
HCO^+	-	-	-
SiO	8.26	$1.0\times10^{-10}\exp(-2.0Av)$	Mitchell, Ginsburg, and Kuntz (1978)

[a] Photodissociation Energy (eV)

[b] Photodissociation Rate

Table 18; Column Densities of Other Clouds[a]

	Diffuse Cloud (ζOph)	Translucent Cloud (HD29647)	High Latitude Cloud	Dense Molecular Cloud (TMC-1) (CP)[b]	(NH$_3$)[c]
C^{16}O	15.08[d]	16-16.95[e]	16.81[f]	17.9[g]	17.9[g]
^{12}CN	12.68[d]	13.74[e]	-	14.48[g]	-
H^{12}CN	-	-	-	14.30[g]	-
H^{12}CO$^+$	-	-	-	14.90[g]	-
HN^{12}C	-	-	-	14.30[g]	-
HC$_3$N	-	-	-	13.78[g]	13.79[h]
NH$_3$	-	-	-	14.30[g]	14.72[h]
CH$_3$OH	-	-	-	13.30[g]	-
SO	-	-	-	13.70[g]	-
C^{32}S	< 13.41[d]	-	-	14.00[g]	12.40[i]
C^{34}S	-	-	-	13.4[i]	-
C$_3$H$_2$	-	-	12.23[f]	14.00[g]	-
^{28}SiO	-	-	-	< 10.38[i]	-

[a] log N values, where column density N is given by cm^{-2} unit.

[b] The Cyanopolyyne Peak in TMC-1.

[c] The Ammonia Peak in TMC-1.

[d] Observed by Snow (1980).

[e] van Dishoeck and Black (1989)

[f] The values are the average of 28 core region in 15 different high-latitude clouds observed by Turner, Rickard, and Xu (1989).

[g] Observed by Ohishi, Irvine, and Kaifu (1992).

[h] Observed by Hirahara et al. (1992).

[i] Observed by Suzuki et al. (1992).

[j] Observed by Ziurys, Friberg, and Irvine (1989).

Table 19; Relative Abundances of the Observed Molecules with respect to $C^{16}O$[a]

Velocity Component (km/s)	^{12}CN	$C^{32}S$	SO	^{28}SiO	$H^{12}CN$
+22	-1.41 (0.50)	≦-3.99	≦-4.71	≦-3.65	-3.14 (0.03)
+3	-2.45 (0.09)	-2.82 (0.18)	-3.79 (0.18)	-3.44 (0.14)	-1.53 (0.05)
-20	-3.72 (0.09)	-3.98 (0.02)	≦-5.83	-4.30 (0.14)	-3.33 (0.03)
-28	-3.72 (0.09)	-3.79 (0.02)	≦-5.56	-4.03 (0.14)	-3.28 (0.03)
-42	-3.81 (0.09)	-4.26 (0.18)	-5.58 (0.15)	-4.93 (0.11)	-3.57 (0.03)
-46	-3.60 (0.07)	-4.26 (0.04)	-5.51 (0.14)	-4.56 (0.08)	-4.02 (0.03)
-76	-2.70 (0.09)	-3.64 (0.02)	≦-5.83	≦-3.65	≦-3.34
-92	-2.70 (0.09)	-3.39 (0.12)	≦-5.83	-3.59	-2.65 (0.03)
-105	-2.35 (0.10)	-2.96 (0.18)	≦-5.83	-3.79	-2.20 (0.02)
(CP)[b]	-3.42	-3.90	-4.20	≦-7.52	-3.60
(NH_3)[c]	-	-5.50	-	-	-

(Table 19, continued)

Velocity Component (km/s)	$HN^{12}C$	$H^{12}CO^+$	NH_3	HC_3N	C_3H_2	CH_3OH
+22	-3.17 (0.02)	-1.90 (0.11)	-	≦-4.76	-4.09 (0.04)	≦-4.66
+3	-2.55 (0.06)	-2.25 (0.07)	-2.75 (0.07)	-3.59 (0.10)	-3.01 (0.12)	-3.75 (0.07)
-20	≦-3.63	-3.79 (0.04)	-3.61 (0.10)	-4.98 (0.05)	-4.28 (0.05)	≦-5.09
-28	≦-3.36	≦-3.58	-3.84 (0.10)	-4.71 (0.05)	-4.05 (0.05)	≦-4.82
-42	≦-4.26	-3.78 (0.04)	-4.57 (0.12)	≦-5.82	-4.86 (0.05)	-5.11 (0.07)
-46	≦-3.89	-3.80 (0.02)	-4.40 (0.11)	-5.42 (0.03)	-4.58 (0.05)	-4.81 (0.07)
-76	≦-3.20	≦-3.42	-3.71 (0.10)	≦-4.76	-4.25 (0.04)	≦-4.66
-92	≦-3.20	≦-3.42	-3.56 (0.10)	-4.73 (0.03)	-4.11 (0.04)	≦-4.66
-105	-2.68 (0.05)	-2.80 (0.04)	-3.15 (0.10)	-3.98 (0.08)	-3.62 (0.07)	≦-4.66
(CP)[b]	-3.60	-3.00	-3.60	-4.12	-3.90	-4.60
(NH_3)[c]	-	-	-3.18	-	-	-4.11

[a] log N(x)/log $N(C^{16}O)$ values, where the column density of $C^{16}O$ ($\log N(C^{16}O)$) is determined from $C^{18}O$ by assuming isotopic ratio of 90. The numbers in parentheses denotes one standard deviation.

[b] The Cyanopolyyne Peak in TMC-1.

[c] The Ammonia Peak in TMC-1.

Figure Captions

Figure 1: A plot of densities and temperatures of dense molecular cloud, translucent cloud, high-latitude cloud, diffuse cloud and HI gas.

Figure 2a: A plot of the column densities of CCS against those of HC_3N by Suzuki et al. (1992). Open and closed marks represent cores with and without sign of star formation, respectively. Open and closed triangle marks the upper limit for CCS.

Figure 2b: A plot of the column densities of CCS against those of NH_3 by Suzuki et al. (1992). Notation of the open and closed marks are the same as that of Fig. 2a.

Figure 3: A 10 GHz continuum map by Handa et al. (1987). The labels on contours indicate brightness temperature in kelvin. The noise level of this map is about 30 mK.

Figure 4: A 43 GHz Continuum map of Sgr B2 by Akabane et al. (1988), beam size = 39" circular, contour unit = 0.42 K. Reference point is MD5 (R.A. (1950) = $17^h44^m10^s.6$, DEC(1950) = -28°22'05").

Figure 5: A frequency range which absorption lines are surveyed from the data of Ohishi et al. (1995) in this thesis.

Figure 6: A profile of the $C^{32}S$ J = 1-0 line at a reference point (MD5). The intensity scale is given in the main beam brightness temperature.

Figure 7: Spectra of the $C^{32}S$ J = 1-0, ^{28}SiO J = 1-0, $H^{13}CO^+$ J = 1-0 lines at a reference point. Absorption lines from diffuse molecular clouds are indicated by straight lines. The intensity scale is given in the main beam brightness temperature.

Figure 8a: Profiles obtained by our observation. The intensity scale is given in the main beam brightness temperature.

Figure 8b: Profiles obtained by Greaves et al. (1992). The intensity scale is the same as that of Fig. 8a.

Figure 8c: Profiles obtained by Ohishi et al. (1995). The intensity scale is the same as that of Fig. 8a.

Figure 8d: Profiles obtained in other papers. The intensity scale is the same as that of Fig. 8a.

$^{12}CO(J = 1\text{-}0)$	:Lis(1989)	HPBW 40"
$^{13}CO(J = 1\text{-}0)$	:Lis(1989)	HPBW 40"
$H^{12}CO^{+}(J = 1\text{-}0)$	:Morimoto et al. (1983)	HPBW 20"

Figure 9: A plot of the rotational temperatures derived using NH_3 against the kinetic temperatures derived using ^{12}CO. Error bars are shown for each plot.

Figure 10a: An optical depth (solid lines) and the excitation temperature (dashed lines) for the $C^{32}S$ J = 1-0 line are calculated against molecular hydrogen density and column density of CS per velocity interval based on the LVG assumption.

Figure 10b: Physical parameters reproducing the observed absorption features of the $C^{32}S$ J = 1-0 lines.

Figure 10c: An optical depth (solid lines) and the excitation temperature (dashed lines) for the $C^{32}S$ J = 2-1 line are calculated against molecular hydrogen density and column density of CS per velocity interval based on the LVG assumption.

Figure 10d: Physical parameters reproducing the observed absorption features of the $C^{32}S$ J = 2-1 lines.

Figure 11a: An optical depth (solid lines) and the excitation temperature (dashed lines) for the ^{28}SiO J = 1-0 line are calculated against molecular hydrogen density and column density of SiO per velocity interval based on the LVG assumption.

Figure 11b: Physical parameters reproducing the observed absorption features of the ^{28}SiO J = 1-0 line.

Figure 11c: An optical depth (solid lines) and the excitation temperature (dashed lines) for the ^{28}SiO J = 2-1 line are calculated against molecular hydrogen density and column density of SiO per velocity interval based on the LVG assumption.

Figure 11d: Physical parameters reproducing the observed absorption features of the ^{28}SiO J = 2-1 line are indicated by solid lines for velocity components.

Figure 12: A plot of the molecular hydrogen densities derived from $C^{32}S$ against those from ^{28}SiO. Error bars are shown for each plot.

Figure 13a: A plot of the column densities of $C^{18}O$, ^{13}CN, $C^{32}S$, $C^{34}S$, SO, and visual extinction against each velocity component. Arrow lines mark the upper limit for molecular abundances.

Figure 13b: A plot of the column densities of ^{28}SiO, $H^{13}CN$, $HN^{13}C$, $H^{13}CO^{+}$, NH_3, and visual extinction against each velocity component. See the caption of Fig. 13a.

Figure 13c: A plot of the column densities of HC_3N, C_3H_2, CH_3OH, and visual extinction against each velocity component. See the caption of Fig. 13a.

Figure 14a: A plot of the column densities of ^{13}CN, $H^{13}CN$, NH_3, and HC_3N against visual extinction. Error bars indicate one standard deviation. Arrow lines mark the upper limit for the molecular abundances. The visual extinction derived using the data of $C^{18}O$ in the range of 1.5-1.8 mag and from the data of ^{13}CO in the range of the below 1.5 mag. Therefore, there is a discrepancy between 1.5-4.1 mag and below 1.5 mag.

Figure 14b: A plot of the column densities of $C^{32}S$, SO, C_3H_2, and CH_3OH against visual extinction. See the caption of Fig. 14a.

Figure 14c: A plot of the column densities of ^{28}SiO, $HN^{13}C$, and $H^{13}CO^+$ against visual extinction. See the caption of Fig. 14a.

Figure 15a: A plot of the brightness temperatures multiplied by velocity width of $H^{13}CN$ against those of ^{13}CN. See the caption of Fig. 14a.

Figure 15b: A plot of the brightness temperatures multiplied by velocity width of C_3H_2 against those of $C^{34}S$. See the caption of Fig. 14a.

Figure 15c: A plot of the brightness temperatures multiplied by velocity width of C_3H_2 against those of $H^{13}CN$. See the caption of Fig. 14a.

Figure 16: A correlation coefficients of the molecular brightness temperature. Open squares in right-upper side denote deficient of the data.

Figure 17a: A plot of the column densities of $H^{13}CN$ against those of ^{13}CN.

Figure 17b: A plot of the column densities of C_3H_2 against those of $C^{34}S$.

Figure 17c: A plot of the column densities of C_3H_2 against those of $H^{13}CN$.

Figure 18: A correlation coefficients of the column densities of molecules. See the caption of Fig. 16.

Figure 19: A plot of the observed densities and temperatures of diffuse molecular clouds toward Sgr B2.

Figure 20: A schematic illustration of the proposed model for the production mechanism of the molecules belonging to A group (^{13}CN, $H^{13}CN$, NH_3, $HN^{13}C$, and HC_3N). Note that an arrow does not necessarily represent a single step reaction.

Figure 21: A schematic illustration of the proposed model for the production mechanism of the molecules belonging to B group ($C^{34}S$, C_3H_2, SO and CH_3OH). Note that an arrow does not necessarily represent a single step reaction.

Figure 22: Comparison of molecular abundances of TMC-1 with those of the diffuse molecular clouds. The straight line shows the locus of equal relative abundances in the two sources. The arrow lines denote the upper limit of molecular abundances. Error bars of each are shown in the upper-left.

(a) The +22 km/s velocity component
(b) The +3 km/s velocity component
(c) The -20 km/s velocity component
(d) The -26 km/s velocity component
(e) The -42 km/s velocity component
(f) The -46 km/s velocity component
(g) The -76 km/s velocity component
(h) The -92 km/s velocity component
(i) The -105 km/s velocity component

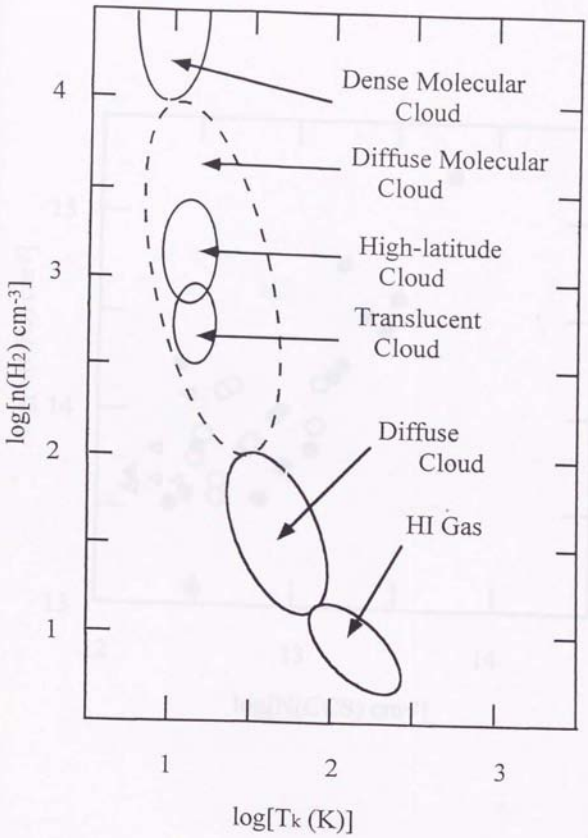
Dense Molecular Cloud
Diffuse Molecular Cloud
High-latitude Cloud
Translucent Cloud
Diffuse Cloud
HI Gas
4
3
2
1
log[n(H2) cm-3]
1
2
3
log[Tk (K)]

Fig. 1

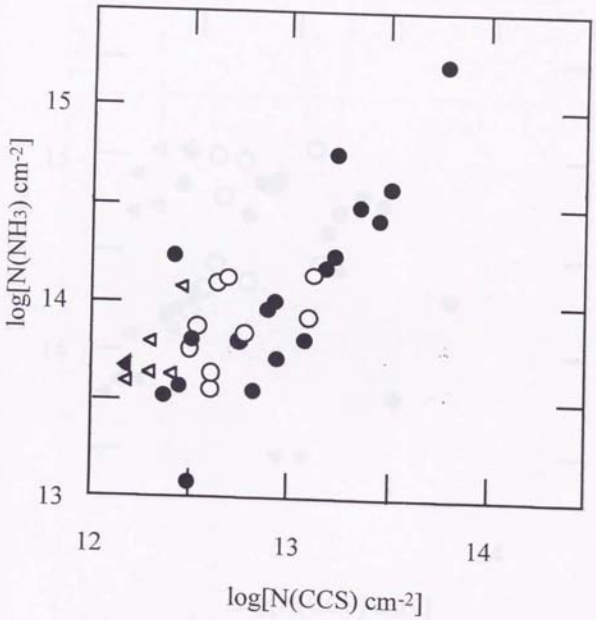

Fig. 2a

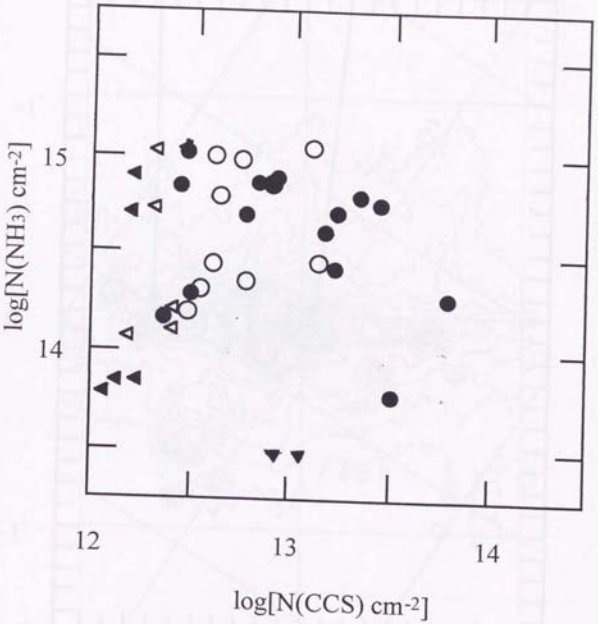

Fig. 2b

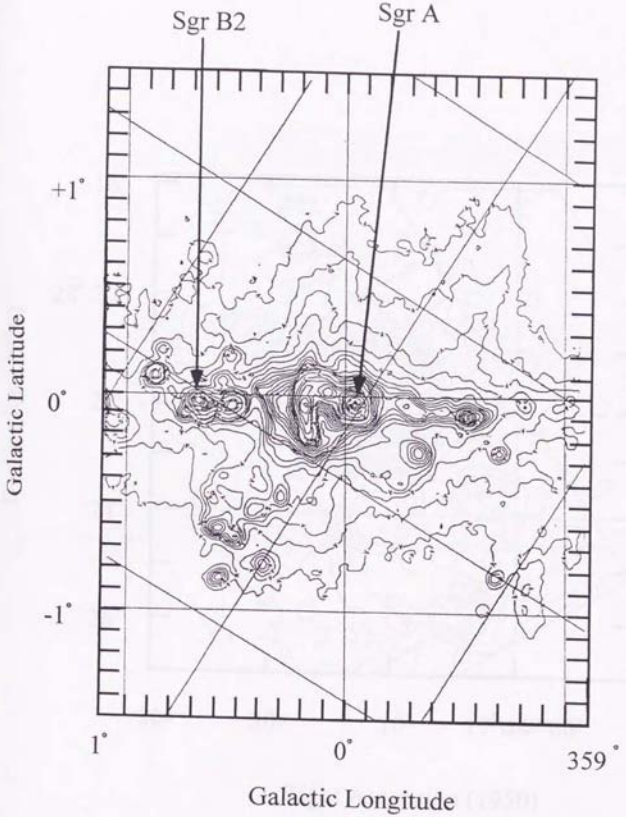
Sgr B2
Sgr A
+1°
0°
-1°
Galactic Latitude
1°
0°
359°
Galactic Longitude

Fig. 3

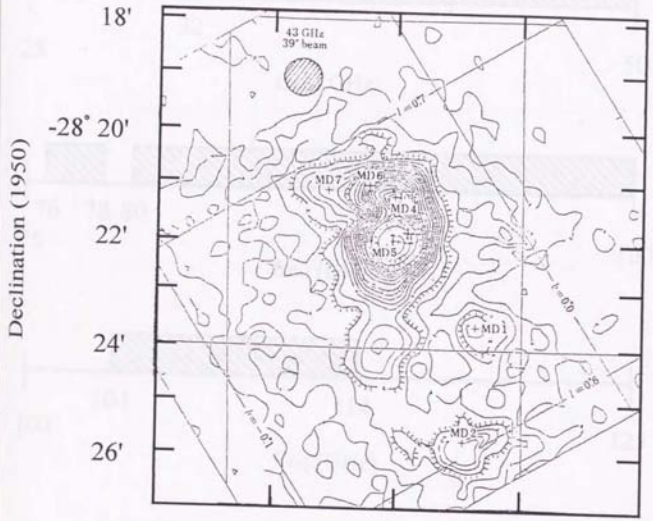
18'
-28° 20'
22'
24'
26'
43 GHz
39" beam
MD7
MD6
MD4
MD5
MD1
MD2
t=.07
t=.09
t=.08
t=.10
30s
20s
10s
17h44m00s
Declination (1950)
Right Ascension (1950)

Fig. 4

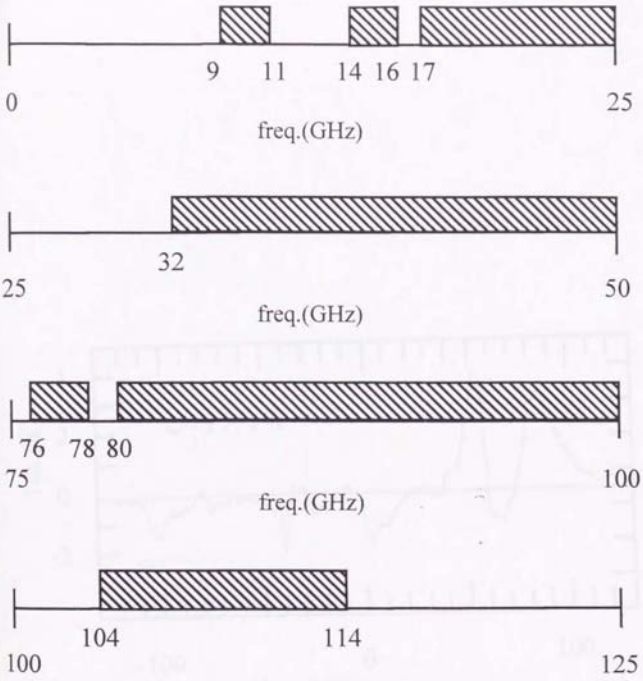
9 11 14 16 17
0
25
freq.(GHz)
32
25
50
freq.(GHz)
76 78 80
75
100
freq.(GHz)
104
114
100
125
freq.(GHz)

Fig. 5

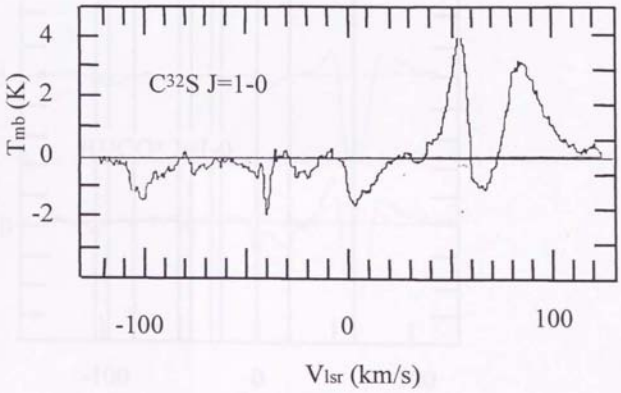

Fig. 6

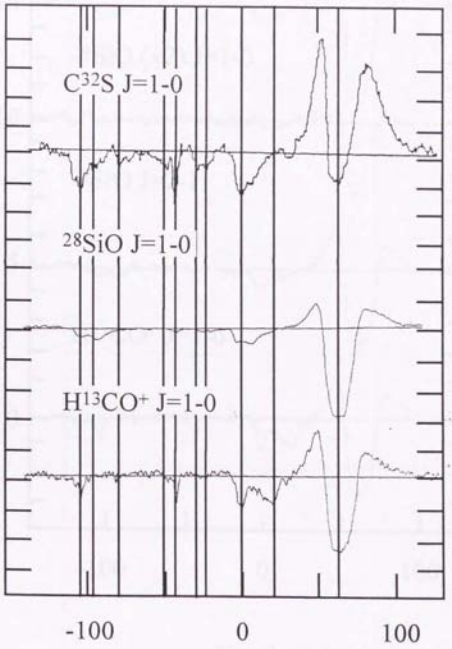

Fig. 7

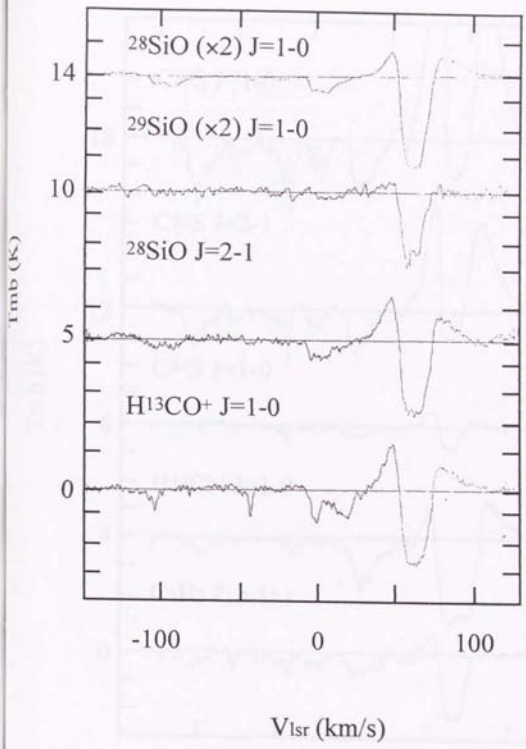
28SiO (×2) J=1-0
29SiO (×2) J=1-0
28SiO J=2-1
H13CO+ J=1-0
14
10
5
0
Tmb (K)
-100
0
100
Vlsr (km/s)

Fig. 8a

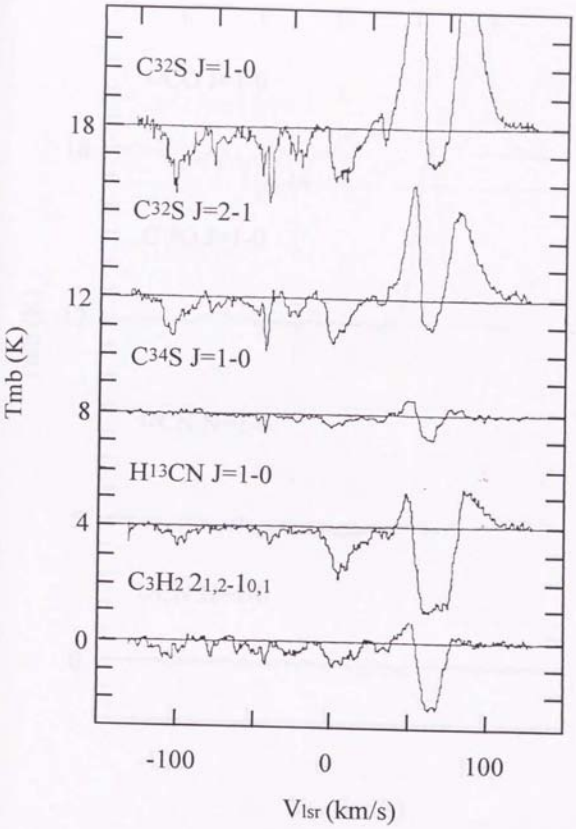
C32S J=1-0
C32S J=2-1
C34S J=1-0
H13CN J=1-0
C3H2 21,2-10,1
18
12
8
4
0
Tmb (K)
-100
0
100
Vlsr (km/s)

Fig. 8b

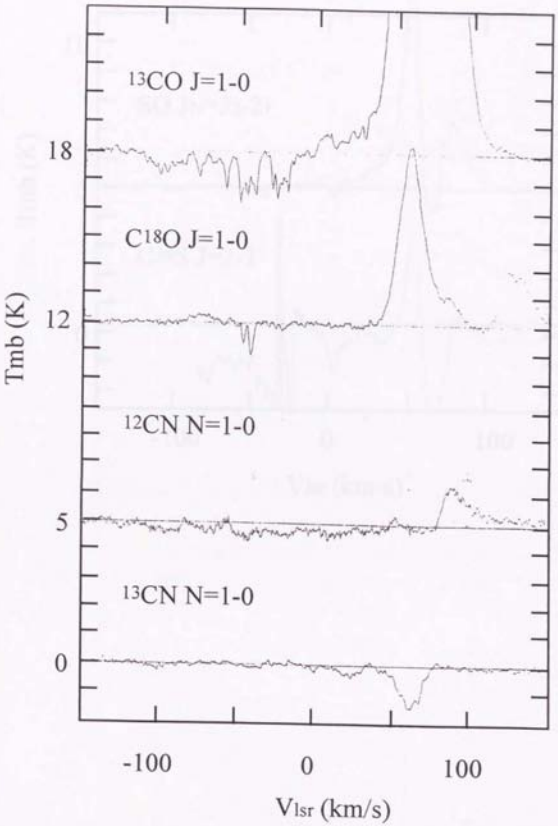

Fig. 8c (Continued.)

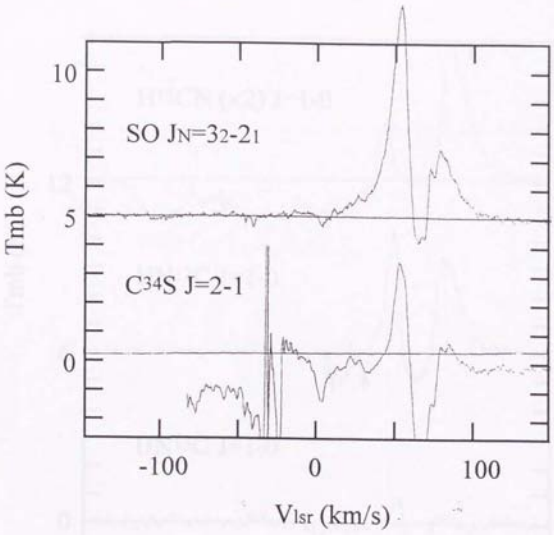

Fig. 8c (Continued.)

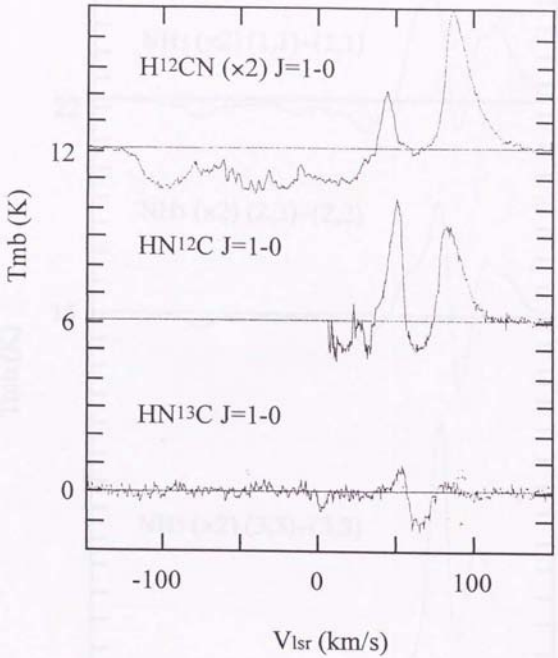

Fig. 8c (Continued.)

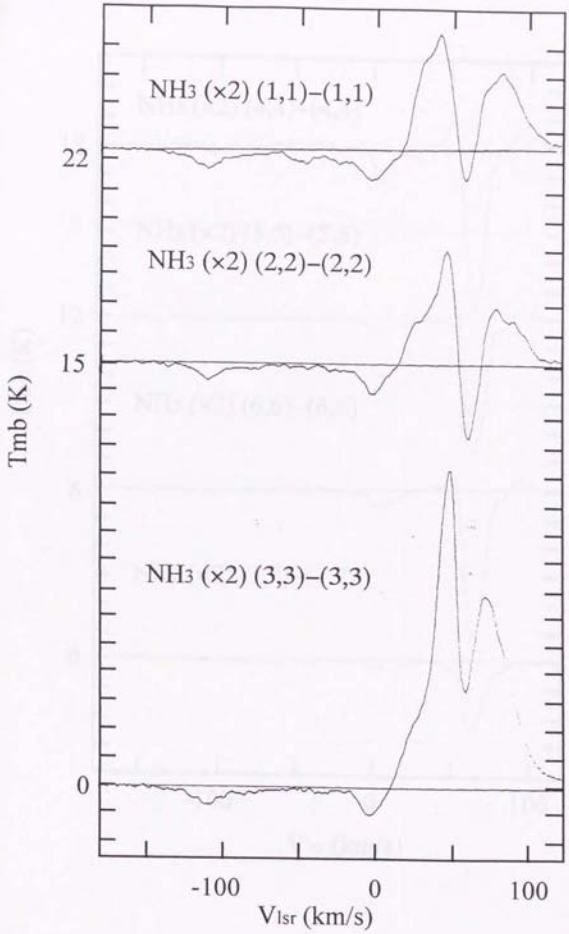

Fig. 8c (Continued.)

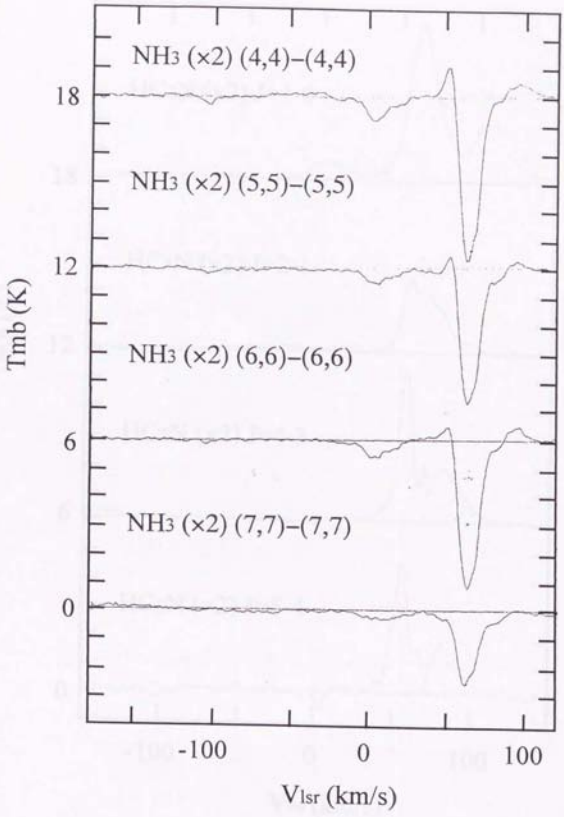

Fig. 8c (Continued.)

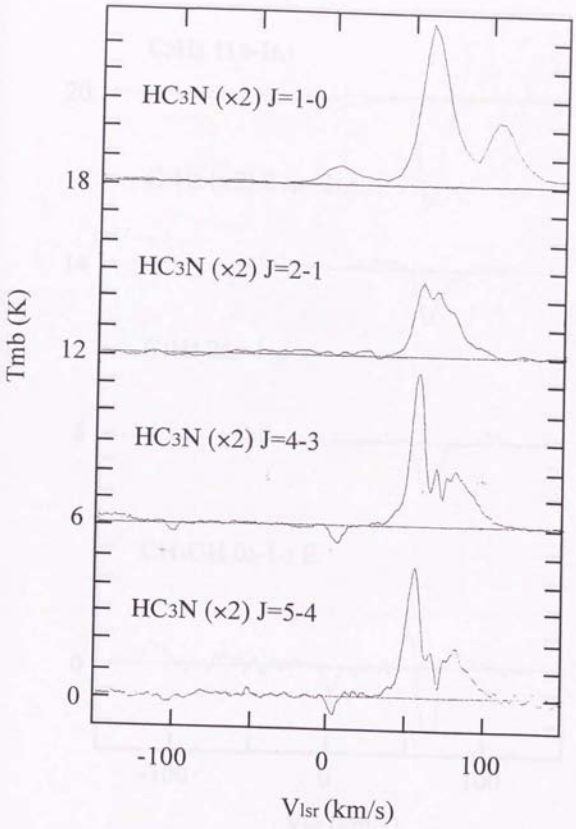

Fig. 8c (Continued.)

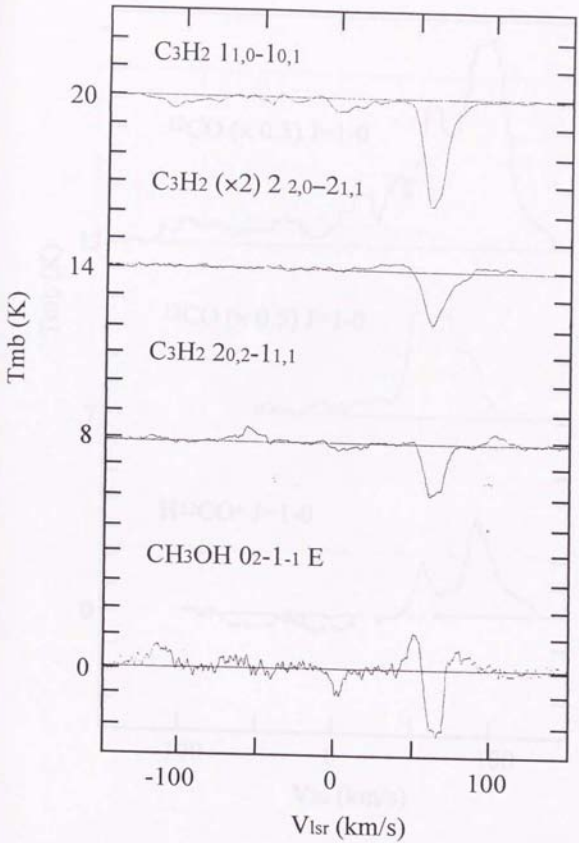
C3H2 11,0-10,1
20
C3H2 (×2) 2 2,0–21,1
14
C3H2 20,2-11,1
8
CH3OH 02-1-1 E
0
Tmb (K)
-100
0
100
Vlsr (km/s)

Fig. 8c

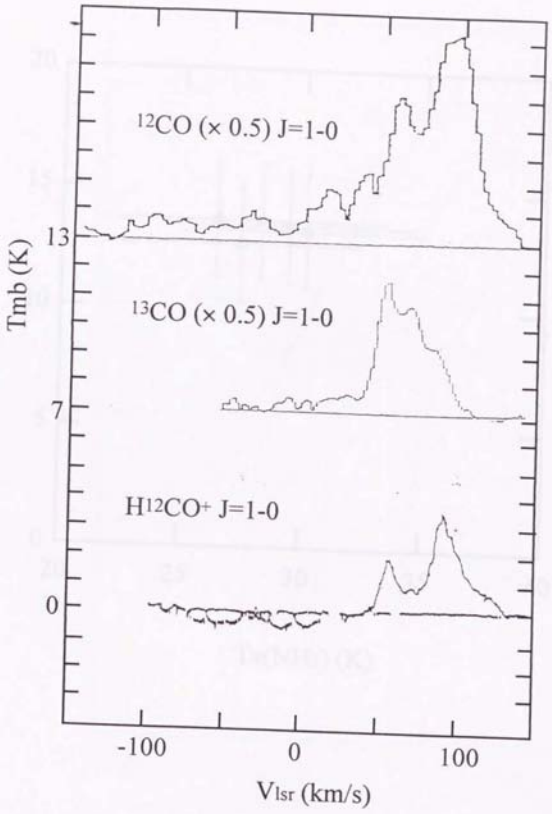

Fig. 8d

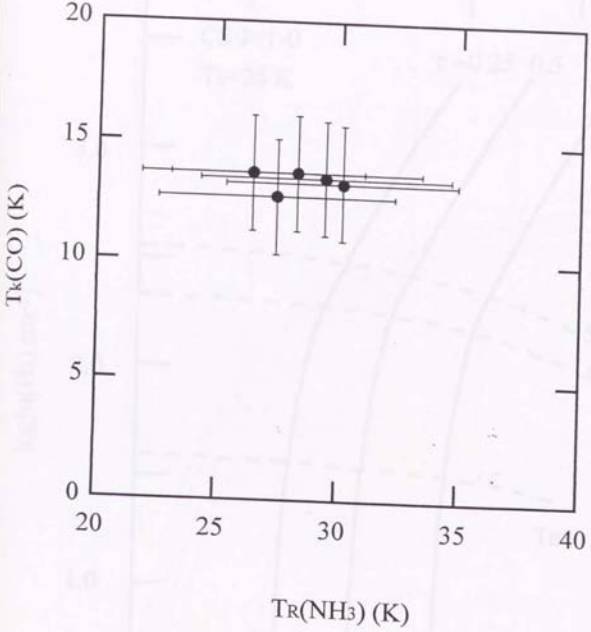

Fig. 9

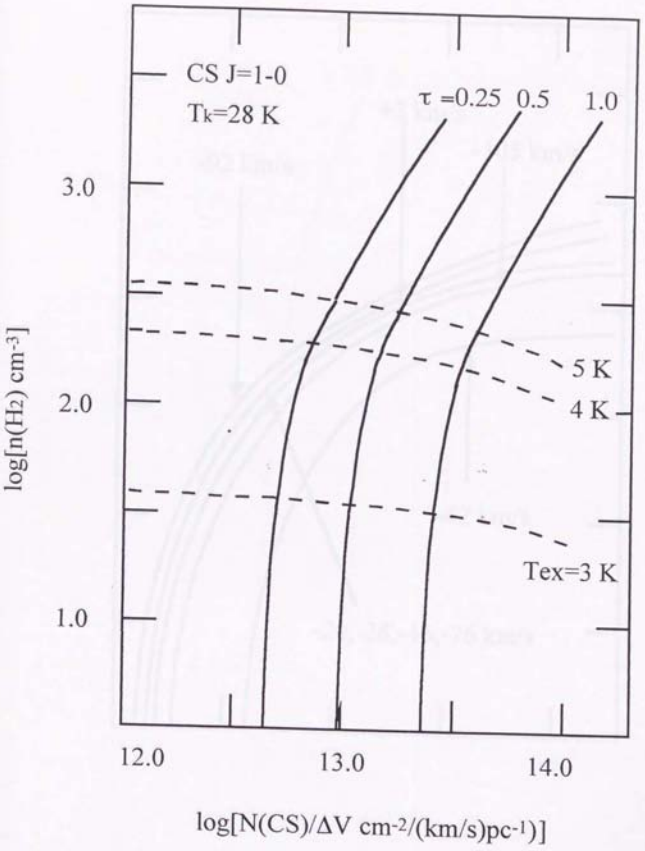
CS J=1-0
Tk=28 K
τ =0.25 0.5 1.0
5 K
4 K
Tex=3 K
3.0
2.0
1.0
12.0
13.0
14.0
log[n(H2) cm-3]
log[N(CS)/ΔV cm-2/(km/s)pc-1)]

Fig. 10a

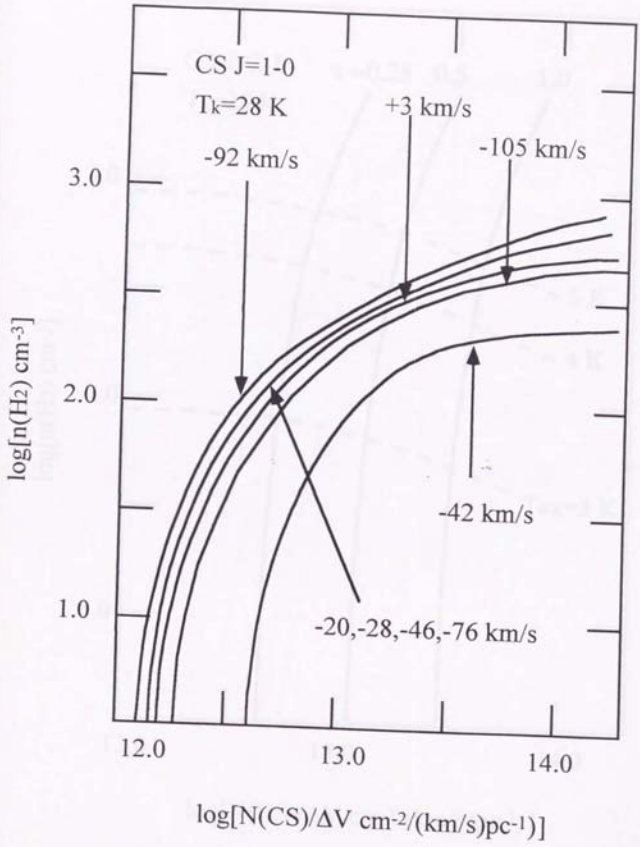
CS J=1-0
Tk=28 K
+3 km/s
-92 km/s
-105 km/s
-42 km/s
-20,-28,-46,-76 km/s
3.0
2.0
1.0
12.0
13.0
14.0
log[n(H2) cm-3]
log[N(CS)/ΔV cm-2/(km/s)pc-1)]

Fig. 10b

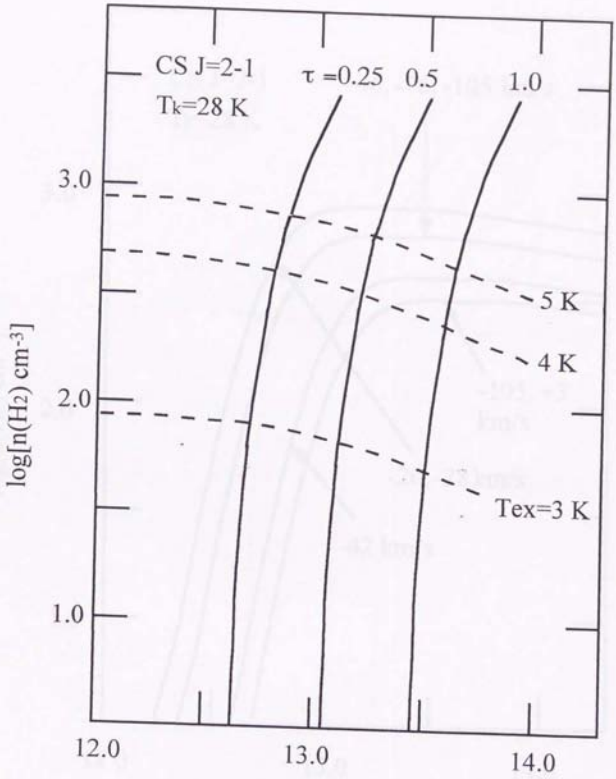
CS J=2-1
Tk=28 K
τ =0.25
0.5
1.0
3.0
2.0
1.0
5 K
4 K
Tex=3 K
log[n(H2) cm-3]
12.0
13.0
14.0
log[N(CS)/ΔV cm-2/(km/s)pc-1)]

Fig. 10c

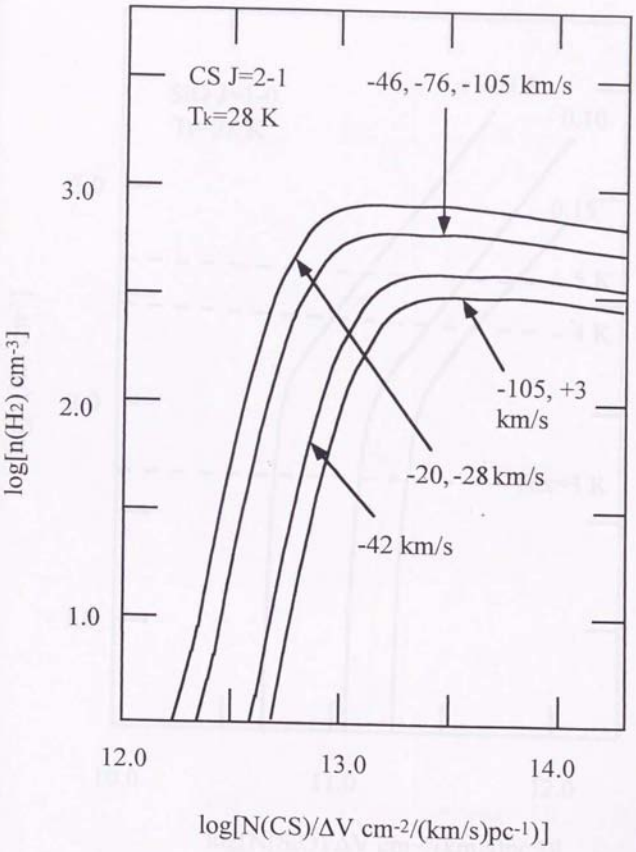
CS J=2-1
Tk=28 K
-46, -76, -105 km/s
-105, +3 km/s
-20, -28 km/s
-42 km/s
3.0
2.0
1.0
log[n(H2) cm-3]
12.0
13.0
14.0
log[N(CS)/ΔV cm-2/(km/s)pc-1)]

Fig. 10d

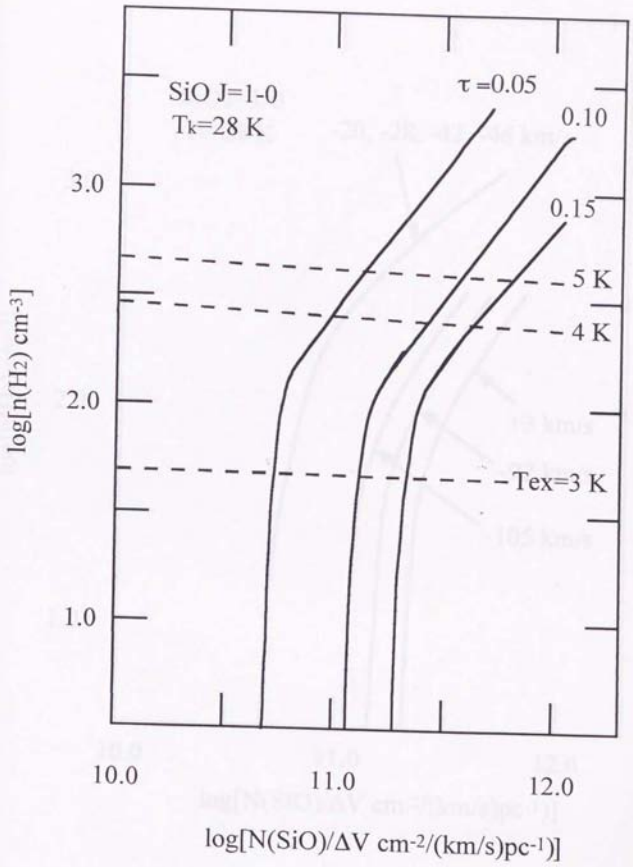
SiO J=1-0
Tk=28 K
τ =0.05
0.10
0.15
5 K
4 K
Tex=3 K
3.0
2.0
1.0
log[n(H2) cm-3]
10.0
11.0
12.0
log[N(SiO)/ΔV cm-2/(km/s)pc-1)]

Fig. 11a

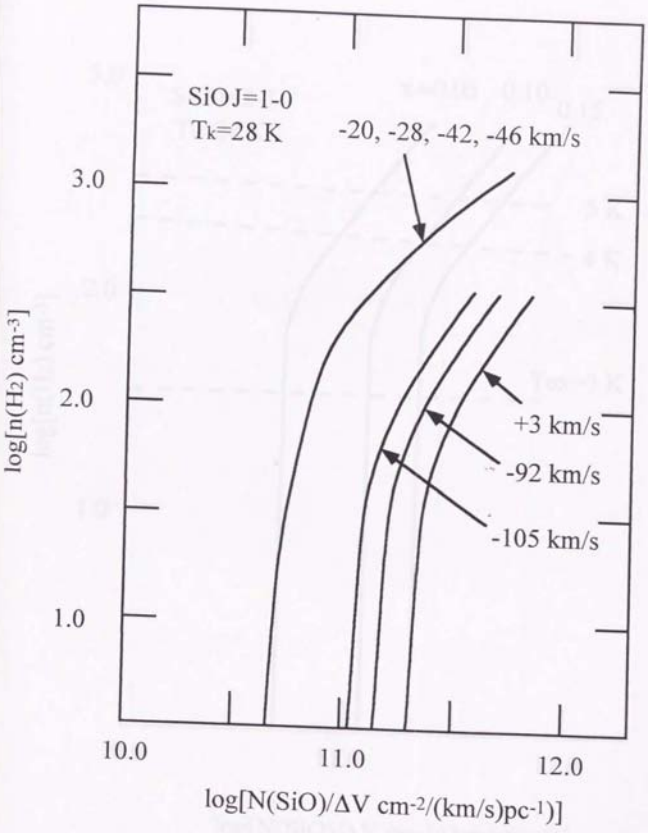
SiOJ=1-0
Tk=28 K
-20, -28, -42, -46 km/s
+3 km/s
-92 km/s
-105 km/s
3.0
2.0
1.0
log[n(H2) cm-3]
10.0
11.0
12.0
log[N(SiO)/ΔV cm-2/(km/s)pc-1)]

Fig. 11b

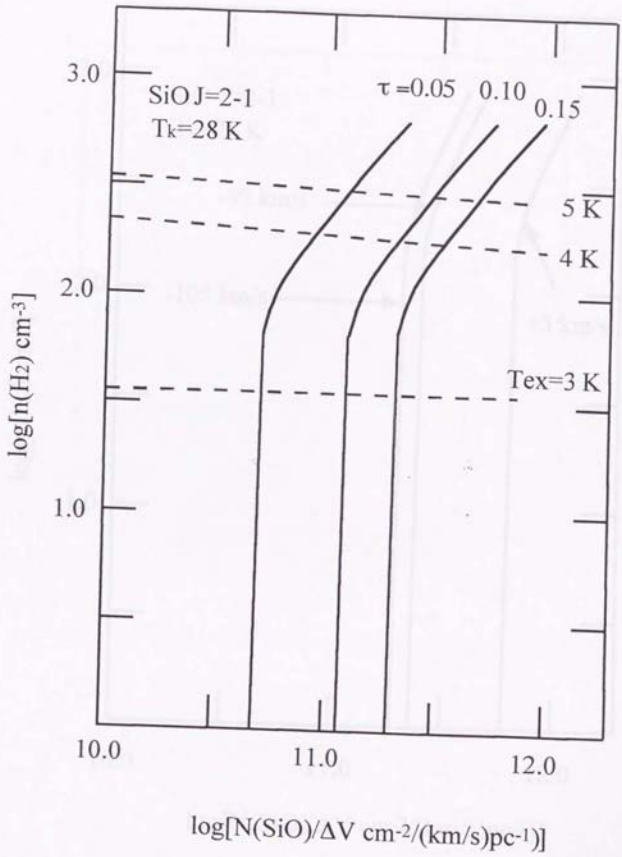
3.0
2.0
1.0
SiO J=2-1
Tk=28 K
τ =0.05
0.10
0.15
5 K
4 K
Tex=3 K
log[n(H2) cm-3]
10.0
11.0
12.0
log[N(SiO)/ΔV cm-2/(km/s)pc-1)]

Fig. 11c

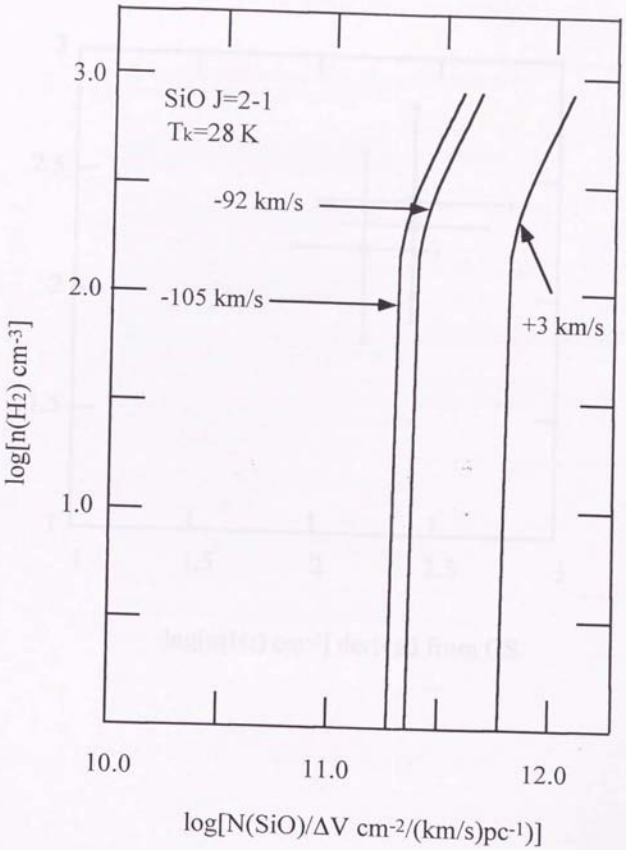
SiO J=2-1
Tk=28 K
-92 km/s
-105 km/s
+3 km/s
3.0
2.0
1.0
10.0
11.0
12.0
log[n(H2) cm-3]
log[N(SiO)/ΔV cm-2/(km/s)pc-1)]

Fig.11d

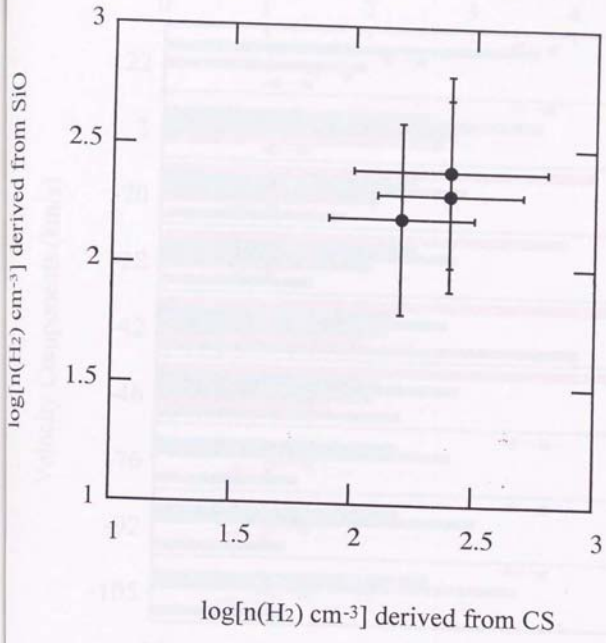
3
2.5
2
1.5
1
1
1.5
2
2.5
3
log[n(H2) cm-3] derived from SiO
log[n(H2) cm-3] derived from CS

Fig. 12

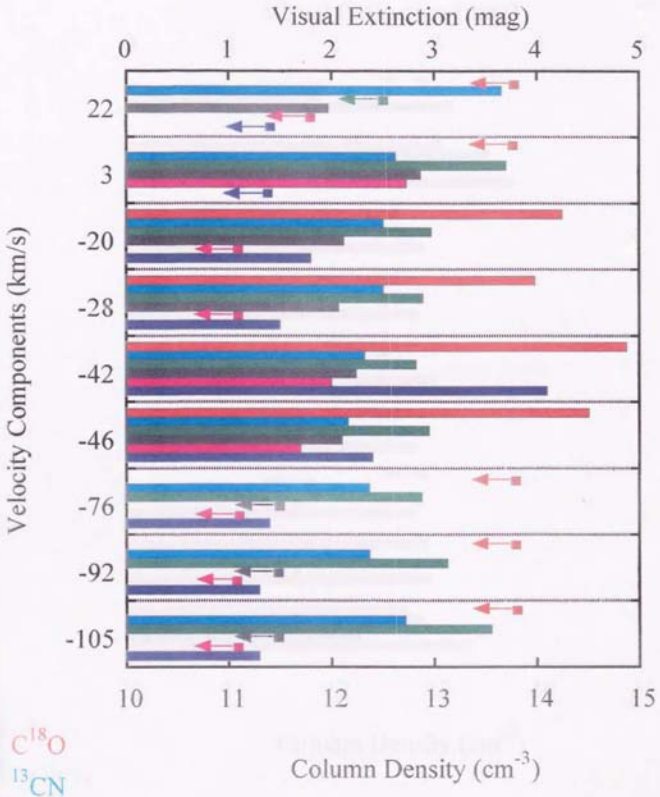
Visual Extinction (mag)
0
1
2
3
4
5
22
3
-20
-28
-42
-46
-76
-92
-105
Velocity Components (km/s)
10
11
12
13
14
15
Column Density (cm-3)
C18O
13CN
C32S
C34S
SO
Visual Extinction

Fig. 13a

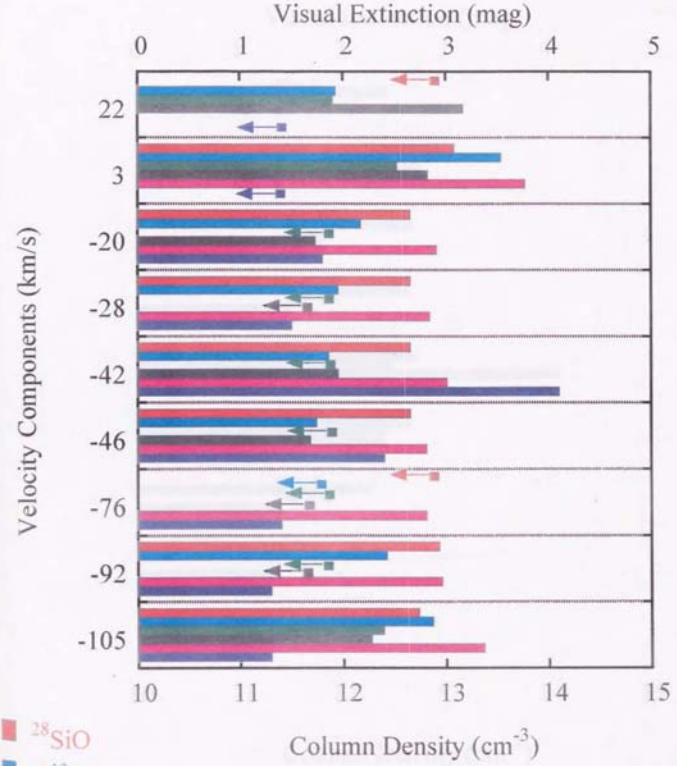
Visual Extinction (mag)
0
1
2
3
4
5
22
3
-20
-28
-42
-46
-76
-92
-105
Velocity Components (km/s)
10
11
12
13
14
15
Column Density (cm-3)
28SiO
H13CN
HN13C
H13CO+
NH3
Visual Extinction

Fig. 13b

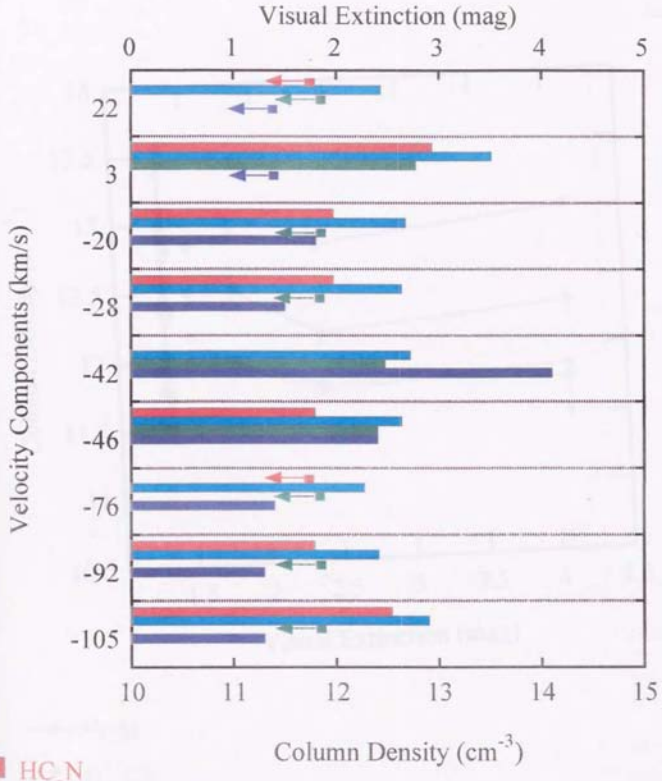
Visual Extinction (mag)
0
1
2
3
4
5
22
3
-20
-28
-42
-46
-76
-92
-105
Velocity Components (km/s)
10
11
12
13
14
15
Column Density (cm-3)
HC3N
C3H2
CH3OH
Visual Extinction

Fig. 13c

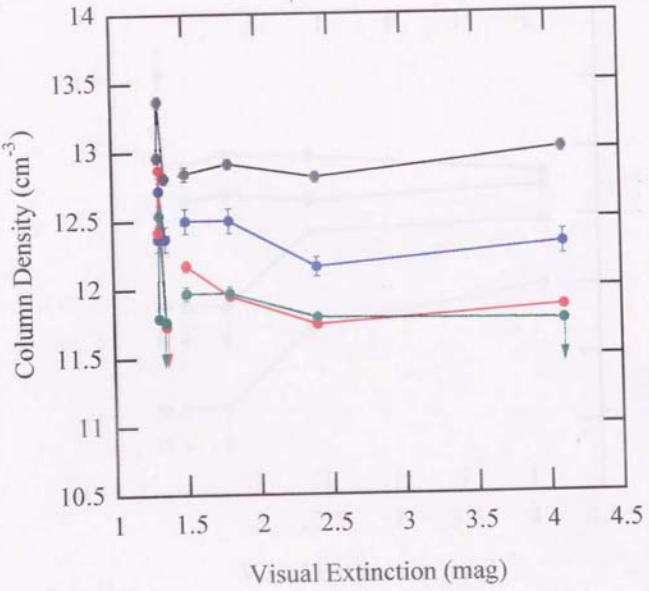
14
13.5
13
12.5
12
11.5
11
10.5
Column Density (cm^{-3})
1
1.5
2
2.5
3
3.5
4
4.5
Visual Extinction (mag)
^{13}CN
H^{13}CN
NH$_3$
HC$_3$N

Fig. 14a

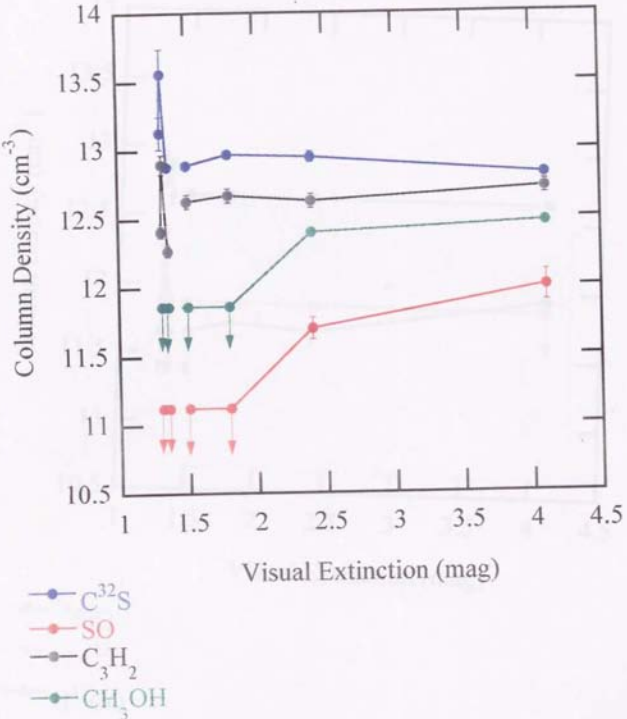
14
13.5
13
12.5
12
11.5
11
10.5
Column Density (cm^{-3})
1
1.5
2
2.5
3
3.5
4
4.5
Visual Extinction (mag)
$C^{32}S$
SO
C_3H_2
CH_3OH

Fig. 14b

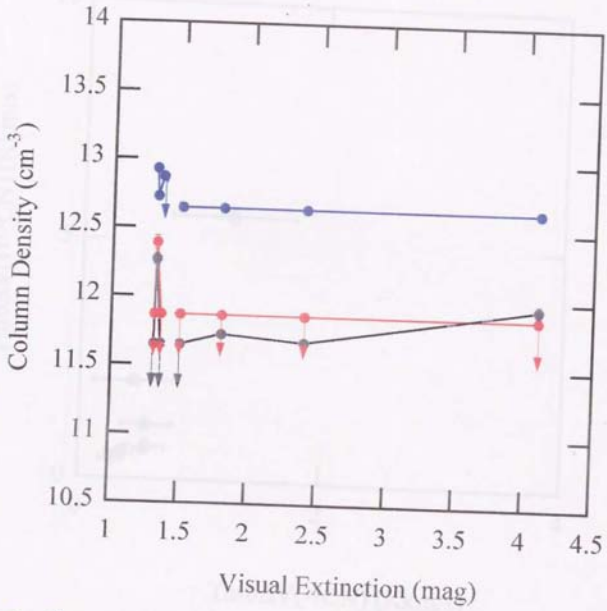
14
13.5
13
12.5
12
11.5
11
10.5
Column Density (cm^{-3})
1
1.5
2
2.5
3
3.5
4
4.5
Visual Extinction (mag)
^{28}SiO
HN^{13}C
H^{13}CO^{+}

Fig. 14c

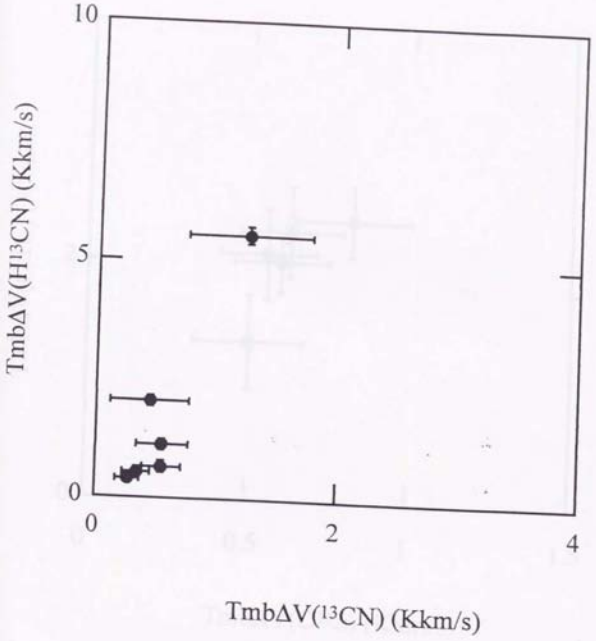

Fig. 15a

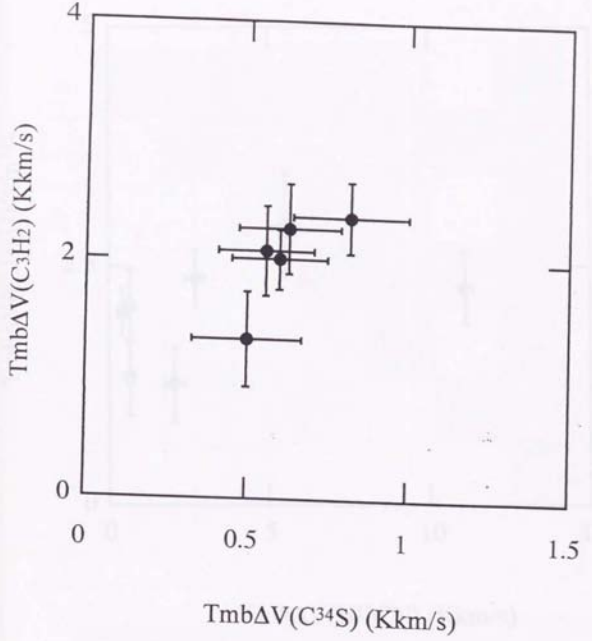

Fig. 15b

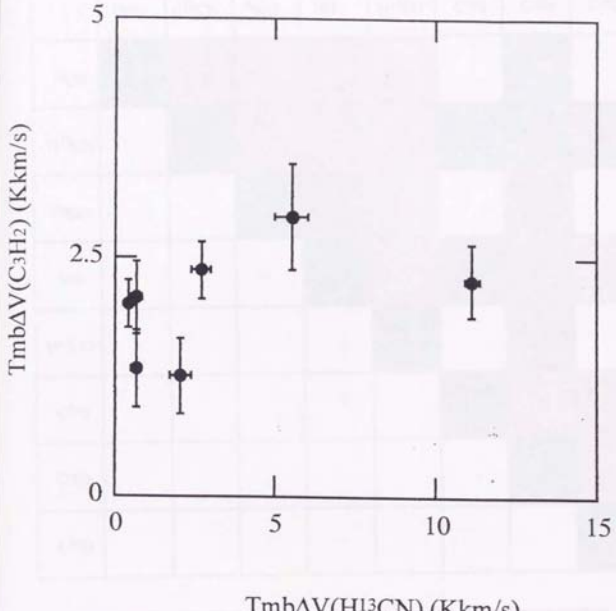

Fig. 15c

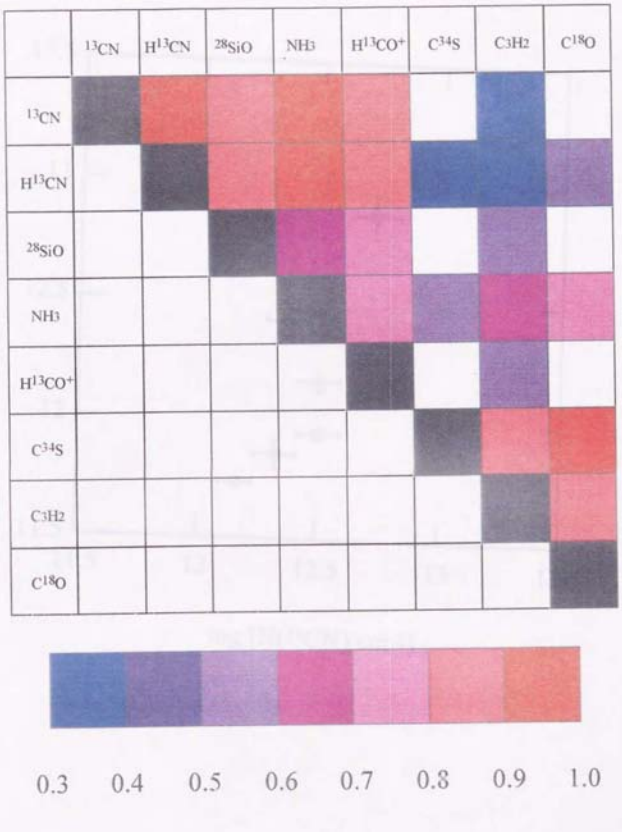
^{13}CN
$H^{13}CN$
^{28}SiO
NH_3
$H^{13}CO^+$
$C^{34}S$
C_3H_2
$C^{18}O$
0.3
0.4
0.5
0.6
0.7
0.8
0.9
1.0

Fig. 16

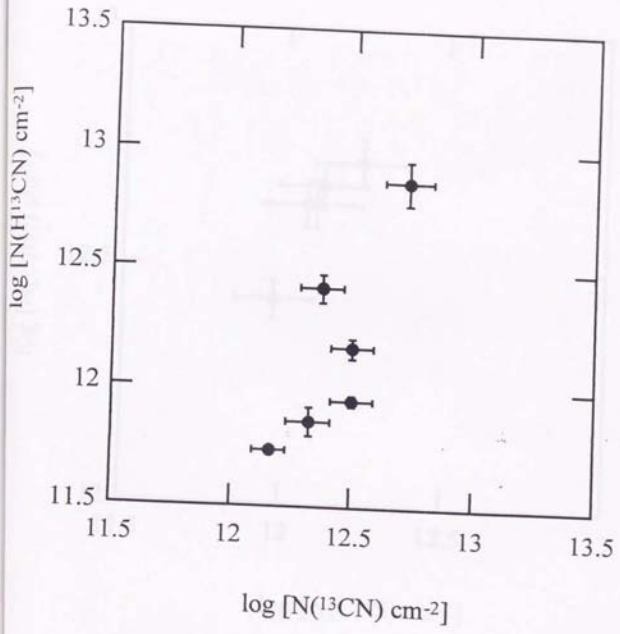

Fig. 17a

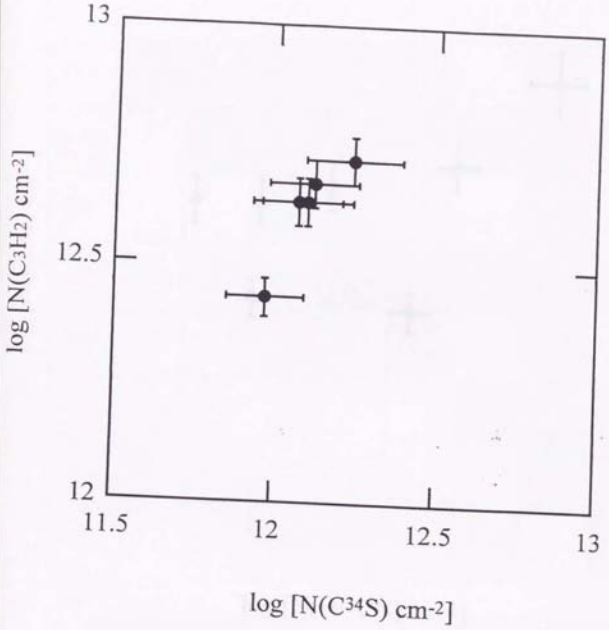

Fig. 17b

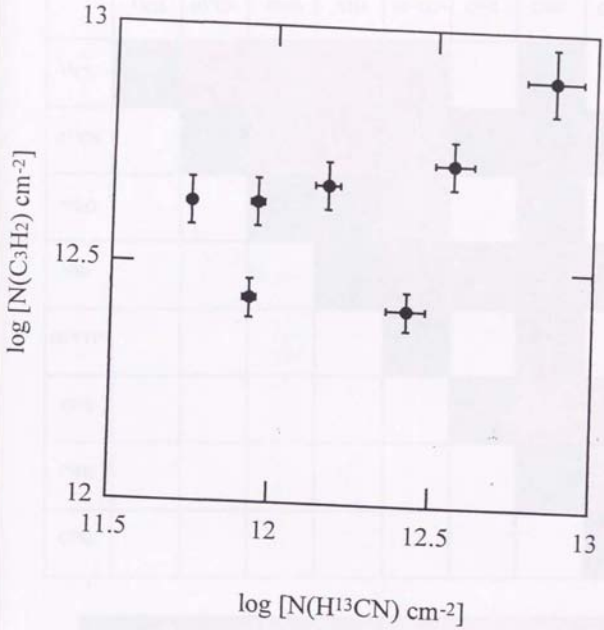

Fig. 17c

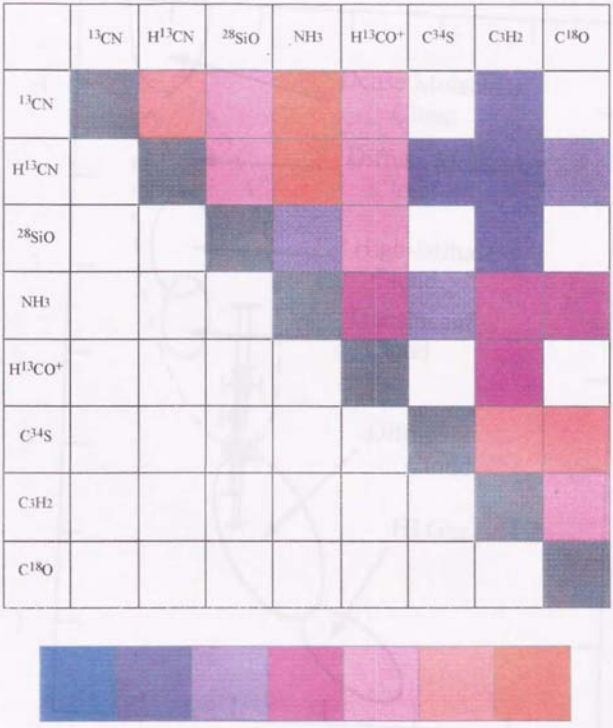
^{13}CN
$H^{13}CN$
^{28}SiO
NH_3
$H^{13}CO^+$
$C^{34}S$
C_3H_2
$C^{18}O$
0.3
0.4
0.5
0.6
0.7
0.8
0.9
1.0

Fig. 18

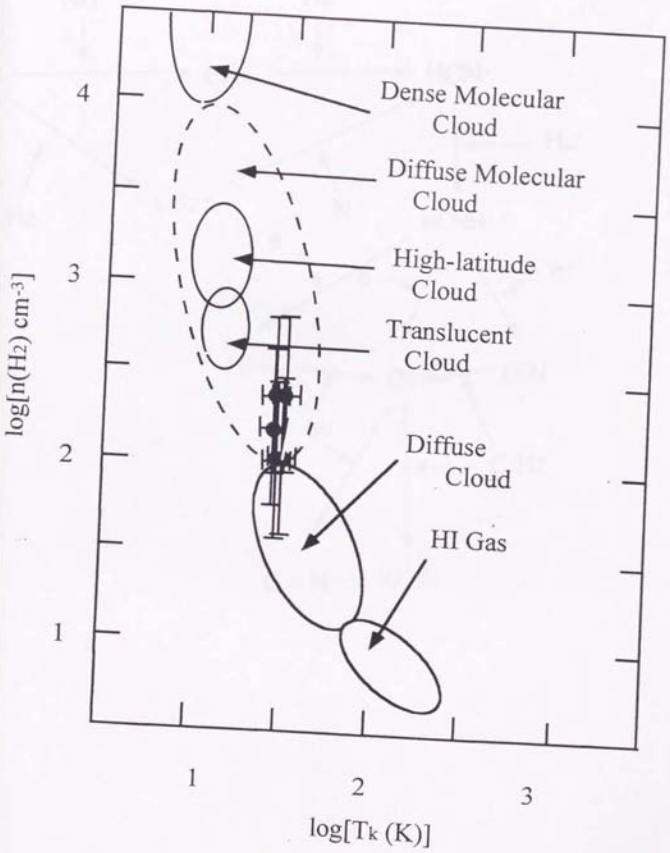
Dense Molecular Cloud
Diffuse Molecular Cloud
High-latitude Cloud
Translucent Cloud
Diffuse Cloud
HI Gas
4
3
2
1
log[n(H2) cm-3]
1
2
3
log[Tk (K)]

Fig. 19

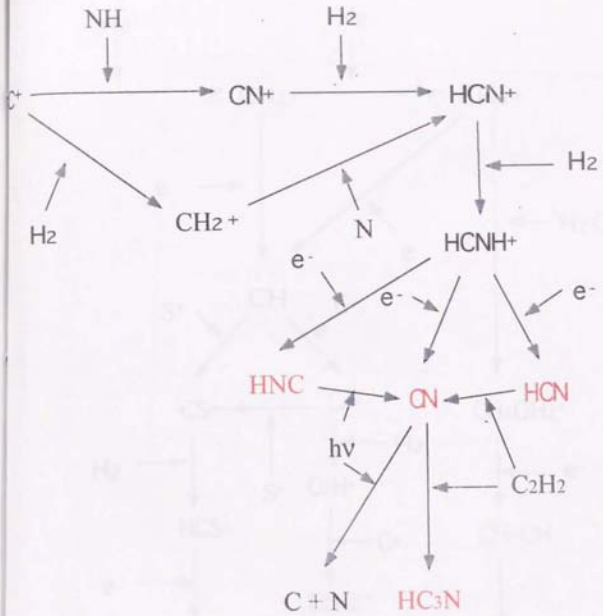

Fig. 20

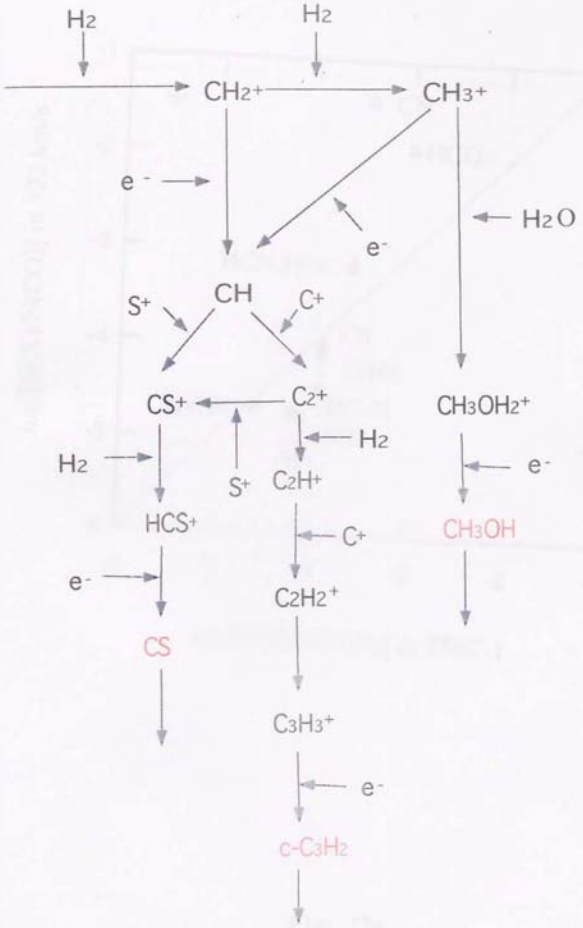
H2
H2
CH2+
CH3+
e -
e-
H2O
S+
CH
C+
CS+
C2+
CH3OH2+
H2
H2
e-
S+
C2H+
HCS+
C+
CH3OH
e-
C2H2+
CS
C3H3+
e-
c-C3H2

Fig. 21

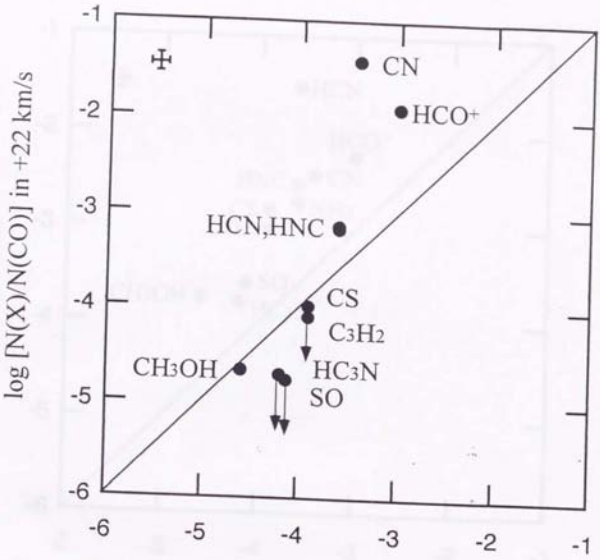
log [N(X)/N(CO)] in +22 km/s
log [N(X) /N(CO)] in TMC-1
-1
-2
-3
-4
-5
-6
-6
-5
-4
-3
-2
-1
CN
HCO+
HCN,HNC
CS
C3H2
CH3OH
HC3N
SO

Fig. 22a

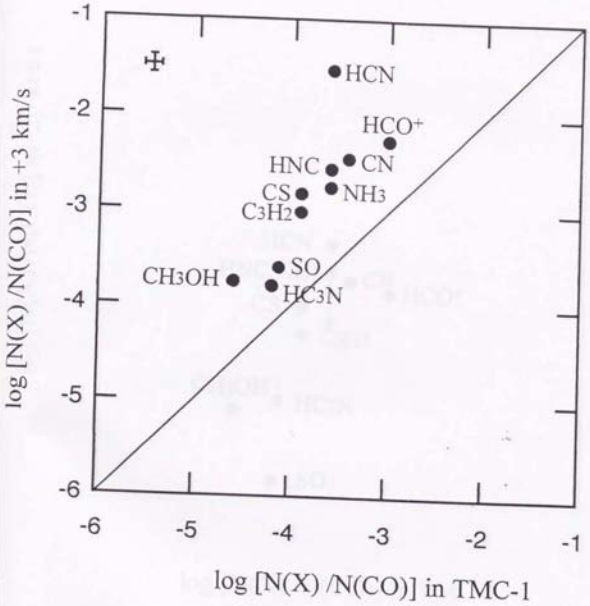
HCN
HCO+
HNC
CN
CS
NH3
C3H2
SO
CH3OH
HC3N
-1
-2
-3
-4
-5
-6
log [N(X) /N(CO)] in +3 km/s
log [N(X) /N(CO)] in TMC-1

Fig. 22b

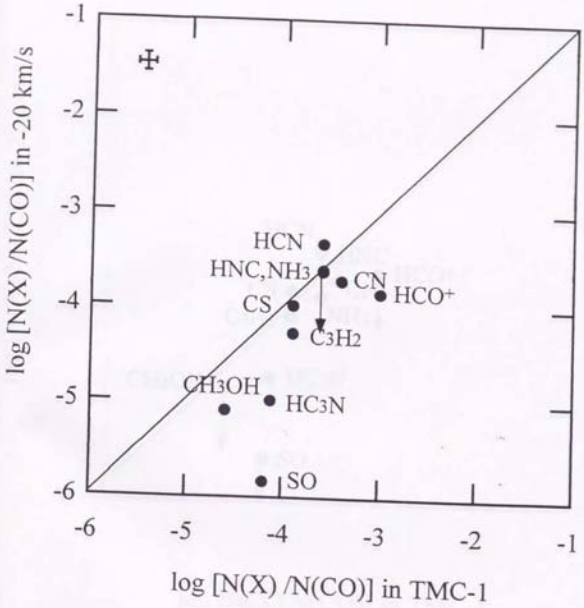
log [N(X) /N(CO)] in -20 km/s
log [N(X) /N(CO)] in TMC-1
-1
-2
-3
-4
-5
-6
HCN
HNC,NH3
CN
HCO+
CS
C3H2
CH3OH
HC3N
SO

Fig. 22c

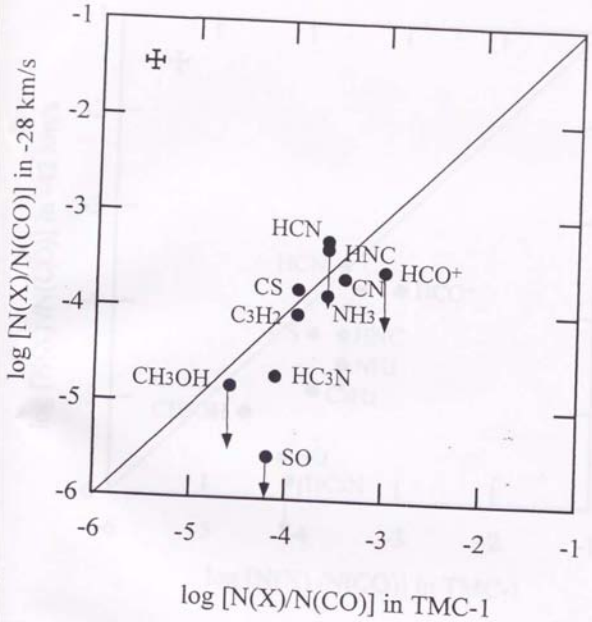
log [N(X)/N(CO)] in -28 km/s
log [N(X)/N(CO)] in TMC-1
-1
-2
-3
-4
-5
-6
HCN
HNC
HCO+
CS
CN
C3H2
NH3
CH3OH
HC3N
SO

Fig. 22d

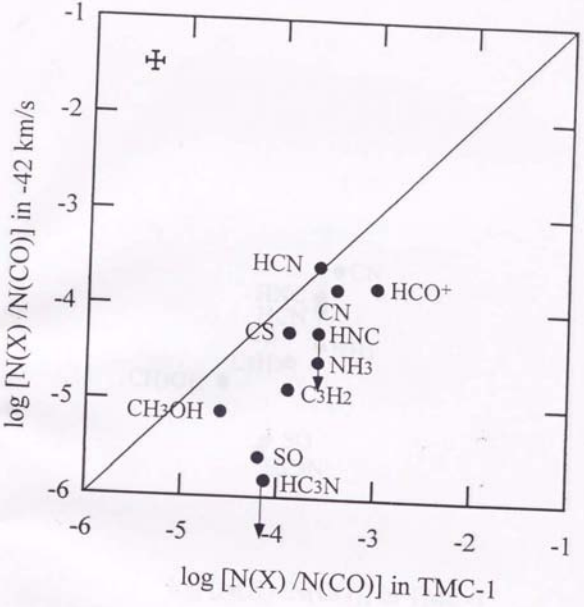
-1
-2
-3
-4
-5
-6
-6
-5
-4
-3
-2
-1
HCN
HCO+
CN
CS
HNC
NH3
C3H2
CH3OH
SO
HC3N
log [N(X) /N(CO)] in -42 km/s
log [N(X) /N(CO)] in TMC-1

Fig. 22e

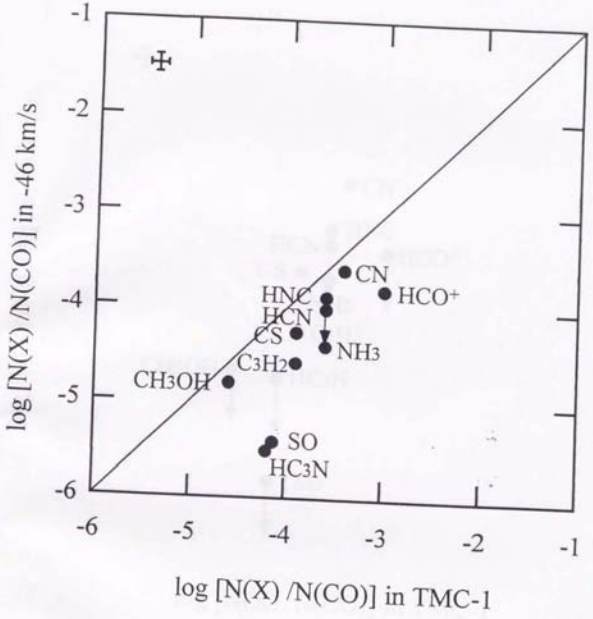
-1
-2
-3
-4
-5
-6
-6
-5
-4
-3
-2
-1
log [N(X) /N(CO)] in -46 km/s
log [N(X) /N(CO)] in TMC-1
CN
HCO+
HNC
HCN
CS
NH3
C3H2
CH3OH
SO
HC3N

Fig. 22f

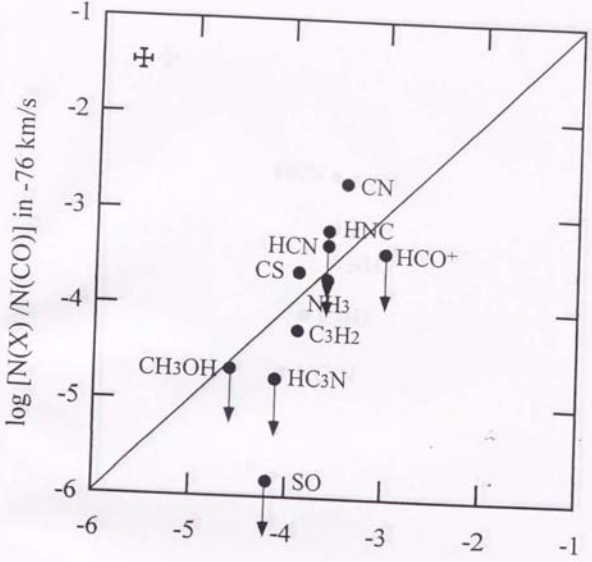
log [N(X) /N(CO)] in -76 km/s
log [N(X) /N(CO)] in TMC-1
-1
-2
-3
-4
-5
-6
CN
HNC
HCN
CS
HCO+
NH3
C3H2
CH3OH
HC3N
SO

Fig. 22g

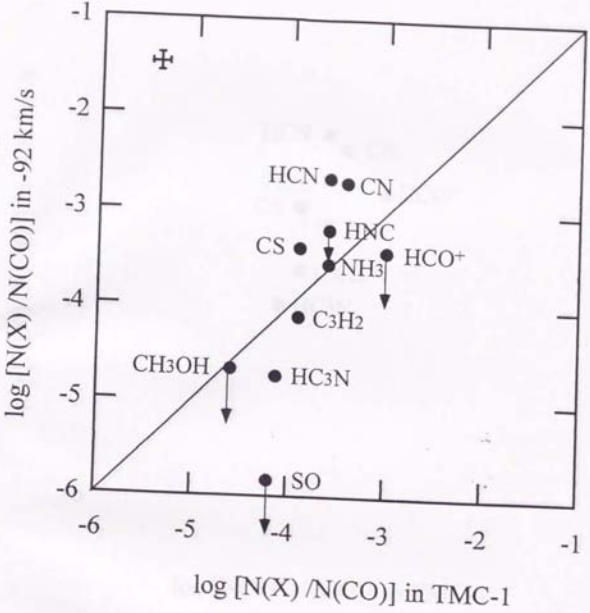
-1
-2
-3
-4
-5
-6
-6
-5
-4
-3
-2
-1
HCN
CN
HNC
CS
NH3
HCO+
C3H2
CH3OH
HC3N
SO
log [N(X) /N(CO)] in -92 km/s
log [N(X) /N(CO)] in TMC-1

Fig. 22h

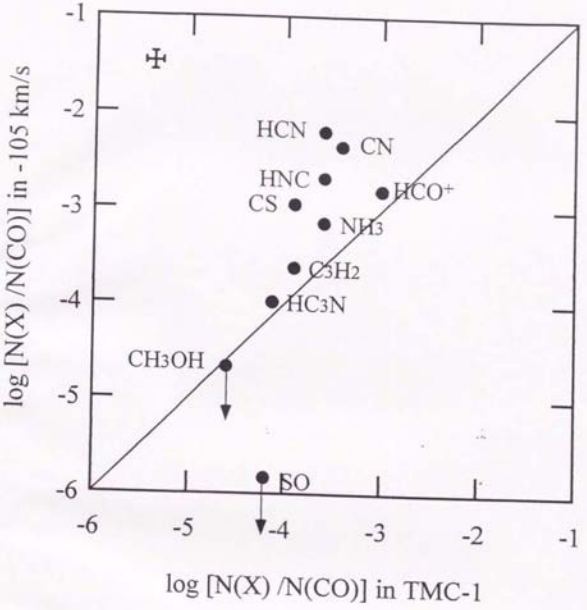
log [N(X) /N(CO)] in -105 km/s
log [N(X) /N(CO)] in TMC-1
HCN
CN
HNC
HCO+
CS
NH3
C3H2
HC3N
CH3OH
SO
-1
-2
-3
-4
-5
-6

Fig. 22i

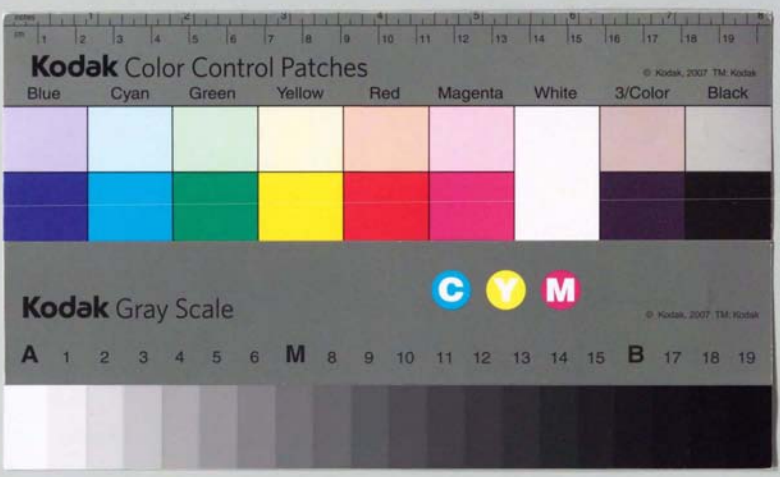
Kodak Color Control Patches
© Kodak, 2007 TM: Kodak
Blue
Cyan
Green
Yellow
Red
Magenta
White
3/Color
Black
Kodak Gray Scale
C
Y
M
© Kodak, 2007 TM: Kodak
A 1 2 3 4 5 6 M 8 9 10 11 12 13 14 15 B 17 18 19